THE STUDY OF PRUSSIAN BLUE AS CATHODE MATERIAL FOR SODIUM-ION BATTERIES

CHEN YUNCAI

University of Malaya

FACULTY OF SCIENCE
UNIVERSITY OF MALAYA
KUALA LUMPUR

2019

THE STUDY OF PRUSSIAN BLUE AS CATHODE MATERIAL FOR SODIUM-ION BATTERIES

CHEN YUNCAI

DISSERTATION SUBMITTED IN FULFILMENT OF THE REQUIREMENTS FOR THE DEGREE OF MASTER OF SCIENCE

DEPARTMENT OF PHYSICS
FACULTY OF SCIENCE
UNIVERSITY OF MALAYA
KUALA LUMPUR

2019

University of Malaya

UNIVERSITY OF MALAYA

ORIGINAL LITERARY WORK DECLARATION

Name of Candidate: **CHEN YUNCAI**

Matric No: **SGR160033**

Name of Degree: **MASTER OF SCIENCE**

Title of Project Paper/Research Report/Dissertation/Thesis ("this Work"):

THE STUDY OF PRUSSIAN BLUE AS CATHODE MATERIAL FOR SODIUM-ION BATTERIES

Field of Study: **EXPERIMENTAL PHYSICS**

I do solemnly and sincerely declare that:

(1) I am the sole author/writer of this Work;
(2) This Work is original;
(3) Any use of any work in which copyright exists was done by way of fair dealing and for permitted purposes and any excerpt or extract from, or reference to or reproduction of any copyright work has been disclosed expressly and sufficiently and the title of the Work and its authorship have been acknowledged in this Work;
(4) I do not have any actual knowledge nor do I ought reasonably to know that the making of this work constitutes an infringement of any copyright work;
(5) I hereby assign all and every rights in the copyright to this Work to the University of Malaya ("UM"), who henceforth shall be owner of the copyright in this Work and that any reproduction or use in any form or by any means whatsoever is prohibited without the written consent of UM having been first had and obtained;
(6) I am fully aware that if in the course of making this Work I have infringed any copyright whether intentionally or otherwise, I may be subject to legal action or any other action as may be determined by UM.

Candidate's Signature Date:

Subscribed and solemnly declared before,

Witness's Signature Date:

Name:

Designation:

University of Malaya

THE STUDY OF PRUSSIAN BLUE AS CATHODE MATERIAL FOR SODIUM-ION BATTERIES

ABSTRACT

The introduction of electric vehicles (EVs) into the automotive market has boosted the advancement of energy storage technology. Although lithium-ion batteries (LIBs) could provide a solution to the emerging EV market, it needs to overcome the issue of high material cost and limited resources. This leads the research direction to sodium-ion batteries (SIBs), the most potential alternative batteries with infinite sodium resource from the ocean and earth crust. In current work, Prussian Blue (PB) was synthesized by the facile one step solution-precipitation method at room-temperature. Ascorbic acid and poly (vinylpyrrolidone) (PVP) were used as the chelating agents. The as-prepared PB was characterized by element analysis, energy dispersive X-ray spectroscopy (EDX), thermogravimetric analysis (TGA), X-ray diffraction (XRD), high resolution transmission electron microscope (HRTEM), field emission scanning electron microscopy (FESEM) and X-ray photoelectron spectroscopy (XPS). The formula of the as-prepared PB has been obtained as $Na_{0.58}Fe[Fe(CN)_6]_{0.93}\square_{0.07}1.67H_2O$ with a 3-5 % water content. Two pairs of redox peaks are shown in cyclic voltammetry (CV) curve. The peaks at 3.15 V / 2.74 V correspond to high-spin Fe^{3+}/Fe^{2+} bonding to N atoms of C≡N and those at 3.78V / 3.63V correspond to low-spin Fe^{3+}/Fe^{2+} bonding to C atoms of C≡N. The battery exhibited a discharge specific capacity (DSC) of 133 mAh g^{-1} with an efficiency of almost 100 % at 0.1 C. At 2 C, a DSC of 102 mAh g^{-1} was obtained and the SIBs exhibited a good cyclability with more than 89 % retention after 200 galvanostatic charge/discharge (GCD) cycles.

Keywords: Sodium-ion battery, cathode, Prussian Blue, low vacancies rate, room-temperature.

University of Malaya

KAJIAN PRUSSIA BIRU SEBAGAI BAHAN KATOD UNTUK BATERI NATRIUM-ION

ABSTRAK

Pengenalan kenderaan elektrik ke pasaran otomotif telah meningkatkan kemajuan teknologi penyimpanan tenaga. Walaupun bateri litium-ion dapat memberikan penyelesaian kepada pasaran kenderaan elektrik yang berkembang, ianya perlu mengatasi masalah kos bahan yang tinggi dan sumber yang terhad. Ini telah mengundang karah penyelidikan bateri natrium-ion, bateri alternatif yang paling berpotensi dengan sumber natrium tanpa had dari lautan dan kerak bumi. Dalam penyelidikan semasa, Prussian Blue (PB) disintesiskan melalui kaedah larutan-pengendapan pada suhu bilik. Asid askorbik dan poly(vinylpyrrolidone) digunakan sebagai ejen celating. PB yang telah disediakan dicirikan oleh analisis unsur, pembelauan sinar-X, spektroskopi penyebaran tenaga sinar-X, mikroskop penghantaran elektron beresolusi tinggi, mikroskopi pengimbasan elektron pelepasan medan dan spektroskopi fotoelektron sinar-X. Formula PB yang disediakan adalah $Na_{0.58}Fe[Fe(CN)_6]_{0.93}\square_{0.07}1 .67H_2O$ dengan kandungan air sebanyak 3-5 %. PB tersebut digunakan sebagai bahan katod untuk bateri natrium-ion. Lengkung kitaran voltammetri menunjukkan terdapat dua pasang puncak redoks. Puncak pada 3.15 V/2.74 V menunjukkan ikatan Fe^{3+}/Fe^{2+} spin tinggi kepada atom N dari C≡N manakala pada 3.78 V/3.63 V menunjukkan ikatan Fe^{3+}/Fe^{2+} spin rendah kepada atom C dari C≡N. Bateri ini menunjukkan kapasiti pelepasan tertentu sebanyak 133 mAh g^{-1} dengan kecekapan hampir 100 % pada arus 0.1 C. Pada kepadatan arus 2 C, pelepasan tertentu sebanyak berkurang ke 102 mAh g^{-1} dan menunjukkan prestasi yang cemerlang dengan pengekalan sebanyak 89 % selepas 200 pusingan caj/pelepasan galvanostatik.

Kata kunci: bateri natrium-ion, katod, Prussian Blue, kadar kekosongan yang rendah, suhu bilik.

University of Malaya

ACKNOWLEDGEMENTS

I would like to take this opportunity to thank all of the people who have helped me during my master career.

My deepest gratitude goes first and foremost to Professor Abdul Kariem Arof and Dr. Woo Haw Jiunn, my supervisors, who have walked me through all the stages of the writing of this thesis. Their critical comments, constant encouragement and guidance have greatly enlightened me not only on the academic pursuit but also on the morals of being a human. Without the consistent and illuminating instruction, this thesis could not have reached its present stage.

Secondly, I would like to express my heartfelt thanks to all the members in Centre for Ionics, University of Malaya, who help me a lot me during my experimental sections. They also helped me a lot in life during my two years as a foreigner in Malaysia. I am feeling very lucky that I can met them in a strange country.

I also greatly thank to the scholars and authors mentioned in the bibliography. Their previous works guided me the direction to explore the world of science. Without their works, the literature review of my thesis would not have been possible.

Last, I am deeply indebted to my beloved families and friends, who always supported me when I am down. Their helps and supports have accompanied me through the difficult moments of my life.

In here, I would like to thank all the people who helped me and accompanied me these 3 years.

University of Malaya

TABLE OF CONTENTS

University of Malaya

University of Malaya

University of Malaya

University of Malaya

LIST OF FIGURES

University of Malaya

University of Malaya

University of Malaya

LIST OF TABLES

University of Malaya

LIST OF SYMBOLS AND ABBREVIATIONS

ω	:	Angular frequency
θ	:	Diffraction angle
λ	:	Incident wavelength
α	:	Lattice parameter
(h, k, l)	:	Miller index
σ	:	Warburg coefficient
□	:	Vacancies
A	:	Superficial area of the electrode
C	:	Capacity
CSC	:	Charge specific capacity
Cspecific	:	Specific capacity
CV	:	Cyclic voltammetry
D	:	Diffusion coefficient
DSC	:	Discharge specific capacity
EC	:	Ethylene carbonate
EDX	:	Energy dispersive X-Ray spectroscopy
EIS	:	Electrochemical impedance spectroscopy
EV	:	Electric vehicle
F	:	Faraday constant
FEC	:	Fluoroethylene carbonate
FESEM	:	Field emission scanning electron microscopy
GCD	:	Galvanostatic charge/discharge
HRTEM	:	High resolution transmission electron microscope
LCE	:	Lithium carbonate equivalent
LIB	:	Lithium-ion batteries
m	:	Mass

University of Malaya

MIB	:	Magnesium ion batteries
n	:	Amount of transfer electron
NASICON	:	Natrium-superionic conductor
NMP	:	N-methyl-2-pyrrolidone
PB	:	Prussian blue
PC	:	Polycarbonate
PIB	:	Potassium-ion batteries
PVDF	:	Poly(vinylidene fluoride)
PVP	:	Poly(vinylpyrrolidone)
R	:	Gas constant
Rct	:	Charge transfer resistance
Rs	:	SPE resistance
SC	:	Specific capacity
SEI	:	Solid electrolyte interphase
SEM	:	Scanning electron microscopy
SHE	:	Standard hydrogen electrode
SIB	:	Sodium-ion battery
T	:	Absolute temperature
TEM	:	Transmission electron microscope
TGA	:	Thermogravimetric analysis
XPS	:	X-ray photoelectron spectroscopy
XRD	:	X-ray diffraction
Zre	:	Real impedance

University of Malaya

CHAPTER 1: INTRODUCTION

1.1 Research Background

Electricity has become an integral part of daily life. Thermal power generators using fossil energies are now the main method to generate electricity. However, with increasing demands for electricity, environmental issues and the fluctuating oil price have created a worldwide energy crisis. This have resulted in the search and development of renewable and clean energy, including wind, solar, tidal and geothermal energies.

Solving the energy storage crisis has been a worldwide challenge. Nowadays, lithium rechargeable battery is the most widely used secondary battery in portable devices. However, the lithium reserve is now depleting. It has been reported that the lithium element in the earth is very limited and the price of lithium has increased to 7200 USD per ton in 2016 (Martin et al., 2017). Alternative secondary batteries that are being studied include sodium-ion batteries (SIBs), magnesium-ion batteries (MIBs) and potassium-ion batteries (KIBs).

1.2 Problem Statement

SIBs may be considered as the most potential secondary batteries in the future as they are more suitable for energy storage systems, like the power grid and EVs because of the low cost and abundant resource. The unique properties of Na pose some hurdles for SIBs application. The ionic radius of Na^+ ion (102 pm) which is bigger than that of lithium ion (76 pm) can slow down its movement and affect the specific capacity (SC) and cycling performance of the SIBs. In addition, Na^+ ion has a more positive reduction potential (2.71 V) than that of Li^+ ion (3.05 V) and consequently result in a lower energy density SIBs.

University of Malaya

For SIBs anode materials, literature survey shows that hard carbon is suitable as anode to replace the graphite as in LIBs. Hard carbon is also the most ideal anode due to its low price, abundance and easiness to synthesize. This leaves the challenge for finding a suitable SIB cathode material. In the present work, Prussian blue (PB) with the formula ($A_xBB'(CN)_6$(A = Na; B and B′ = Fe) is synthesized as cathode active material for SIBs because it has an open-framework structure, low cost and non-toxic.

1.3 Objectives of the Research

In view of the problem descried above, the objectives of this work include

1. To synthesize the PB with low interstitial water.
2. To measure the structure properties and morphology of as-prepared PB using energy dispersive X-Ray spectroscopy (EDX), elemental analysis, X-ray diffraction (XRD), thermogravimetric analysis (TGA), field emission scanning electron microscopy (FESEM) and high-resolution transmission electron microscope (HRTEM).
3. To analyze the electrochemical performance of half-cell sodium-ion battery using as-prepared PB as the cathode by using cyclic voltammetry (CV), electrochemical impedance spectroscopy (EIS) and galvanostatic charge/discharge (GCD).

1.4 Dissertation Organization

This dissertation comprises 7 chapters.

Chapter 1 introduces the nature of the work, issues to address and research objectives.

Chapter 2 presents the literature review and previous studies relevant to this work. Development of SIBs are covered, following by a brief introduction of some typical electrode materials for SIBs. This is followed with PB structure and its characteristics.

University of Malaya

Chapter 3 introduces the conventional synthesis method and explains the solution-precipitation method used for this work in detail. The characterizations of PB are described. The last section of this chapter covers the electrochemical characterizations of SIBs using as-prepared PB as the cathode material.

Chapter 4 presents the results of crystal structure and chemical composition of PB. Elemental analysis and EDX results are used to calculate the molecular formula. Base on TGA, the water content and the decomposition temperature of as-prepared PB are acquired. XRD is used to study the lattice structure of as-prepared PB while HRTEM and FESEM are used to determine the morphology properties.

Chapter 5 presents the electrochemical performance of half-cell SIBs using as-prepared PB as cathode material. The first section is the CV, describing the material electrochemical active potential. EIS is used to study the kinetics of cells. From the GCD process, the SC is calculated. The last section describes the different GCD characteristic from which the rate performance of the PB is obtained.

Chapter 6 discusses all results obtained in this work.

Chapter 7 makes a conclusion of this work together with some suggestions for future works.

University of Malaya

CHAPTER 2: LITERATURE REVIEW

2.1 Introduction

Energy is the core section in the development of human society. The use of fire is the flag of a birth of civilization. In the information age, the energy demand is even increasing. However, traditional energies (coal, petroleum and natural gas) are not renewable. The demands of energy will lead to fossil fuels depletion. Excessive usage of fossil fuels can lead to a series of chain effect related to the environmental issues that include thermal pollution, acid rain and greenhouse effect. Therefore, clean and easy to harvest renewable energy is the best alternative to replace fossil fuels as the main energy source. These renewable energies include solar, tidal, wind, hydropower, geothermal, biomass and ocean energies. However, the applications of these renewable energies should be paired with the energy storage system due to the unsustainability of the renewable energies. LIBs should be the best candidate for the energy storage system. However, it suffers from the resource limitation (Zheng et al., 2019). SIBs have similar electrochemical behaviors to LIBs and would be an alternative candidate for LIBs (Zhao et al., 2018). The mechanism of the SIBs is displayed in Figure 2.1 (a). During charge, the electricity is obtained from the renewable energies by the generator. However, the use of this electricity is sometimes at a valley period. Thus, the over output of this electricity should be storage in the energy storage systems and be released at the peak period which is the discharge process. Batteries is the best candidate for this application due to its high energy density (Ren et al., 2017). The general coin-cell structure is presented in Figure 2.1 (b). It consists of cathode cover, spring, current collector, cathode, separator, anode, anode current collector and anode cover. The movement between electrodes leads to the generation of current.

University of Malaya

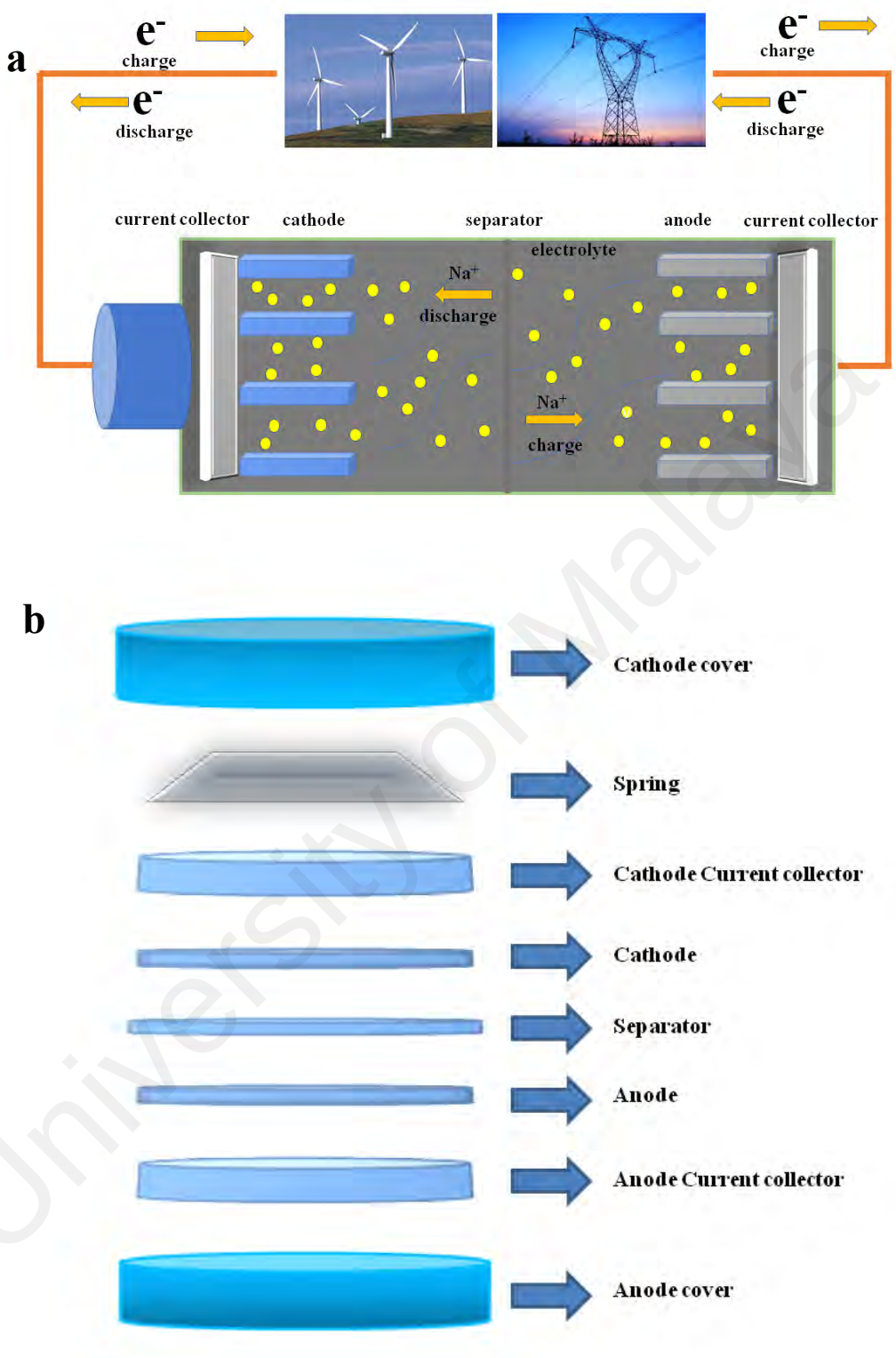

Figure 2.1: (a) The mechanism of the batteries and (b) the structure of a coin-cell.

University of Malawi

2.2 Development of Sodium-ion Batteries (SIBs)

LIBs have been the most wildly used secondary batteries, widely used in commercial system due to its long cycling performance, high operating voltage and high energy density. However, Li reserve is limited and the price of Li has increased over the years and can possibly limit the application of LIBs in medium or large-scale energy system, such as EVs and electricity storage systems.

In a report of Martin (Yoshida et al., 2014), the demand of Li will increase from about 173,000 ton/year lithium carbonate equivalent (LCE) in 2015 to 270,000 ton/year LCE in 2020. With the increasing demands for secondary batteries and the scarcity and uneven distribution of lithium resources, the search on alternative candidates are necessary and urgent. Alternative candidates including SIBs, MIBs and PIBs are being studied. SIBs have gained a lot of attention. Sodium, Na is abundant element in the earth crust (Huang et al., 2018). SIBs are the most promising alternative because of (1) it's abundance in nature (2) low cost and (3) environmentally friendly. Sodium is also in the same group as lithium in the periodic table. Hence the chemical, physical properties of sodium are similar to lithium. SIB is a kind of rocking chair battery likes LIB. SIB consists of cathode, anode, electrolyte, separator and current collector. During GCD process, Na^+ ion moves in between cathode and anode through electrolyte. The electrons move through the external circuit.

Literature review has shown that SIBs research was started together with LIBs in the 1980s. Na_xCoO_2 was used as cathode and sodium-lead was used as the anode (Delmas et al., 1981). However, this SIBs exhibited a lower voltage than LIBs at that time. Hence researchers gave up on SIB research and concentrated on LIBs. After a few decades, due to over-demand and lack of Li resources, SIBs have once again gained the limelight.

University of Malaya

However, due to the large size of Na^+ ions, the diffusion kinetics of sodium is slower. It is a major challenge to synthesize suitable electrodes for SIBs. A suitable SIB electrode should possess the following features: (1) high capacity, (2) high voltage, (3) high energy density, (4) high conductivity, (5) high structural stability, (6) low cost and (7) environmentally friendly. For anode material, different kind of materials have successfully been developed (Hwang et al., 2017; Ye et al., 2016). However, the cathode still suffers the issue of low theoretical SC.

2.3 Anode Materials for SIBs

Na metal is an active metal with a voltage of -2.70 V (vs. standard hydrogen electrode, SHE). The theoretical SC of Na is 1160 mAh h^{-1} and the melting point is 97.7 ℃. But Na metal cannot be used as the anode for commercial SIBs because Na metal dendrite will grow and impale the separator, which will lead to short circuit and possible explosion.

The general requirements for SIB anode are:

1. High energy density and high SC
2. Low potential compared with Na.
3. High structural stability
4. Good ions kinetics
5. No reaction to electrolyte
6. High thermal stability
7. Low-cost and environmentally friendly

2.3.1 Hard Carbon Anode

For the commercial market, graphite is used as the anode candidate for LIBs. Unfortunately, the graphite is not suitable for SIBs because Na^+ has large radius, which is bigger than the inter layer spacing of the graphite (Balogun et al., 2016). This leads to

University of Malaya

the discovery of another member of carbon family, hard carbon to be used as the anode for SIBs. Cao et al. had studied hollow-carbon nanowire anode for SIBs that could exhibited a SC of 251 mAh g^{-1}. This hollow-carbon nanowire still demonstrated a SC of 206.3 mAh g^{-1} after 400 cycles (Figure 2.2). However, at high current density this hollow-carbon nanowire performed quite badly and only exhibited a capacity of 149 mAh g^{-1}.

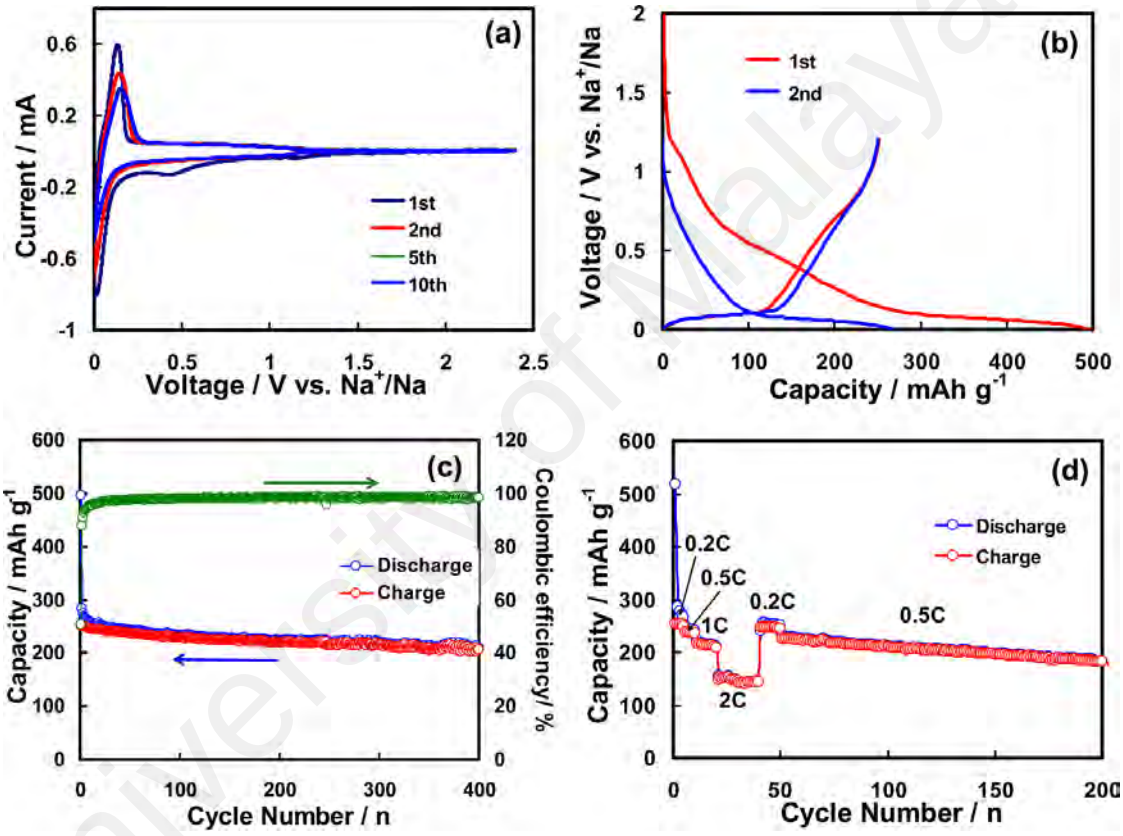

Figure 2.2: (a) CV curves (0 and 2.5 V, 0.1 mV s^{-1}), (b) First two GCD profiles, (c) Cycle performance and (d) Discharge capacity, respectively of hollow-carbon nanowire. (Cao et al., 2012)

University of Malaya

2.3.2 Alloy Materials

Besides hard carbon, alloy materials are also considered as another one promising anode candidate for SIBs. The high SC of alloy materials draws the main attraction but it suffers from the issue of structural change and volume expansion. Figure 2.3 shows an example of alloyed anode, antimony-carbon (Sb-C) nanofibers.

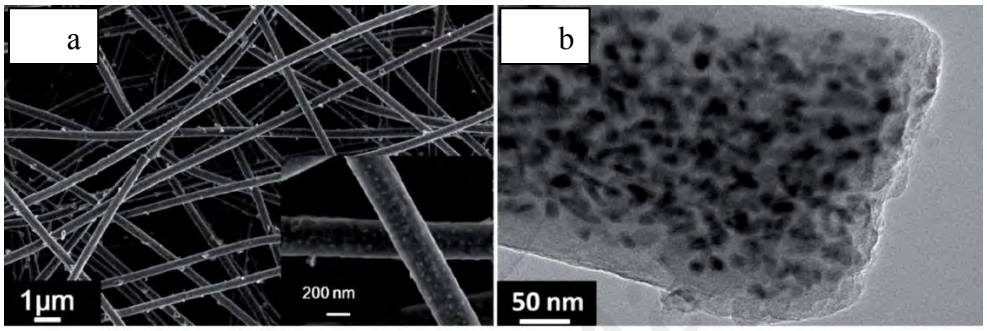

Figure 2.3: (a) SEM images, (b) TEM image of the Sb–C nanofibers (Wu et al., 2014)**.**

Another group, Wu's group. synthesized Sb–C nanofibers (Figure 2.4) anode for SIBs. This Sb–C material could deliver a SC of 631 mAh g^{-1} at C/15. The SC remained 90 % over 400 cycles at the current of C/3 (Wu et al., 2014). Unfortunately, it dropped quickly in higher current density.

University of Malaya

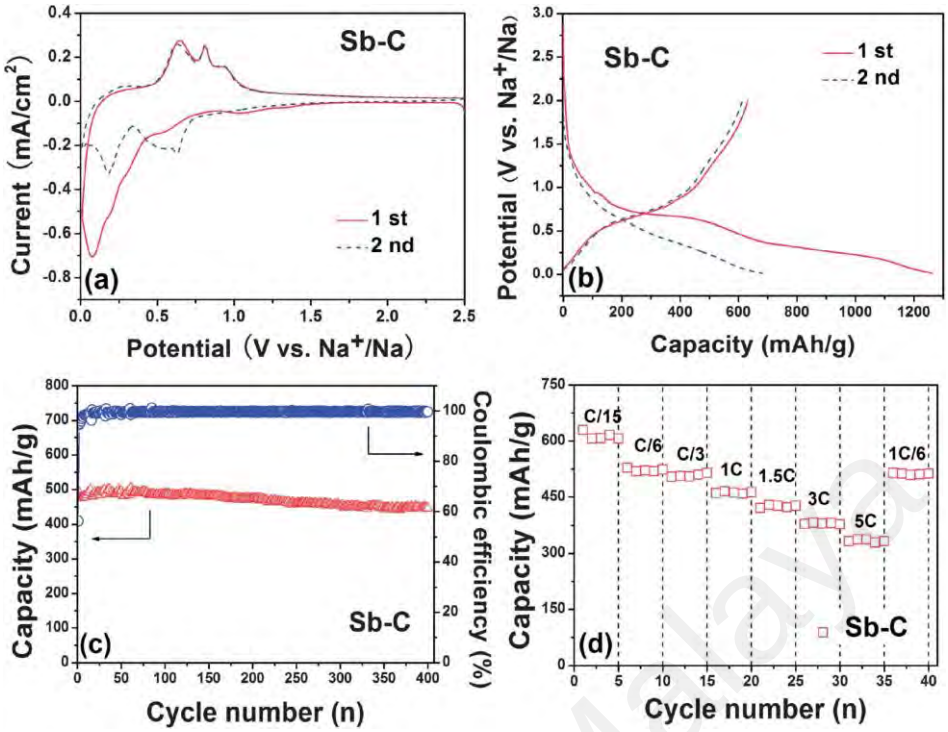

Figure 2.4: (a) CV curves, (b) the initial GCD profiles (0.01 V and 2.0 V, C/15), (c) cycling performance (C/3), and (d) C rate capability (current rates from C/15 to 5 C) of the Sb-C nanofibers (Wu et al., 2014).

2.4 Cathode Materials for SIBs

Electrode plays a major character in the performances of SIBs. The capacity, reversibility and voltage are based on the electrode materials. Capacity is the most important parameter for a battery. The capacity of the anode for SIBs is generally in between 250 - 500 mAh g^{-1}, with some exceptional material reaching 1000 mAh g^{-1}. However, the specific capacities of cathode for SIBs are only around 80 mAh g^{-1} - 200 mAh g^{-1} (Hwang et al., 2017). Therefore, a lot of attempts have been made to improve the cathode performance. This section presents some of the important cathode candidates, such as polyanion compounds, transition metal oxides, organic compounds, polymers and metal hexacyanometalates.

University of Malaya

2.4.1 Transition Metal Oxides

Na_xMO_2 (M = Fe, Co, Ni, Mn, etc.), transition metal oxides are popular cathodes for SIBs due to their facile, controllable method of synthesis and wide ion movement path. There are two typical structures of transition metal oxide, tunnel structure ($x<0.5$) and layer structure ($0.5<x<1$). Due to the different coordination mode and stack mode, layer transition metal oxide can be divided into O2, O3, P2 and P3 phases (O is octahedral, P is the prism, the number is the layer amount of oxygen atom of each unit) (Delmas et al., 1981).

2.4.1.1 Na_xCoO_2

Delmas et al. (1981) pointed out that Na_xCoO_2 can be used as cathode material for SIBs. Under 1 bar oxygen pressure and over the temperature range 500 – 800 °C. The products had different Na contents according to the respective temperature. The observed compositions were: $x = 1$ (O3), $x = 0.77$ (O'3), $0.64 \leq x \leq 0.74$ (P2) and $0.55 \leq x \leq 0.60$ (P'3) and all the compositions showed the ability of Na^+ insertion/extraction (Figure 2.5). XRD analysis indicated that the Na^+ distribution was responsible for the structural changes. More recently, Baster and co-workers (Baster et al., 2015) studied the structures of P2 type ($P6_3/mmc$) $Na_{0.72}CoO_2$ at temperature between -260 to 800 °C and found that thermal expansion differed along a-axis and c-axis. The unit cell parameters exhibited nonlinear dependence on temperature. At the same time, unit cell volume increases linearly for this material above 100 °C, average thermal expansion coefficient equaled to 1.52×10^{-5} ℃ $^{-1}$. But c/a ratio increased significantly up to 400 °C and the changes were somewhat irregular. This behavior can be related to changes in the oxygen stoichiometry. The authors also indicated the redox peaks between 2.0 – 4.0 V vis CV. In order to increase the cycling performance, $Na_{0.6}Ca_{0.7}CoO_2$ was synthesized (Han et al., 2015). The substitution of one Ca^{2+} for two Na^+ helps to contract the unit cell volume without in

University of Malaya

phase (P2), which increased the cycling performance with retained capacity from 109 to74 mAh g^{-1} (0.56 mAh g^{-1} $cycle^{-1}$ for 60 cycles).

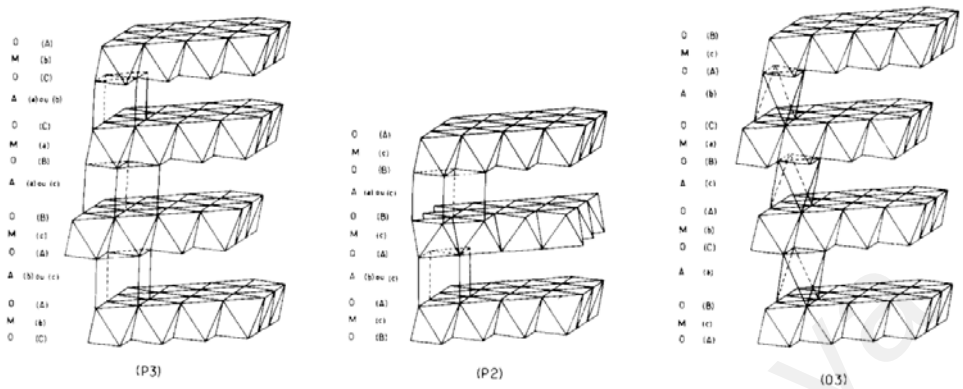

(a)

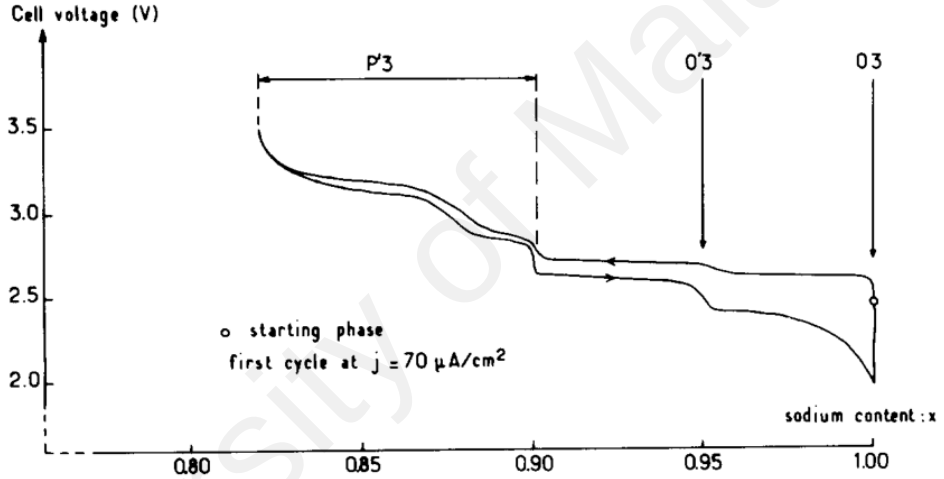

(b)

Figure 2.5: (a)Various types of packing in na_xcoo_2 layered oxides, (b)emf composition curve obtained from $NaCoO_2$ (O3), (c)electrochemical behavior of Na_xCoO_2 phases with P'3, O3 and O'3 packing (d)electrochemical behavior of a P2-type phase (Delmas et al., 1981).

University of Malaya

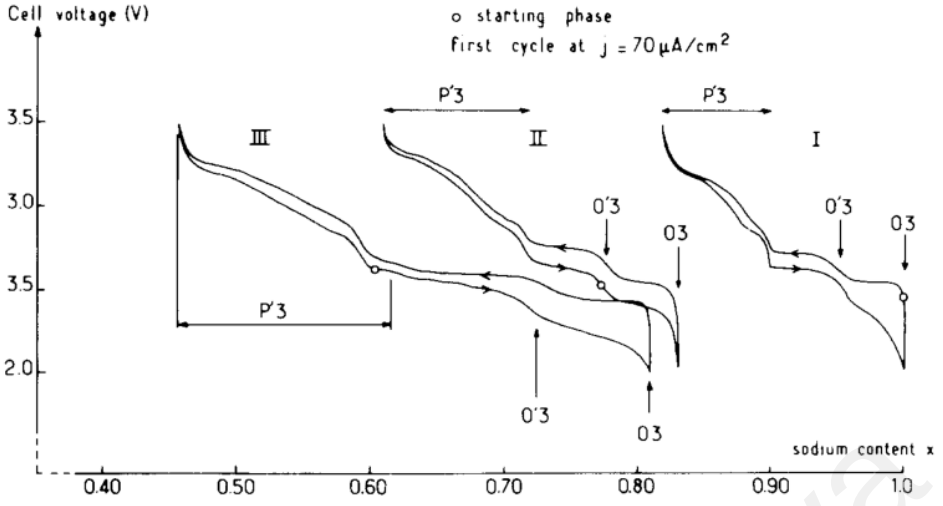

(c)

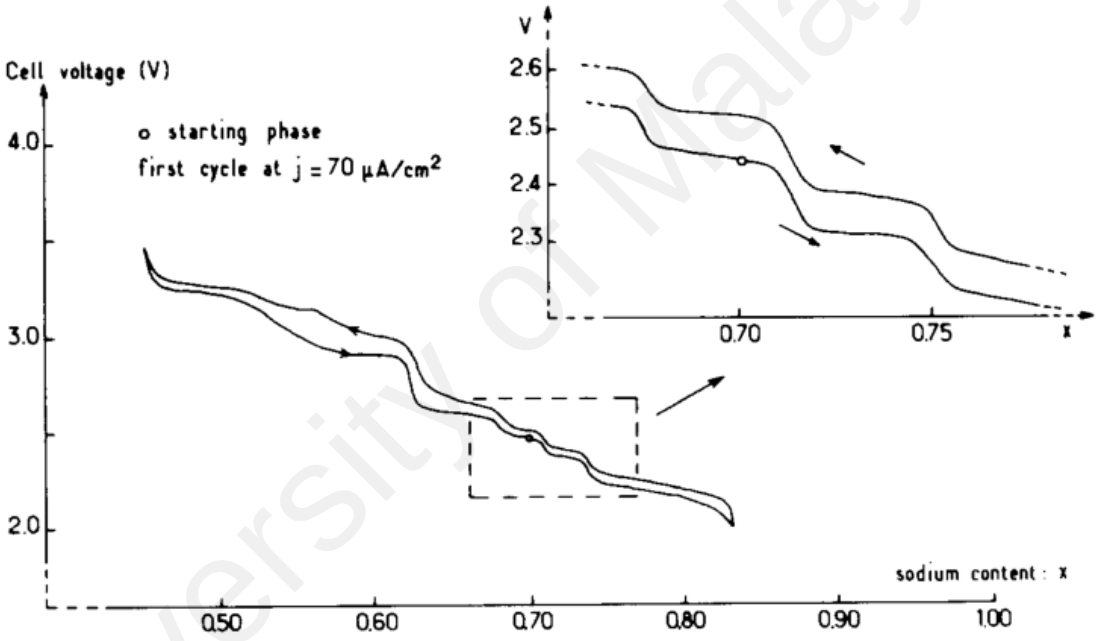

(d)

Figure 2.5, continued.

2.4.1.2 Na_xMnO_2

Mn-based cathode candidate is one of the most popular nanomaterials due to their low cost. There are two typical structures of Mn-based materials for SIBs, tunnel (x = 0 to 0.44) and layer structure ($x > 0.5$) (Parant et al., 1971). In a later report by Mendiboure (Mendiboure et al., 1985), $Na_{0.40}MnO_2$ with tunnel structure, $Na_{0.70}MnO_{2+y}$ with P2

University of Malaya

structure, α-$NaMnO_2$ with O'3 structure and β-$NaMnO_2$ with layer structure (Figure 2.6) were investigated.

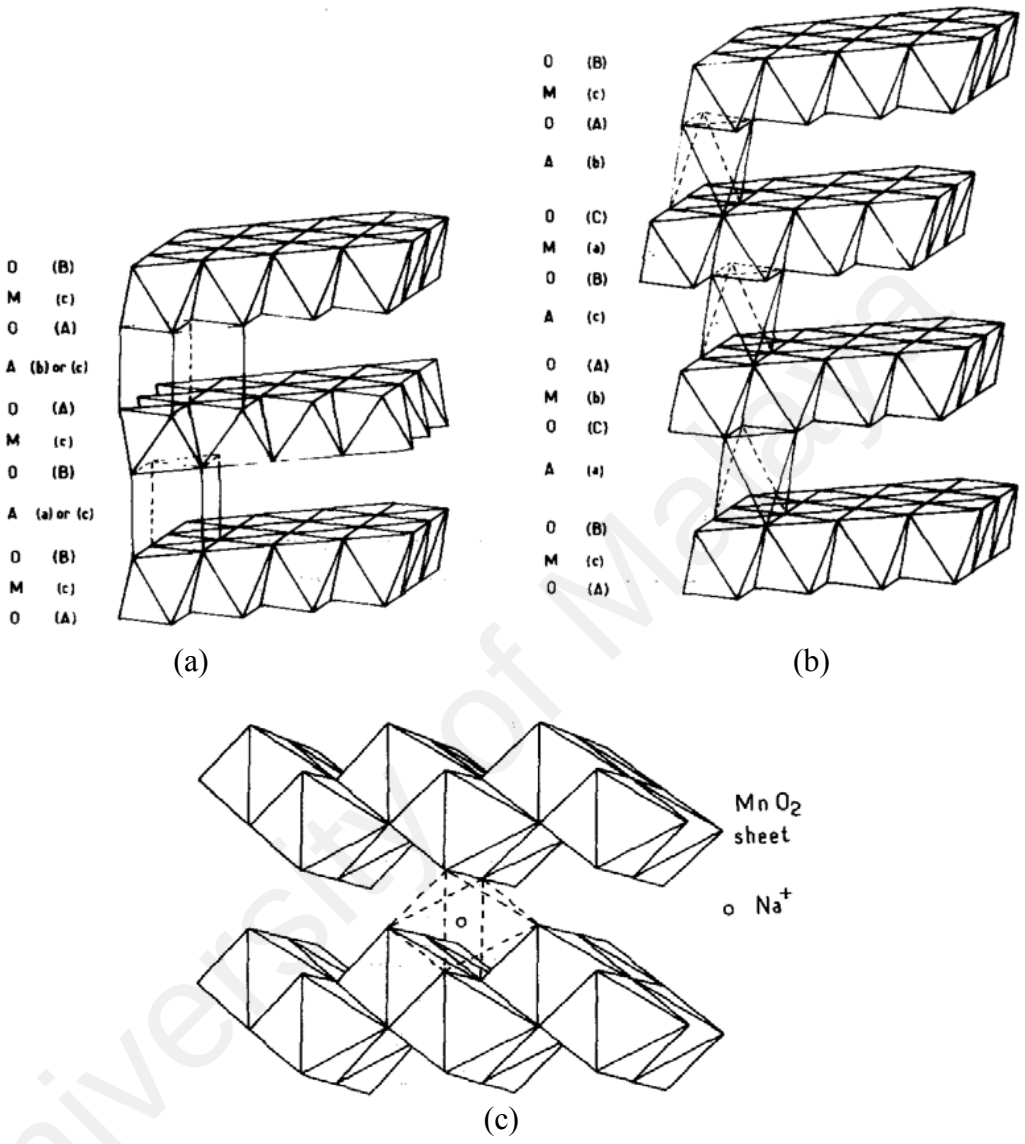

Figure 2.6: (a) $Na_{0.7}MnO_2$(P2), (b) α-$NaMnO_2$ (0'3) structures and (c) β-$NaMnO_2$ structure. O: oxygen, M: manganese, A: sodium (Mendiboure et al., 1985).

The α and β type $NaMnO_2$ have been re-investigated By Su's group (2013). The researchers synthesized the α and β type $NaMnO_2$ nanorods using a hydrothermal method. The α and β type $NaMnO_2$ nanorods delivered the first cycle SC of 278 mAh g^{-1} and 298 mAh g^{-1}, respectively (Su et al., 2013). The β-$NaMnO_2$ has also investigated by Billaud's group (2014). In their report, the β-$NaMnO_2$ material showed a SC of near 190 mAh g^{-1}

University of Malaya

in the 1st cycle and 50 % retention after 100 cycles (Billaud et al., 2014). The cycling performance of both materials are barely satisfactory. Compared to α-$NaMnO_2$, *β*-$NaMnO_2$ showed a better cycling performance due to its compact tunnel structure.

Orthorhombic $Na_{0.44}MnO_2$ is more stable than $NaMnO_2$. Recently, Sauvage's group (Sauvage et al., 2007) studied the mechanism of $Na_{0.44}MnO_2$ and revealed that there were six biphasic transitions during the GCD process. The reversible process is for $0.25 < x < 0.65$ (x is number of Na in each formula) and for irreversible process when values of x is below 0.25. Later, He's group (He et al., 2016) synthesized $Na_{0.44}MnO_2$ nanoplate that exhibited long cycling stability. The nanoplate was synthesized using a template-assisted method. The SC was 108 mAh g^{-1} and reduced by 2.2 % to 105 mAh g^{-1} after 100 cycles. Liu et al (Liu et al., 2017) used a reverse microemulsion method to prepare $Na_{0.44}MnO_2$. The cycling performance was improved., The capacity remained 72.8 mAh g^{-1} over 2000 cycles at 1000 mA g^{-1} (8.3 C). This significant performance provided a new insight of this kind of manganese oxides.

2.4.1.3 Na_xFeO_2

Na_xFeO_2 is a non-toxic and low-cost cathode material for SIBs, because of the abundance and low price of Fe. α-Na_xFeO_2 (O3 type) have been investigated by many researches. The α-Na_xFeO_2 was synthesized (Yabuuchi et al., 2012) via solid-state reaction. The capacity was between 80 - 100 mAh g^{-1} with a plateau voltage profile at ~3.3 V vs. Na/Na^+, but when $x < 0.5$, the electrochemical performance decreased dramatically due to the irreversible structural change, therefore the authors suggested that x should higher than 0.55 to avoid the limitation of the performances. For further understanding the mechanism of the irreversible SC, ex-situ Mössbauer spectroscopy analysis was used to study the instability of Fe^{4+} (Lee et al., 2015) and found that more than 20 % of Fe^{4+} change to Fe^{3+} during the charging process; In addition, the synchrotron

University of Malaya

X-ray diffraction further revealed that there is a new layer phase O″3 when the Na^+ ions were extracting from cathode. The transformation of the structure decreases the reversible SC of α-Na_xFeO_2. Due to this nature, the pure Na_xFeO_2 is hard to get the desired performance, but the substitution of elemental can help to increase the stability of the structure. These kinds of materials will be presented later.

2.4.1.4 Na_xNiO_2

Na_xNiO_2 is one of the earliest researched materials for SIBs application. There is two stable structures of $NaNiO_2$, the O3 structure with a monoclinic structural distortion and a higher temperature rhombohedral structure (Delmas et al., 1994). In a later report (Vassilaras et al., 2013), the authors re-studied the rhombohedral $NaxNiO_2$. At between 1.25 - 3.75 V, 0.63 Na can be extracted and 0.52 Na can be inserted back with a charge specific capacity (CSC) of 147 mAh g^{-1} and the discharge specific capacity (DSC) of 123 mAh g^{-1}; 0.82 Na can be extracted and 0.58 Na can be inserted back with a CSC of 199 mAh g^{-1} and DSC of 147 mAh g^{-1} at between 2.0 - 4.0 V. Compared these two different voltage ranges, the material showed stable cycling performance without significant structural change in a low voltage range, while at the higher voltage range the material showed high SC but unstable cycling performance.

Similar to Na_xFeO_2, Jahn–Teller effect is the main barrier to the application of Na_xNiO_2. Due to this effect, the structure of Na_xNiO_2 changed during GCD process and this unstable change can lead to the increase of irreversible SC. The addition of other transition metals can help to suppress the distortion of the structure.

2.4.1.5 Na_xCrO_2

Na_xCrO_2 has a typical O3 structure. Although it can be used as a cathode candidate for SIBs, the SC is low. Komaba et al. (2009) re-investigated the $NaCrO_2$. Between 2 - 3.5 V, the $NaCrO_2$ showed a DC of about 100 mAh g^{-1} with satisfactory capacity fading

University of Malaya

(Komaba et al., 2009). The $NaCrO_2$ was prepared using a solid-state reaction. They used XRD to investigate the structural transformation and thermal stability (Xia & Dahn, 2012). They found that the final product was ~ $Na_{0.5}CrO_2$ because of the minimal oxygen release. The carbon-coated $NaCrO_2$ using citric acid was investigated (Ding et al., 2012), and compared the product to bare $NaCrO_2$. The $NaCrO_2$ coated by carbon showed a better cycling performance and higher SC, which decrease from 135 mAh g^{-1} to 116 mAh g^{-1} over 40 cycles. This result proved that carbon coating is an effective modified method for electrode materials for SIBs. Recently, O3-type $NaCrO_2$ was synthesized by an emulsion-drying method and was coated carbon using pitch carbon source (Yu et al., 2015). The material delivered a SC of 121 mAh g^{-1} at the current of 20 mA g^{-1} with near 90 % retention after 300 cycles and even maintain 99 mAh g^{-1} at the current density of 16.5 A g^{-1}.

2.4.1.6 Na_xVO_2

Two structures of Na_xVO_2, $NaVO_2$ with O3 structure and $Na_{0.72}VO_2$ with P2 structure were prepared (Onoda, 2008). Both materials can be used as cathode material. $NaVO_2$ and $Na_{0.72}VO_2$ delivered ~120 mAh g^{-1} with 0.5 Na atom insertion (Hamani et al., 2011). Na_xVO_2 with P'3 structure and O'3 structure have been investigated (Delmas et al., 2013; Didier et al., 2011; Guignard et al., 2013; Szajwaj et al., 2009). Although they delivered satisfactory SC (~140 mAh g^{-1}), they did not attract much attention due to the narrow voltage window. In the attempt to investigate the phase transformation in P2- Na_xVO_2, four main single-phase domains were formed for x=1/2, $0.53 \leq x \leq 0.57$, $5/8 \leq x \leq 2/3$, $0.74 \leq x \leq 0.8$ within the $0.5 \leq x \leq 0.9$ range.

2.4.1.7 Multi metal oxide

Multi-metal elemental substitution is the most common method to improve electrochemical performances of a SIB. The element used for multi-metal oxide includes

University of Malaya

Ti, Cr, Mn, Fe, Co and Ni etc. Many researches had been done to explore the eligible ratio and element selection of multi-metal oxide materials for SIBs. The character of Co was to enhance the rate performance and cycling performance (Li et al., 2016). The substitution of Co enlarged the sodium-ion d-spacing diffusion, improved structural stability and enhanced electronic conductivity. Increasing Ni^{+} ion can enhance SC but the rate and cycling performances become poorer. Portion substitution of Mn ion was increased to improve the thermal stability and capacity retention (Hwang et al., 2016).

Similar to Na_xMnO_2, multi Mn oxide is a widely research cathode material for SIBs because of its stable structure, non-toxicity and low-cost. However, the low theoretical SC hiders it becoming a practical cathode material. A stable structure and wide GCD voltage range are the important factors to improve the performance of a battery. Jiang et al. (2015) synthesized a tunnel structure $Na_{0.54}Mn_{0.50}Ti_{0.51}O_2$/C nanorods. This nanorod showed a stable SC of 85 mAh g^{-1}. Liu et al. (2015) obtain a SC of 88.5 mAh g^{-1} for a SIB with P2-$Na_{2/3}Ni_{1/3}Mn_{2/3}O_2$ between 2.0 - 4.0 V. When the voltage range changed from 4.0 V - 4.5 V, the SC raised to 158 mAh g^{-1}. However, the structure of P2-$Na_{2/3}Ni_{1/3}Mn_{2/3}O_2$ is unstable under this voltage range. It changed from P2 to O2 and led to a huge SC fading. Similar to P2-$Na_{2/3}Ni_{1/3}Mn_{2/3}O_2$, the stopped voltage was changed from 4.0 V to 4.2 V, the SC of $Na_x(Fe_{1/2}Mn_{1/2})O_2$ suffered a rapid fading with a series of phase transitions. Thus, a potential range between 2.0 - 4.0 V is suggested (Pang et al., 2015). Chen et al. (2015) synthesized a P3/P2 $Na_{0.66}Co_{0.5}Mn_{0.5}O_2$ and increased the voltage range to 4.3 V, the material exhibited a SC of 156.1 mAh g^{-1} and it still retained more 100 mAh g^{-1} at the current density of 1 C over 100 cycles. Yoshida et al. (2014) used Ti to replace some of the Ni in synthesizing P2-type $Na_{2/3}Ni_{1/3}Mn_{2/3-x}Ti_xO_2$ which showed a SC of 127 mAh g^{-1}. Wang et al. prepared $NaNi_{1/3}Fe_{1/3}Mn_{1/3}O_2$ using a hydroxide co-precipitation reaction to fabricate soft-packed batteries. After 200 cycles, the battery retained about 70 % of the capacity and tend to be stable until 500 cycles. The synthesis

University of Malaya

method and electrochemical performance of this battery is beneficial for industrial production (Wang et al., 2016a). Zhu et al. (2016) synthesized a hierarchical architecture P2-$Na_{0.67}Co_{0.5}Mn_{0.5}O_2$. This hierarchical structure P2-$Na_{0.67}Co_{0.5}Mn_{0.5}O_2$ exhibited good cyclability and delivered a SC of 132 mAh g^{-1} and only very small amount fading (130 mAh g^{-1}) over 100 cycles.

2.4.2 Polyanion Compounds

Like the Li polyanion compounds, Na polyanion compounds have become the most studied materials due to its structural and thermal stabilities (Zhu et al., 2013). However, the insertion/extraction kinetics of Na^+ ions in Na polyanion compounds is different with that of Li, thus the technology and experience of LIBs cannot be transferred to SIBs directly. The general formula of polyanion compounds is $A_xM[(BO_h)^k]_c$, where A is alkali-ion, M is some of transition metal, B is P, S, V or Si etc. At the present, phosphate, pyrophosphate and sulfate are outstanding polyanion compounds materials for SIBs.

2.4.2.1 Phosphate

$NaFePO_4$ is an analogue of $LiFePO_4$, which achieved a satisfactory performance. There are two typical structures of $NaFePO_4$ which are olivine and maricite. By a high-temperature progress, the olivine structure $NaFePO_4$ transformed to the maricite structure $NaFePO_4$ (Figure 2.7). Compared to olivine structure $NaFePO_4$, maricite structure $NaFePO_4$ is more stable. However, the unit structure limits the application of maricite structure $NaFePO_4$. Both of two structures consist of FeO_6 octahedra unit and PO_4 tetrahedra unit. For maricite structure $NaFePO_4$, two FeO_6 octahedra units were connected by the edge and share the corner with near PO_4 tetrahedra unit. This structure makes the path of Na^+ ions narrow. On the contrary, for olivine structure $NaFePO_4$, two FeO_6 octahedra units were connected by the corner and share the edge with near PO_4

University of Malaya

tetrahedra unit. Due to this, there is a spacious and stable path for the movement of Na^+ (Avdeev et al., 2013; Sun et al., 2012).

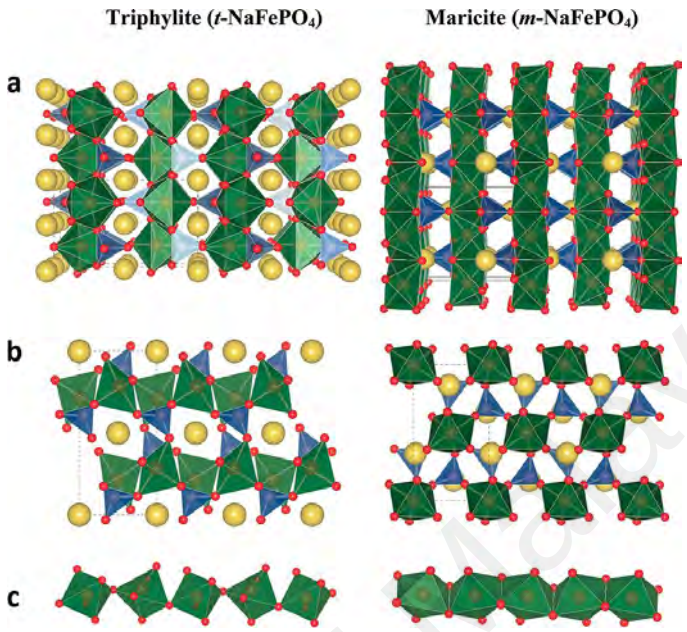

Figure 2.7: Schematic presentation of orthorhombic structured triphylite $NaFePO_4$ (left) and maricite $NaFePO_4$ (right) polymorphs (a and b). (c) Corner-sharing and edge-sharing coordination (Avdeev et al., 2013).

Zhu et al. (2013) compared the electrochemical performances of SIBs using $NaFePO_4$ and LIBs using $LiFePO_4$ as the cathode material. The rate performance and the SC of $NaFePO_4$ is worse than that of $LiFePO_4$ because of the lower Na^+ ions diffusion speed. On the other hand, for cycling performance, $NaFePO_4$ is approximately equal to that of $LiFePO_4$ due to the help of the stable olivine structure. The morphologies were depending on synthesis methods and solvent conditions could influence the electrochemical performances of $LiFePO_4$ (Whiteside et al., 2014).

2.4.2.2 Pyrophosphate

$Na_2FeP_2O_7$, $Na_2MnP_2O_7$ and $Na_2CoP_2O_7$ are the most investigated pyrophosphate (Kim et al., 2016). Barpanda's group (2013) and Kim's group (2013) reported newly this

University of Malaya

pyrophosphate cathode material $Na_2FeP_2O_7$ with a triclinic structure for SIBs almost at the same time and this material delivered a SC of near 80 mAh g^{-1}, which implied pyrophosphate is a suitable cathode candidate for SIBs. Barpanda's group synthesized a series of pyrophosphate analogues including $Na_2MnP_2O_7$, $Na_2CoP_2O_7$ and $Na_{2-x}(Fe_{1-y}Mn_y)P_2O_7$ and then investigated the thermal stability of $Na_2FeP_2O_7$. $Na_2MnP_2O_7$ exhibited a SC of near 80 mAh g^{-1} (Barpanda et al., 2012; Barpanda et al., 2014; Barpanda et al., 2013b). Compared these three pyrophosphate analogues, $Na_2FeP_2O_7$ seems most likely the promising cathode material for SIBs. The thermal stability of $Na_2FeP_2O_7$ was studied by the same group, when the temperature increased to above 560 ℃, the structure turned to ground state monoclinic from triclinic but with decomposition (Barpanda et al., 2013a). Another group studied the operating temperature between 253 K - 363 K of $Na_2FeP_2O_7$ as the cathode material for SIB cell and achieved a stable GCD performance with the SC of about 90 mAh g^{-1} and near 100 % retention over 300 cycles (Chen et al., 2014). Carbon coating is a method to optimize this product. Niu et at. (2015) synthesized $Na_{3.12}Fe_{2.44}(P_2O_7)_2$/multi-walled and tested the electrochemical performance as cathode for SIB half-cell and SIB full-cell, compared to the pure $Na_{3.12}Fe_{2.44}(P_2O_7)_2$, the performance of half-cell which used the $Na_{3.12}Fe_{2.44}(P_2O_7)_2$/multi-walled as the cathode was significantly better than that of bare $Na_{3.12}Fe_{2.44}(P_2O_7)_2$. Furthermore, the full-cell delivered a SC of 145 mAh g^{-1}, but only retained 81 mAh g^{-1} over 50 cycles with the efficiency of 70 % (Niu et al., 2015). Recently this group reported another graphene optimized $Na_{6.24}Fe_{4.88}(P_2O_7)_4$ composite nanofibers using electrospinning method. The SC is ~100 mAh g^{-1} after 320 cycles. Unfortunately, improvement in terms of the efficiency is required (Niu et al., 2016).

University of Malaya

2.4.2.3 Mixed phosphate and pyrophosphate

Mixed phosphate and pyrophosphate were built up by PO_4 tetrahedra and FO_6 octahedra with shared corners. The $Fe_3P_2O_{13}$ groups connected along the a-axis with P_2O_7 groups. Na^+ located in large tunnels. See Figure 2.8 (Kim et al., 2012).

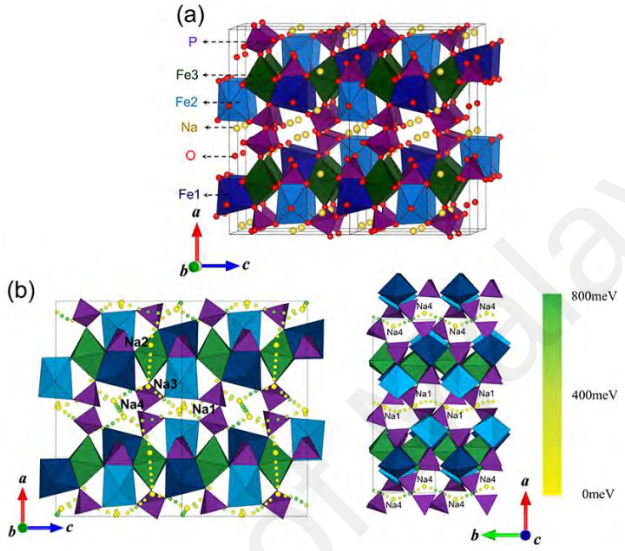

Figure 2.8: (a) Schematic representation and (b) the 3D Na diffusion channel in the $Na_4Fe_3(PO_4)_2(P_2O_7)$ (Kim et al., 2012).

The insertion/extraction of the Na^+ occurred by a single-phase reaction of Fe^{2+}/Fe^{3+} redox reaction and the volumetric change was 4 % (Kim et al., 2013). This small volumetric change can be owing to the open structure of P_2O_7 and make it promising to be an alternative candidate for SIBs cathode. To understand the mechanism of Na^+ migration, the intrinsic defects voltage trends of $Na_4M_3(PO_4)_2P_2O_7$ (M = Fe, Co, Ni, Mn) was investigated by Wood et al (2015) via density functional theory, molecular dynamics and atomistic energy minimization simulations. The activation barrier was 0.20 - 0.24 eV. The diffusion coefficients were 10^{-10} - 10^{-11} cm^2 s^{-1} at 325 K which implied a good rate capability. The metal substitution increased the active voltage and enhanced the energy density (Wood et al., 2015).

University of Malaya

Nose et al. (2013a and 2013b) investigated the $Na_4Co_3(PO_4)_2(P_2O_7)$ and $Na_4Co_{2.4}Mn_{0.3}Ni_{0.3}(PO_4)_2P_2O_7$, respectively. $Na_4Co_3(PO_4)_2(P_2O_7)$ showed a SC of about 95 mAh g^{-1} with a high active voltage of 4.5 V while $Na_4Co_{2.4}Mn_{0.3}Ni_{0.3}(PO_4)_2P_2O_7$ exhibited a SC of about 103 mAh g^{-1} with a high active potential of 4.5 V as well. Co^{2+}, Mn^{2+} and Ni^{2+} ions reacted simultaneously to the charging process and provided a high mixed potential. The higher active potential implies the higher energy density which is an important parameter for SIBs.

2.4.2.4 Fluorophosphates and carbonophosphates

Fluorine can be used as the dopant to increase the operating voltage. Carbon-coating becomes an efficient method to improve the conductivity of materials. Kawabe et al. (2011) synthesized carbon-coated Na_2FePO_4F using ascorbic acid as the carbon source and obtained a SC of 110 mAh g^{-1} with two small polarized voltage plateaus. Langrock et al. (2013) used sucrose (carbon source) to synthesize the carbon-coated porous hollow Na_2FePO_4F with a SC of 89 mAh g^{-1} with 80 % retention after 750 cycles. The electrolyte permeated into the hollow which increased the reaction area and transfer reaction kinetics during GCD and enhanced the electronic conductivity (Langrock et al., 2013).

Chen's group introduced a new compound family which was carbonophosphates with a general formula $A_xM(YO_3)(XO_4)$ (M = redox-active metal, Y = S, P, Si, As, A = Li, Na; X = C, B and x = 1−3) (Chen et al., 2012). Later one of the carbonophosphates ($Na_3MnPO_4CO_3$) was used as SIB cathode material and exhibited a SC of about 125 mAh g^{-1} (Chen et al., 2013).

2.4.2.5 Na-superionic conductor (NASICON, $Na_3V_2(PO_4)_3$)

$Na_3V_2(PO_4)_3$ has a Na-superionic conductor (NASICON) structure built up via VO_6 octahedra corner-sharing with three PO_4 tetrahedrons. Na^+ ions occupy in the tetrahedral sites and octahedral sites as shown in Figure 2.9 (Jian et al., 2012). Lim et al. (2012)

University of Malaya

reported a NASICON type $Na_3V_2(PO_4)_3$ and this material exhibited a SC of 84.8 mAh g^{-1}. This was not a high SC for SIB cathode. To improve the properties of NASICON, Jian' group synthesized carbon-coated $Na_3V_2(PO_4)_3$ and the SC of the as-prepared sample increased to 93 mAh g^{-1}. But the rate performance was not satisfactory.

Saravanan et al. (2013) synthesized porous $Na_3V_2(PO_4)_3$/C using a solution-based method and achieved a satisfactory electrochemical performance. The SC of the $Na_3V_2(PO_4)_3$/C could reach 116 mAh g^{-1} at 1 C and about 90 mAh g^{-1} at 20 C. The SC remained at 90 mAh g^{-1} after 30,000 cycles GCD. Using carbon as the matrix is an effective method for improvement of NASICON performance. By the report of Li's group, different carbon including acetylene carbon nanospheres, carbon nanotubes and graphite nanosheets had been used as matrix for NASICON and the acetylene carbon nanospheres was the best of three matrices, delivering a SC of 117.5 mAh g^{-1} at 0.5 C and 96.4 % SC retention at 5 C over 200 cycling (Li et al., 2014). Acetylene carbon framework provides the 3D pathways for Na and electron transportation, stability for the structure during cycling. Zhu et al. (2017) synthesized another $Na_3V_2(PO_4)_3$ particles embedded in carbon with the SC of 101 mAh g^{-1} and 44 mAh g^{-1} at 1 C and 22 C, respectively. Fang et al. (2015) used a facile mechanically assisted pre-reduction and calcination method for synthesis of crystallized $Na_3V_2(PO_4)_3$ particle and achieved a SC of 115 mAh g^{-1}. This SC is near theoretical SC, the authors attribute this to hierarchical carbon framework and interconnected nanofibers. Rui et al. (2015) synthesized carbon coated $Na_3V_2(PO_4)_3$ in the porous graphene framework by a feasible freeze-drying-assisted method and showed a good rate SC of 115 mAh g^{-1}, specifically. Liu et al. (2016) synthesized core/double-shell structure $Na_3V_2(PO_4)_3@C_D$ with a SC 116 mAh g^{-1}. Li et al. (2017) synthesized double carbon-wrapped $Na_3V_2(PO_4)_3$ composite by rheological phase method and showed a SC of 99.8 mAh g^{-1}.

University of Malaya

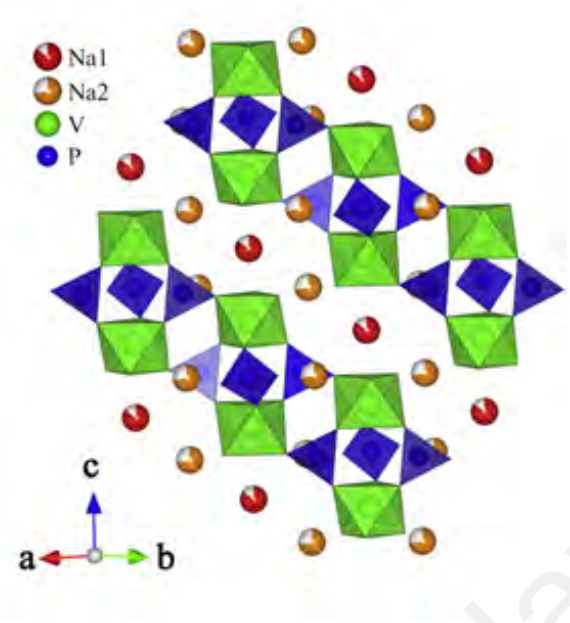

Figure 2.9: Structure of $Na_3V_2(PO_4)_3$ (Jian et al., 2012).

This carbon network plays multiple roles, such as enhance the material's conductivity. It provides sufficient conducting pathways, acts as the barriers to prevent particle aggregation and functions as a frame scaffold to buffer large volume strains (Wang et al., 2017). Element doped NASICON is another useful method to improve the material performance. N-doping can change the disorder and graphitic character of the carbon layer, strongly impact the overall performance of the $Na_3V_2(PO_4)_3$. The appropriate amount of N-doping can decrease voltage hysteresis, improved capacity and superior cycling stability with higher redox kinetic and lower solid-electrolyte interface film resistance (Zhang et al., 2017). Liang et al. (2017) synthesized the $Na_3V_2(PO_4)_3$ nanoparticles, the sulfur and nitrogen co-doped carbon layer can improve the electron transport and shorten Na^+ diffusion paths, resulting in the ideal electrochemical reaction kinetics. Xiao et al. (2018) used folic acid to synthesize a series of $Na_3V_2(PO_4)_3$/N doped carbon composites and tested the electrochemical properties. The best carbon-nitrogen ratio was 3.3 wt % with a SC of 95 mAh g^{-1} over 3000 cycles.

University of Malaya

2.4.2.6 Sulfate

Compared to $(PO_4)_3$, $(SO_4)_2$ group has lower ionic conductivity. Mason et al. (2014) suggested that iron (III) sulfate ($Fe_2(SO_4)_3$) can be applied as a SIBs cathode material. $Fe_2(SO_4)_3$ group by corner-sharing tetrahedra SO_4 and octahedra FeO_6 with a theoretical SC of 134 mAh g^{-1} due to 2 Na^+ ion insertion/extraction but the experimental SC of $Fe_2(SO_4)_3$ only exhibited 65 mAh g^{-1}. Barpanda et al. (2014) presented an alluaudite-type $Na_2Fe_2(SO_4)_3$ which exhibited a SC of near 102 mAh g^{-1}. Based on alluaudite-type $Na_2Fe_2(SO_4)_3$, Wong et al. (2015) investigated the migration of Na^+ ion in monoclinic $Na_{2+\delta}Fe_{2-\delta/2}(SO_4)_3$ by classical molecular dynamics, bond-valence site energy modelling and density functional theory simulations. The room temperature conductivity of this alluaudite-type $Na_2Fe_2(SO_4)_3$ is 2×10^{-7} S cm^1.

2.4.3 Organic Compounds

The organic compounds and polymer can be used as both the anode and cathode materials for SIBs, but in here we only introduce the part for the cathode.

The research of organic compound and polymer cathode materials for SIBs are still at the preliminary stage. The compounds including carboxylates, anhydrides, imide and quinone compound had been investigated (Hwang et al., 2017; Skundin et al., 2018). Most of them can be obtained from nature or synthesized by the natural products in a mild synthesized condition, which simplifies undoubtedly the process of synthesis and lowers the cost. However, many challenges need to be overcome. For example, organic compounds can be only dissolved in the electrolyte which consists of another organic solvent. Secondly, most of organic compounds are insulators, hence limiting the rate performance. Although the theoretical SC of organic compounds and polymer is quite high, the experimental SC is low. The redox voltage also limited the energy density of

University of Malaya

the cathode materials. Due to this, such cathode materials have not been investigated extensively.

Wang's group reported an organic salt of 2,5-dihydroxyterephthalic acid as cathode and anode for SIBs. Two Na^+ ions can be inserted/extracted by 2,5-dihydroxyterephthalic acid and 2,5-dihydroxyterephthalic acid showed a SC of about 180 mAh g^{-1} between 1.6 - 2.8 V vs 0.1 - 1.8 V (Wang et al., 2014). For anhydrides, perylene 3,4,9,10-tetracarboxylic dianhydride exhibited a SC of 150 mAh g^{-1} with 2 Na^+ accommodation. 15 Na^+ ions can be inserted/extracted to the material with the discharge cut-off voltage of 0.01 V, (Luo et al., 2014). Monomer imide cannot be served as the cathode for SIBs because it can dissolve in the organic electrolytes. Hence diimide and poly-imide can overcome this issue. Perylene diimide has a π-conjugated structure and two Na^+ ions can be inserted/extracted per molecular unit. It showed a SC of 140 mAh g^{-1} with 90 % SC retention after 300 cycles.

Chihara et al. (2013) studied the properties of $Na_2C_6O_6$ which can show the SC of 170 mAh g^{-1}. On increasing the voltage to 3.2 V, the compound started to dissolve in the electrolyte and suffered a fast SC fading. Later, Yu's group (2016) prepared different morphologies (micro-bulk, microrod, and nanorod) $Na_2C_6O_6$ and their performances were investigated. Among the $Na_2C_6O_6$ with different morphologies, $Na_2C_6O_6$ nanorod delivered the best performance whit the SC of near 190 mAh g^{-1} and 90 % retention over 100 cycles. In order to understand the GCD mechanisms of $Na_2C_6O_6$, Yamashita et al. (2016) used first-principles calculations and evolutionary algorithm to predict the structural transition during GCD. In the latest report by Lee at al. (2017), a four Na^+ ion insertion/extraction $Na_2C_6O_6$ has been studied with a SC of 484 mAh g^{-1} by controlling the particle size and using diethylene glycol dimethyl ether.

University of Malaya

2.4.4 Polymers

Pure polymer cannot apply as the electrode active material for SIBs due to their insulativity (no conductivity), but after p-doping/n-doping, it becomes possible to be the electrode for SIBs. This review only discusses the p-doping polymers as a suitable cathode for SIBs. Compared to organic compounds, polymers are insoluble in organic electrolyte due to their long carbon chain.

Although the polymers solubility in the electrolyte is better than organic compounds, other performances such as the SC, cycling stability and average voltage must be improved. Sulfonyl-based polyimide showed a SC of about 122 mAh g^{-1} at a low average voltage of 2.0 V (Xu et al., 2016). Anthraquinone-based polyimide showed a better SC of 190 mAh g^{-1} with a retention of 180 mAh g^{-1} after 150 cycles (Xu et al., 2015). Su et al. (2015) synthesized a polypyrrole hollow nanosphere, it showed a higher average voltage of about 3.0 V. But the SC is not quite high which is 100 mAh g^{-1} and 70 % specific retention over 1000 cycles. Another high voltage material is Na-rich poly(diphenylaminesulfonic acid sodium) as reported by Shen et al. (2014). It can reach 3.4 V and about 100 mAh g^{-1}. A sulfonated polyaniline was synthesized by Zhou et al. (Zhou et al., 2015), this $–SO_3Na$ withdrawn enhance the high Na density and electron-withdrawing ability and showed a SC of 133 mAh g^{-1} and 96.7 % SC remained over 200 cycles.

2.5 Prussian Blue (PB) and its Analogues

PB become the popular material only a few years ago, as reported by Wessells et al. (2011) and Lu et al. (2012). Buser et al. (1977) reported the structure of PB, as a three-dimension network with the formula $AxMM'(CN)_6$ (A = K, Na, M and M′ = Co, Fe, Mn, Ni. The open-framework structure of PB make it a potential cathode for SIBs. As shown in Figure 2.10, Fe(II) and Fe(III) are bridged by linear (C≡N) group. The C≡N bond opens

University of Malaya

the faces of the elementary cubes, which can help Na^+ ions to move easily in the body-center positions. The whole unit is a cubic structure. Due to this unique structure, the movement of Na^+ ion will be fast and stable (Lu et al., 2012).

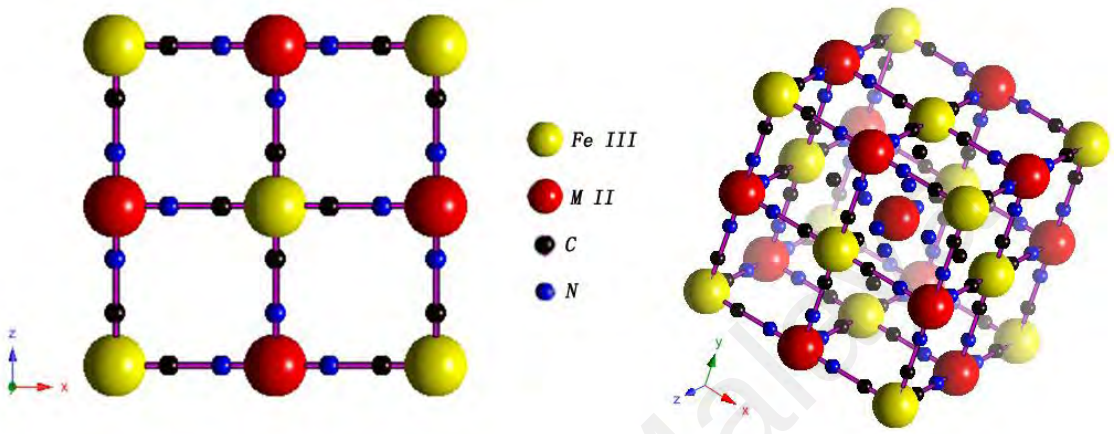

Figure 2.10: 3D structure of PB.

2.5.1 $Na_xFeFe(CN)_6$

$Na_xFeFe(CN)_6$ is a typical compound of hexacyanometalates family named PB. The major issues of PB are the high interstitial water and the high vacancies rate. Controlling the purity and the crystalline can improve the performance of PB. Qian's group synthesized $Na_4Fe(CN)_6$/C, a nanomaterial that showed a near theoretical SC of 90 mAh g^{-1}. It was low because only one electron is redox during GCD process (Qian et al., 2012). Later Qian's group optimized the method to prepare a single crystal $FeFe(CN)_6$, two pairs of redox couple were detected and increased the SC to 120 mAh g^{-1} and 87 % retention after 500 cycles (Wu et al., 2013). This group also used the $NaSO_4$ as the electrolyte to obtain a SC of 125 mAh g^{-1} and 83 % retention over 500 cycles (Wu et al., 2015). You et al. (2014) reported $Na_{0.61}Fe[Fe(CN)_6]_{0.94}\square_{0.06}$ using a single iron source method to synthesize ($\square$ is the vacancies rate). The interstitial water and vacancies rate were low and achieved high performance SC of 170 mAh g^{-1} at a rate of 0.15 C. Unfortunately,

University of Malaya

when the current density was increased to 0.3 C, the SC decreased quickly. In that report, the authors also compared the PB prepared by mixing $[Fe(CN)_6]^{4-}$ and Fe^{3+} vs PB using single iron source method. They concluded that the $[Fe(CN)_6]$ vacancies in PB crystal lattice may prevent the diffusion of electrons along the C≡N framework. In addition, the interstitial water may occupy the interstitial sites and thus inhibit Na^+ diffusion. Li et al. (2015) synthesized different Na^+ content PB to study the influence of Na^+ content to SIBs. The study showed that the Na^+ insertion to the PB structure was enhanced with the decrease of interstitial water and vacancies and improved the cycling performance and columbic efficiency.

2.5.2 $Na_xCoFe(CN)_6$

The substitution of Co element can offer another active site for hexacyanometalates. By studying $Na_xCo[Fe(CN)_6]_{0.90}\cdot 2.9H_2O$, prepared by Takachi and co-workers (2013), the voltage plateaus were located at 3.8 V and 3.4 V corresponding to Co and Fe with a SC of 135 mAh g^{-1}. But this material suffers high capacity fading. Yuan's group reported a $Na_2Co_3[Fe(CN)_6]_2$ nanomaterial which can be applied as LIBs cathode as well and exhibited an acceptable performance (Yuan et al., 2016). Wu et al. (2016) presented $Na_2CoFe(CN)_6$ and obtained a capacity of near 150 mAh g^{-1} and about 90 % SC retention over 200 cycles. The success of this material can be ascribed to the high crystalline and purity of the product.

2.5.3 $Na_xFeMn(CN)_6$

Manganese, one of the low-cost transition metal element, was investigated as the M element for PB. It exhibited an unnegligible performance. Song et al. (2015) dried the $Na_2MnFe(CN)_6\cdot zH_2O$ two methods, under air-dried and vacuum dried to investigate the influence of interstitial water. They found that the product dried at a vacuum environment contained less interstitial water with a better electrochemical performance (150 mAh g^{-1}

University of Malaya

for vacuum dried vs 135 mAh g^{-1} for air dried) and smooth GCD curve. The $Na_2MnFe(CN)_6 \cdot zH_2O$ with less interstitial water showed a smaller volume change and cooperative distortion during GCD (Song et al., 2015; Wang et al., 2015). Cui's group presented a monoclinic $Na_2Mn^{II}[Mn^{II}(CN)_6]$ with a $P2_1/n$ space group. The material showed a four-state-reaction as:

$$\begin{array}{lll} \mathbf{Na_3Mn^{II}[Mn^{I}(CN)_6]} & \Leftrightarrow & \mathbf{Na_2Mn^{II}[Mn^{II}(CN)_6]} \Leftrightarrow \\ \text{monoclinic space group } P2_1 & & \text{monoclinic space group } P2_{1/n} \end{array}$$

$$\begin{array}{lll} \mathbf{Na_1Mn^{II}[Mn^{III}(CN)_6]} & \Leftrightarrow & \mathbf{Na_0Mn^{III}[Mn^{III}(CN)_6]} \\ \text{orthorhombic space group } P222_1 & & \text{cubic space group Fm-3m} \end{array} \quad (2.1)$$

Corresponding the phase of monoclinic space group $P2_1$, monoclinic space group $P2_{1/n}$, orthorhombic space group $P222_1$, cubic space group Fm-3m, respectively. With the four-state-reaction, the material showed a SC of ~209 mAh g^{-1} for about 70 mAh g^{-1} each state (Lee et al., 2014).

2.5.4 Mixed Metal Hexacyanometalates

Ni^{2+} ion is an electrochemically inert metal for SIBs, but the addition of Ni^{2+} ion can serve as the structure support site for PB. Chen et al (2016) used Ni^{2+} ion to substitute some of the Mn^{2+} of $Na_2Mn_2Fe(CN)_6$. The $Na_2Ni_xMn_yFe(CN)_6$ exhibited a better cycling performance with a SC of 150 mAh g^{-1} over 400 cycles. Jiang et al. (2016) synthesized a PB@C composite, the synergistic effect of C and PB resulted in a superior electron conductivity of the composite with a SC of 90 mAh g^{-1} at 90 C and 90 % SC retention over 2000 cycles GCD (Figure 2.11 shows the crystal structure.).

University of Malaya

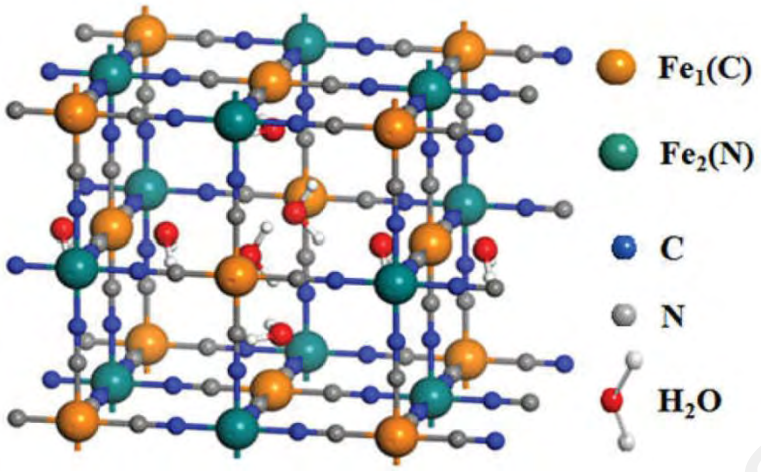

Figure 2.11: Crystal structure with Fe[s]

2.6 Summary

- This chapter briefs the development of SIBs. The GCD mechanism of the SIBs is similar to that of LIBs.
- Some typical anode materials are reviewed by the morphology properties and its' respective electrochemical performance of SIBs.
- The cathode materials are surveyed in great length including all the recent development of SIBs.
- An independent section for PB is presented. This section expounds the insertion/extraction mechanism of Na^+ in PB and the morphology of various PB.

University of Malaya

CHAPTER 3: EXPERMENTAL METHODS

3.1 Introduction

In this chapter, three sections will be included, the synthesis method of PB, characterizations of PB and electrochemical testing of SIBs using as-prepared PB as cathode material.

In the first section, the conventional synthesis methods of PB will be presented. In this work, the aim is to synthesize pure, low interstitial water and low vacancies PB by a facile one step single iron source solution-precipitation method. A single iron source is used to avoid the mixing of another element. The synthesis was carried out at room-temperature with very low reaction rate in order to reduce the interstitial water and vacancies of PB.

The second section is the characterization methods of PB. In this section, a series of characterization methods including element analysis, EDX, TGA, XRD, HRTEM, FESEM and XPS will be presented.

The final section of this chapter overs the electrochemical characterizations of SIBs. In this section, CV, EIS, GCD will be used for studying the electrochemical performances of SIBs using as-prepared PB as cathode material.

3.2 Synthesis of PB

3.2.1 Conventional Method

The conventional method to synthesize PB as pigment was using $FeCl_3$ and $K_4[Fe(CN)_6]$ in an acid environmental solution. The obtained blue color precipitation is PB. However, the PB synthesized by this method had high interstitial water rate and vacancies rate, the electrochemical performance was every low, thus it could not be applied as SIBs cathode material.

University of Malaya

A facile method to synthesize low interstitial water and low vacancies rate PB was employed in this work. In the following section, solution-precipitation method will be introduced.

3.2.2 Solution-precipitation Method

In solution-precipitation method, the precipitation process was started by adding the precipitator to the metal ion solution. After few rounds of washing or filtration, the insoluble pure precipitate was obtained. The obtained precipitate was vacuum dried to desorb moisture.

The advantages of the method are listed below:

1. Low reaction temperature.
2. Smaller and more uniform particles.
3. Easy preparation and operation.
4. Low-cost.

PB powder is shown in Figure 3.1 and Figure 3.2 shows the schematic diagram of the procedure. 100 ml 0.1M HCl was prepared which was marked as solution A. In the second step, the ascorbic acid was added to A, which was then marked as solution B. The third step was adding the polyvinyl pyrrolidone (PVP) to B slowly under magnetic stirring. This was marked as solution C. The fourth step was adding the $Na_4Fe(CN)_6$ to C, magnetic stirring for 24 h and then standing for another 24 h. A faint yellow solution was obtained with blue powder precipitate at the bottom of the beaker. The faint yellow solution was then sucked out and distilled water/ethanol were added for washing. After few times of washing, the precipitate emerged as a suspension. The suspension was transferred to the centrifuge tubes. After centrifugation, the supernatant liquid that overlie on top was removed and new distilled water/ethanol was added. After few rounds of

University of Malaya

centrifugation, the supernatant liquid became transparent. The precipitate was finally kept in the vacuum oven for 24 h.

When the $Na_4Fe(CN)_6$ was in an acid environment, $Fe(CN)_6^{4-}$ decomposed and produced Fe^{2+}. Some Fe^{2+} was then oxidized to Fe^{3+}. Fe^{2+} and Fe^{+3} reacted with the remaining $Fe(CN)_6^{4-}$ to form blue precipitate. The addition of PVP and ascorbic acid were used as the chelating agents to slow down the reaction rate so that a low defect product was formed.

Figure 3.1: Photograph of PB.

University of Malaya

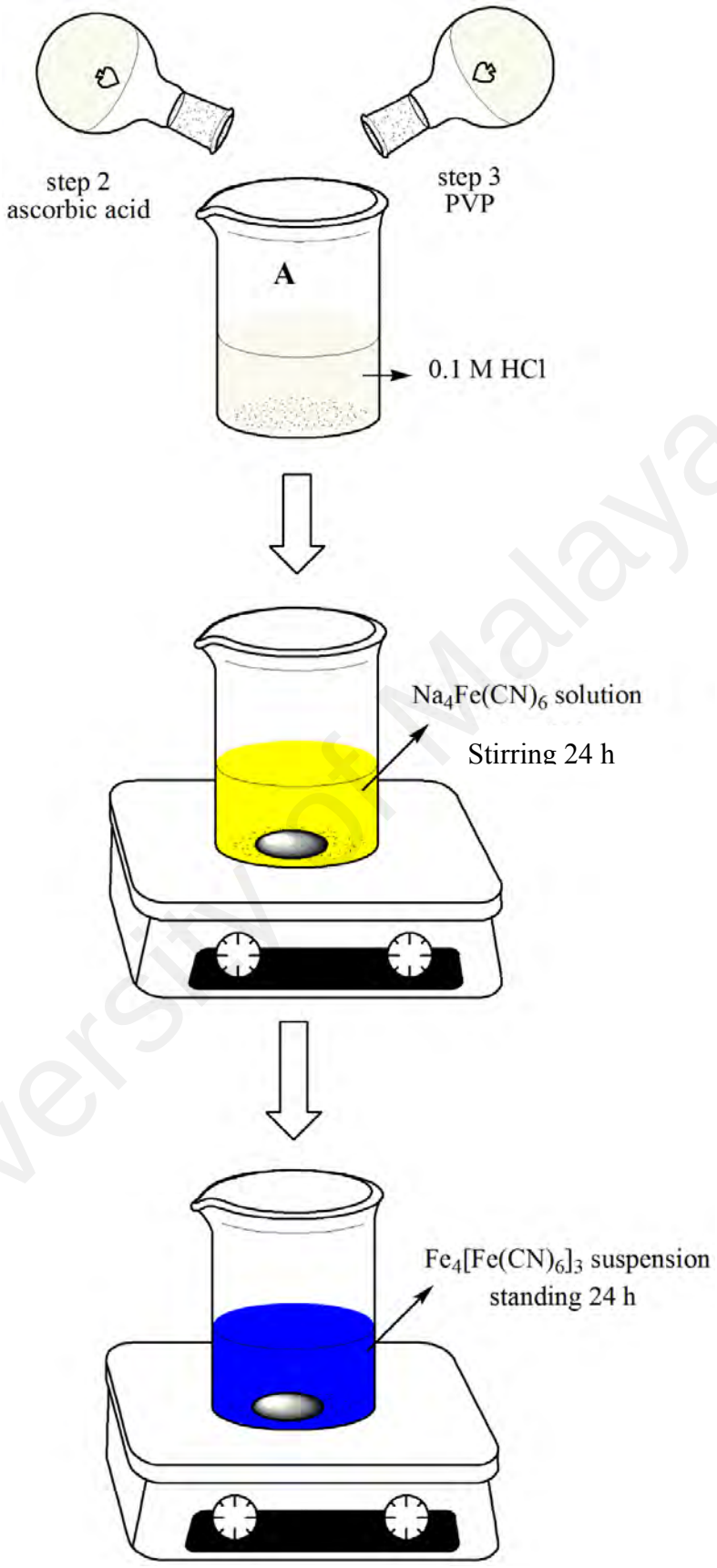

Figure 3.2: Schematic diagram of the precipitation procedure.

University of Malaya

3.3 Characterizations of PB

3.3.1 Elemental Analysis

Elemental analysis is the method to analyze carbon, hydrogen and nitrogen element contents of composites. Briefly, the sample is hold in a tin capsule and burned in a high temperature. Then the emission gases are detected by gas chromatography to confirm the content of C, H and N of each sample.

In this work, CHNS/O 2400 Series II was used to analyze the C, H, N elements content of the as-prepared PB. The sample was combusted with O_2 in a tin capsule at a high temperature. The produced NO_2, CO_2 and H_2O gas were absorbed by different reagents and analyzed using temperature programmed desorption.

3.3.2 Thermogravimetric Analysis (TGA)

In this work, TGA was used for thermal characterization. TGA is the method to investigate the thermal stability of the material by recording the weight change in a series of temperature.

The material was hold by a precise balance in a closed chamber under inert gas. The material was heated until a set temperature and decompose. The loss of weight was detected by the balance to plot the TGA curve.

In this work, TGA was carried out using TGA-Q500. The measurement of mass was acquired from 50 ℃ to 800 ℃ at a heating rate of 50 ℃ per minute under N_2 flow.

3.3.3 X-ray diffraction (XRD)

The transition of inner - layer electron under the bombardment of high-speed moving electron produces the light radiation (X-ray). Crystals is used as X-ray grating, and the coherence scattering of the particles will interfere with the interference of light, so that the scattered x-rays intensity is increasing or decreasing. Due to the superposition of a lot

University of Malaya

of particles scattered wave, the beams with the highest intensity produced by interference are called XRD lines.

XRD is a method to study the lattice structure of materials. Each material has their unique XRD pattern. In this work, the XRD data was collected using the Olympus Innov in-Xitu BTX-II, with Cu Kα radiation (wavelength, λ=1.54056Å, 2θ from 5 to 50°). The results were compared with the standard PDF card of PB (JCPDS No. 52-1907) to study the structure.

The lattice parameters of each sample were calculated by

$$\alpha = \frac{\lambda}{2\theta\sqrt{h^2 + k^2 + l^2}} \tag{3.1}$$

Where α is lattice parameter, θ is diffraction angle, λ is incident wavelength, (h, k, l) is Miller index.

3.3.4 High Resolution Transmission Electron Microscope (HRTEM) and Field Emission Scanning Electron Microscope (FESEM)

HRTEM images were recorded using JEOL JEM-2100F. From these images, the particle size of the PB crystals is estimated.

In order to determine the compositional element and vacancies of the product, elemental analysis and EDX were carried out using JEOL JEM-2100F. C, H, N were determined by CHNS/O 2400 Series II element analysis and the contents of Na and Fe are carried out using EDX.

3.3.5 X-ray Photoelectron Spectroscopy (XPS)

The principle of XPS is to radiate the sample with x-rays so that the inner electrons or valence electrons of an atom or molecule are excited out. The photons excite electrons which are called photoelectrons. The energies of photoelectrons are recorded. The binding

University of Malaya

energies of photoelectron are obtained via recording the kinetic energy/binding energy of photoelectron as the horizontal axis. The relative strength is to be the vertical axis.

In this work, XPS (ESCALB 250Xi) was used to determine the different valence states irons.

3.4 Electrochemical Characterization of SIBs

3.4.1 The Preparation of Cell

In this work, the cathode material is the research focus. Thus, a half-cell, sodium metal | separator | PB cell was assembled to avoid the influence by anode, especially carbon anode. The working electrode was prepared by mixing polyvinylidene fluoride (PVDF) (10 wt %), PB (80 wt %) and Super P (10 wt %). After mixing all the mentioned materials in N-methyl-2-pyrrolidone (NMP) and stirring for 24 h, a dark slurry was obtained, which was coated onto an aluminium foil as thinly as possible and vacuum dried at 60 ℃ for another 24 h to eliminate residual solvent. The working PB electrode was cut into a circular piece of diameter 1.2 cm which can be fitted into a coin cell. The electrode mass density was about 2 mg cm^{-2} excluding aluminium foil active material, PVDF and Super P. The electrolyte includes 1.0 M sodium hexafluorophosphate ($NaPF_6$) in ethylene carbonate (EC): propylene carbonate (PC) with 5 % fluoroethylene carbonate (FEC). There are two kinds of solvent, which are EC: PC (1: 1 volume ratio) and EC: PC: FEC (49: 49: 1 volume ratio). The fabrication of half-cell was carried out in a glove-box filled up with Ar gas, where both oxygen and moisture levels were below 1 ppm. The separator was glass fiber filter and counter electrode was sodium foil. The fabrication of SIB cell is following Figure 3.3.

University of Malaya

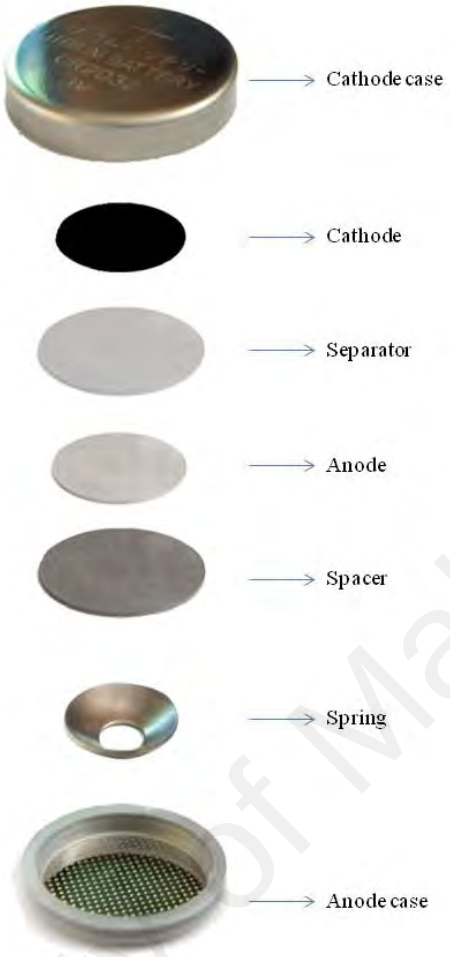

Figure 3.3: Fabrication of SIB cell.

3.4.2 Cyclic Voltammetry (CV)

The cyclic voltammetry (CV) is a method for electrochemistry. The potential of the electrode is controlled at a serious of current rates and re-scans the electrode using a triangular waveform over time. In a voltage range, a potential-current curve is obtained.

According to the trend of the curve, the degree of reversibility between electrodes or electrolyte reaction and the properties of coupling reaction can be investigated. It is

University of Malaya

usually used to be a method for the electrode chemical reaction parameters, to determine the control steps and to understand the reaction mechanism.

In a batteries system, CV is usually carried out to determine the redox peaks and polarization level. In this work, CV was carried out using Autolab. The testing voltage range is between 2.0 - 4.0 V under 0.1 mV s^{-1}.

3.4.3 Electrochemical Impedance Spectroscopy (EIS)

EIS is a frequency domain measurement made by applying a sinusoidal perturbation, often a voltage, to a system. The impedance at a given frequency is related to processes occurring at timescales of the inverse frequency. EIS is a method to study the interface reaction between electrode and electrolyte. From the EIS results, the kinetic of system can be obtained.

In a classical battery system, Nyquist plot shows two semicircles and a radial line. As shown in Figure 3.4, R_s is the ohmic resistance of the system. The first semicircle presents the ions transportation process through the solid electrolyte interphase (SEI). Second semicircle presents the transportation of charges while the radial line presents the diffusion of ions inside the active materials.

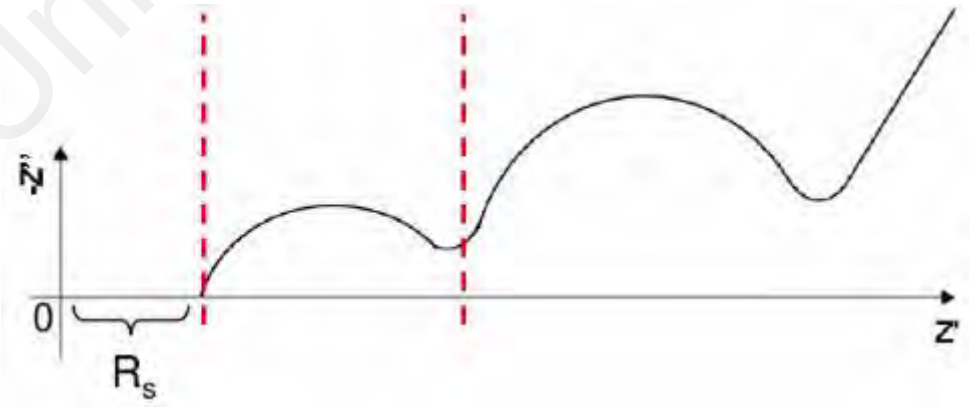

Figure 3.4: Classical Nyquist plot.

University of Malaya

In an open circuit situation, a different frequency sinusoidal signals are added to the half-cell and the resistance corresponding to the frequency can be detected. The results can help to analyze the kinetics of the batteries system during the GCD. The EIS measurement is recorded in the frequency between 0.1 - 100 kHz.The Diffusion coefficient D can be calculated by

$$D = \frac{R^2T^2}{2A^2n^4F^4C^2\sigma^2} \tag{3.2}$$

$$Z_{re} = R_s + R_{ct} + \sigma\omega^{1/2} \tag{3.3}$$

Where, n is the amount of transfer electron during the redox process, F is faraday constant, R is gas constant, A is the superficial area of the electrode, D is diffusion coefficient of Na^+, C is sodium ionic concentration, T is absolute temperature, σ is Warburg coefficient. Z_{re} is real impedance, Rs is the internal resistance (subscript s from solution), ω is angular frequency, Rct is charge transfer resistance (Li et al., 2014). From the equation above, σ^2 is inversely proportional to diffusion coefficient D at the same other conditions.

3.4.4 Galvanostatic Charge/Discharge (GCD)

To investigate the rechargeable performance, Galvanostatic charge/discharge (GCD) is carried out. Base on the redox peaks of CV, an initial potential and final potential are set. Within this potential range, a constant positive current is applied to the batteries and stop once the potential reaches the final value. In reverse direction, a negative current is used to the batteries until the battery's potential changes to a set value. The GCD process will be repeated as long as the specific capacity (SC) remains 80 %.

The rate performance and cycling performance are the main parameters to measure the property of the batteries. The results of GCD are collected by Neware charge-discharge

University of Malaya

machine. The measurements of the fabricated half-cells are performed in a voltage range between 2.0 - 3.6 V or 2.0 - 3.8 V vs. Na^+/Na under different C at room temperature.

Firstly, the cell will be GCD at a current of 0.1 C, 0.2 C, 0.3 C from the voltage between 2.0 V - 3.6 V. At the same time, another half-cell is GCD in the same current but in a different voltage range (2.0 V - 4.0 V). This is due to the observation of two redox pairs in CV curve. Two different voltage ranges are to investigate the SC given by two different active spots, respectively. After rate performance, the half-cell is GCD at the current of 2 C for more than 200 cycles in a voltage range between 2.0 - 4.0 V.

The current 2 C is the current when the half-cell charges from start voltage to stop voltage or discharge from stop voltage to start voltage within 0.5 h under the theoretical SC. The SC is calculated by

$$C_{Specific} = \frac{C}{m} \tag{3.4}$$

Where, $C_{specific}$ is SC, C is capacity, m is the active material mass. The mass of active material is 80 % of the mass of electrode material.

University of Malaya

CHAPTER 4: CHARACTERIZATIONS OF PB

4.1 Introduction

In this chapter, the crystal structure and chemical composition of the product were studied using elemental analysis, energy dispersive X-Ray spectroscopy (EDX), thermogravimetric analysis (TGA), X-ray diffraction (XRD), high resolution transmission electron microscope (HRTEM), field emission scanning electron microscope (FESEM) and X-ray photoelectron spectroscopy (XPS).

4.1.1 Elemental Analysis and Energy Dispersive X-Ray Spectroscopy (EDX)

The general molecular formula of PB is written as Na_xFe^{III} $[Fe^{II}(CN)_6]_y\square_{1-y}\cdot nH_2O$ with $\square$ represents $[Fe^{II}(CN)_6]$ vacancies in the structure, x, y, n are stoichiometric coefficients representing the amount of Na, $[Fe^{II}(CN)_6]$ and H_2O, respectively, per unit PB crystal. For example, Na_2Fe^{III} $[Fe^{II}(CN)_6]_{0.9}\square_{0.1}\cdot 3H_2O$, means in this PB, there are two Na atoms, one Fe^{III} atom, 0.9 $[Fe^{II}(CN)_6]$ molecule, 0.1 vacancies and three H_2O per unit PB crystal. Vacancies here mean the defects of $[Fe^{II}(CN)_6]$ in the PB crystal. If there is no vacancy, the formula should be $Na_2Fe^{III}Fe^{II}(CN)_6\cdot 3H_2O$. According to the report by Song's group (Song et al., 2015), high vacancies were associated with instability of crystal structure and eventually resulting poor batteries performance. In this work, a low vacancies PB is aimed because it may improve the overall performance of PB to be cathode material for SIBs. n refers to the interstitial water content. A low value of n is aimed because the interstitial water may react with electrolyte limiting the electrochemical performance of PB. Further discussion will be presented in later chapter.

To determine all the element content of the prepared PB, EDX is used to determine the Na and Fe contents while elemental analysis is used to determine C, H, N elements and XPS is used to determine the valence of Fe (Fe^{II} and Fe^{III}). Table 4.1 shows part of

University of Malaya

element ratio of as-prepared PB. In here, the concentration ratio of O is not available but its' content could be estimated from the relationship with atom H of H_2O.

Table 4.1: The element ratio of as-prepared PB.

	Na	**Fe^{III}**	**Fe^{II}**	**C**	**N**	**H**
Concentration ratio	4.12	17.28	16.16	21.18	23.66	1.05
Mole ratio (concentration ratio/molar mass)	0.179	0.309	0.289	1.765	1.690	1.05

The concentration ratio is divided by atomic weight of each element to obtain the mole ratio. The prepared PB is written according to $Na_xFe^{III}[Fe^{II}(CN)_6]_y\square_{1-y}\cdot nH_2O$. As such, the real formula of PB is determined as $Na_{0.179}Fe^{III}_{0.309}[Fe^{II}(CN)_6]_{0.289}\square_{0.711}\cdot 0.525H_2O$. Then, the mole ratio of PB is simplified by normalising Fe^{III} mole ratio to 1. All the subscripts are divided by 0.309 to obtain $Na_{0.58}Fe^{III}[Fe^{II}(CN)_6]_{0.93}\square_{0.07}\cdot 1.67H_2O$. As a result, a low vacancy (0.07) and low interstitial water (1.67) PB product is obtained and therefore it is expected to obtain good SIBs performance in Chapter 5.

4.1.2 Thermogravimetric Analysis (TGA)

Refer to Figure 4.1, the TGA curves of the as-prepared PB present the weight-loss process. In the range of 50 ℃ < T < 225 ℃, around 3 % of weight loss is detected and can be ascribed to the loss of adsorbed and interstitial water (Song et al., 2015). Low interstitial water content was reported to contribute high sodium storage during GCD

University of Malaya

process (Wu et al., 2016). Therefore, it is expected that an excellent overall performance and good SC of SIBs in the GCD process will be demonstrated in Chapter 5.

At 345 ℃, a sharp decrease of weight loss is observed and can be ascribed to the decomposition of PB framework. From this temperature, the C≡N molecular bond starts to open up and decompose. The decomposition process ends at 420 ℃. This means that PB has wide operating temperature range and can withstand high temperature before decompose. The mass of residue (C, Fe and Na composite) after 445 ℃ is about 57.4 % which matches well to the weight ratio of C, Fe and Na in Table 4.1.

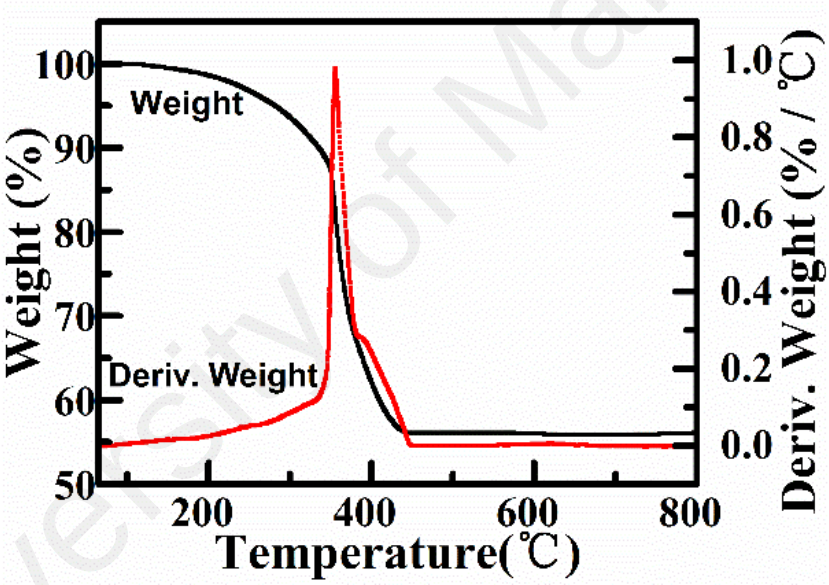

Figure 4.1: TGA and DTG curve of as-prepared PB under N_2 flow.

4.1.3 X-ray Diffraction (XRD)

To further study the structure of as-prepared PB, XRD was carried out. The XRD result of the PB is shown in Figure 4.2. The XRD result was compared with the standard XRD pattern of PB (JCPDS No. 52-1907). The peaks of the as-prepared PB are similar to the standard XRD diffraction pattern of PB. From the XRD results, PB can be indexed to the face-center-cubic structure. The main peaks at 2θ 17.45°, 24.70°, 35.20°, 39.45°, 43.45°,

University of Malaya

50.50°, 53.80° correspond to the lattice planes of (200), (220), (400), (420), (422), (440), (600), respectively. These peaks are sharp and well define. There is no other weak peak in the XRD result indicating the purity of the as-prepared PB. The lattice constant of as-prepared PB is calculated as 10.19Å. This result indicates that the as-prepared PB has a well-defined and highly pure crystal structure.

This nearly perfect cubic structure should help to improve the batteries performance due to the stable structure. A stable structure is a basic feature of an electrode material because the structure space (tunnel) is used for insertion/extraction of Na^+. If the structure is unstable and would collapse, the ability of Na storage is lost which lead to the SIB capacity fading.

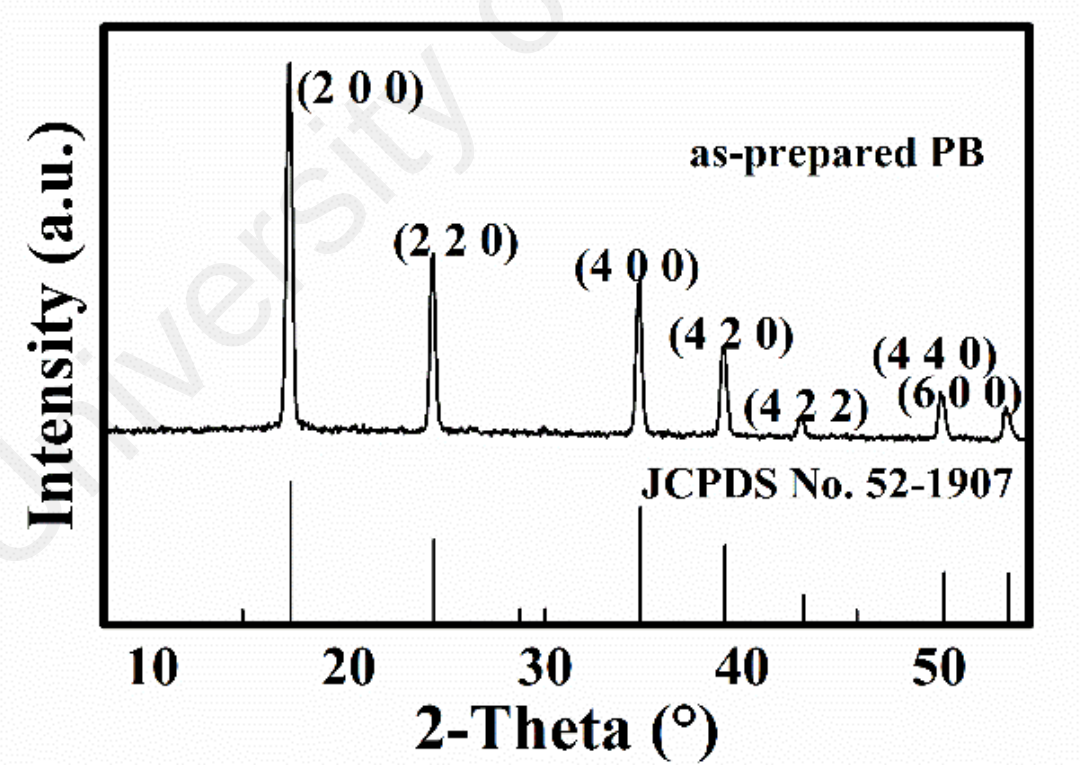

(a)

Figure 4.2: (a) XRD curves and (b) Grating diffraction of the as-prepared PB.

University of Malaya

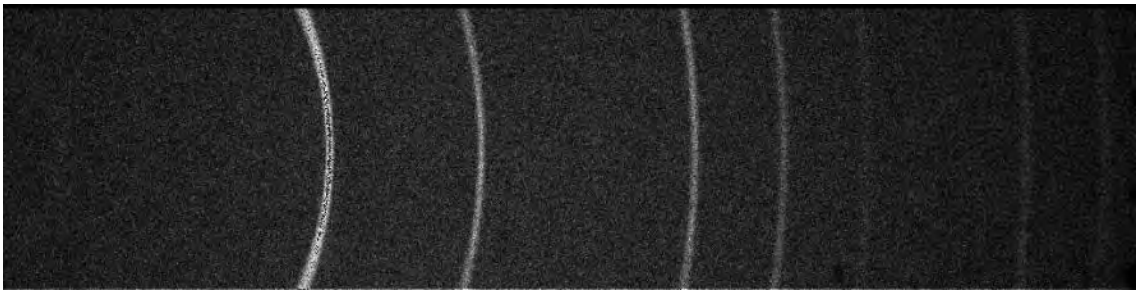

(b)

Figure 4.2, Continued.

4.1.4 High Resolution Transmission Electron Microscope (HRTEM) and Field Emission Scanning Electron Microscope (FESEM)

The synthesized schematic figure of PB is shown in Figure 4.3. As shown in Figure 4.3, there are 3 steps in the formation of PB: First of all, the $Na_4[Fe(CN)_6]$ will dissolve in an acid environment to Na, Fe^{2+} and $(CN)_6$ where Fe^{2+} will then be oxidized to Fe^{3+}, forming a yellow solution. In the second step, Fe^{3+}, Fe^{2+} and $(CN)_6$ will interact to form PB and the solution becomes light blue. In the last step, the solution becomes dark blue which means the $Na_4[Fe(CN)_6]$ have all reacted to PB.

University of Malaya

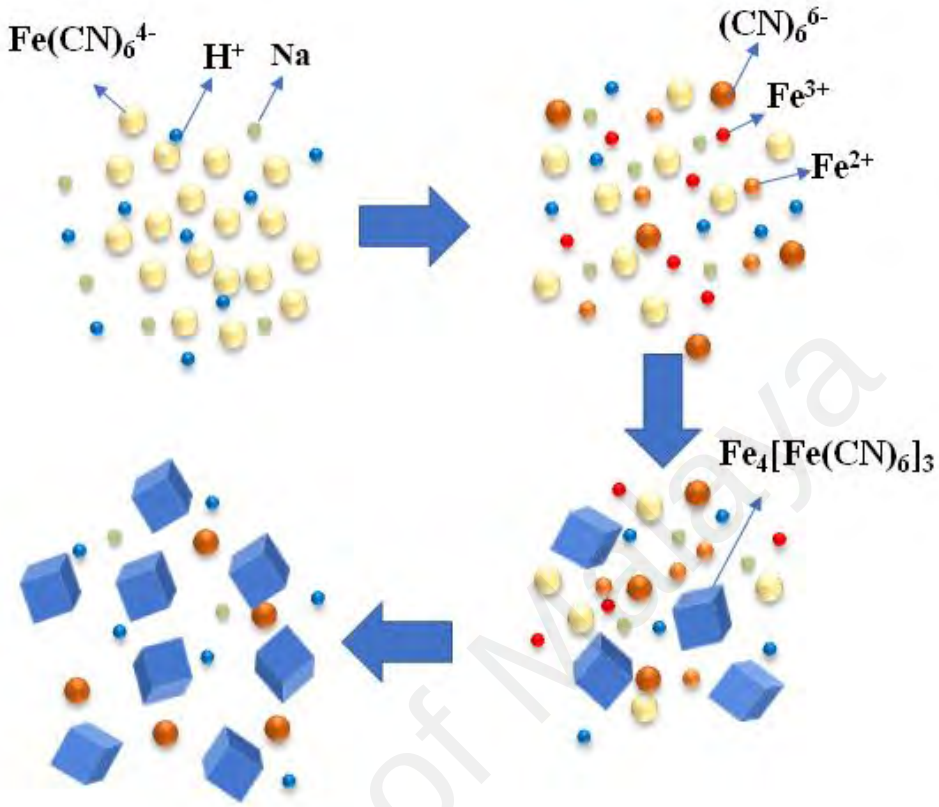

Figure 4.3: The synthesized schematic of PB.

The main issue that hinders the electrochemical performance of PB as SIB cathode material is the interstitial water content and the defects. Water will react with the electrolyte and decompose during the GCD process. One of the decomposed product, O_2 can oxidize the electrolytes and electrode materials. In order to prevent high content of interstitial water and high crystal defect, PVP and CA are added as the chelating agents in the synthesize process. Furthermore, the synthesize process is allowed to go through slow reaction rate at room temperature.

Figure 4.4 (a-f) show the FESEM and HRTEM images of the as-prepared PB. According to the TEM and SEM images, the size of as-prepared PB particles is between 0.4 μm - 1 μm. The crystals of the as-prepared PB in Fig. 4.4 (a) show near perfect cubic

University of Malaya

structure with 575 nm width. Therefore, it is expected that the as-prepared PB has minimum crystal defect and the vacancies inside the crystal lattice should be significantly low.

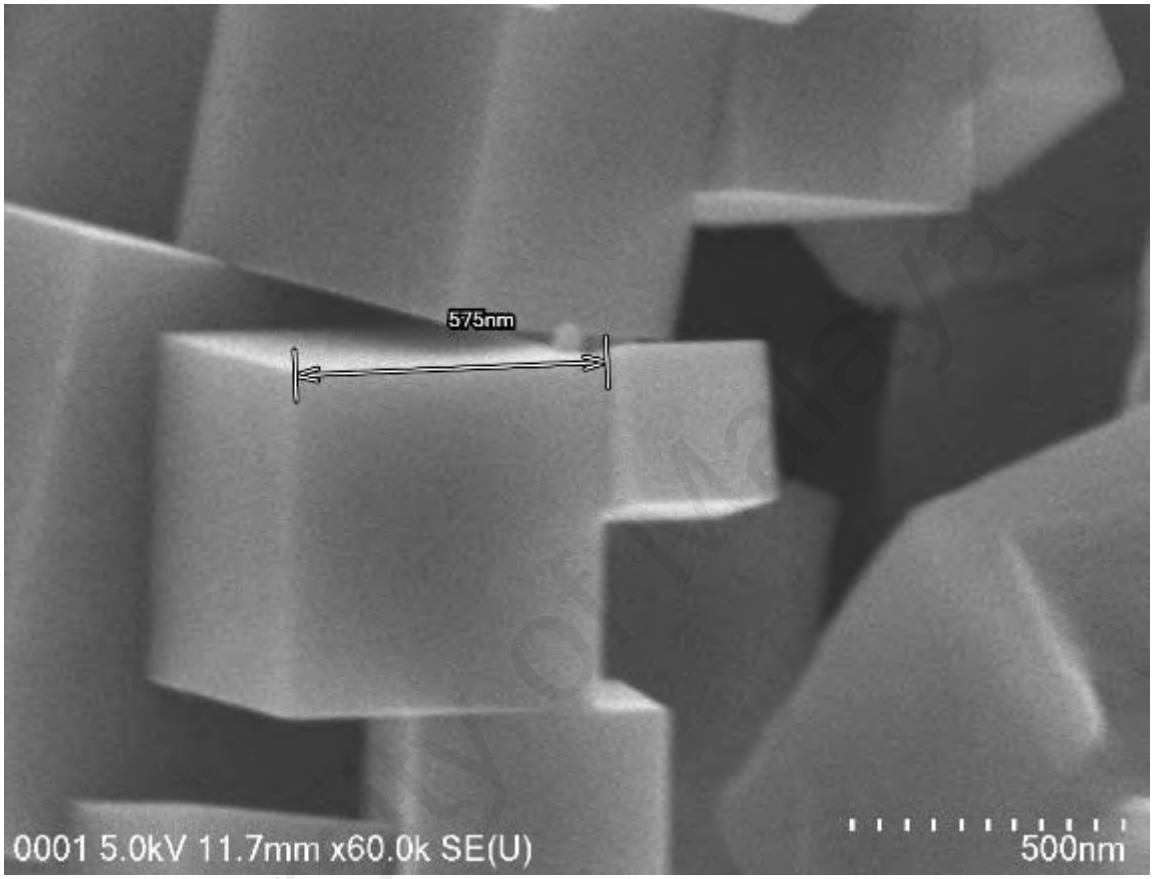

(a)

Figure 4.4: (a) and (b) FESEM images at different magnification and (c) EDX elemental analysis and (d), (e) and (f) HRTEM images at different magnification of as-prepared PB.

University of Malaya

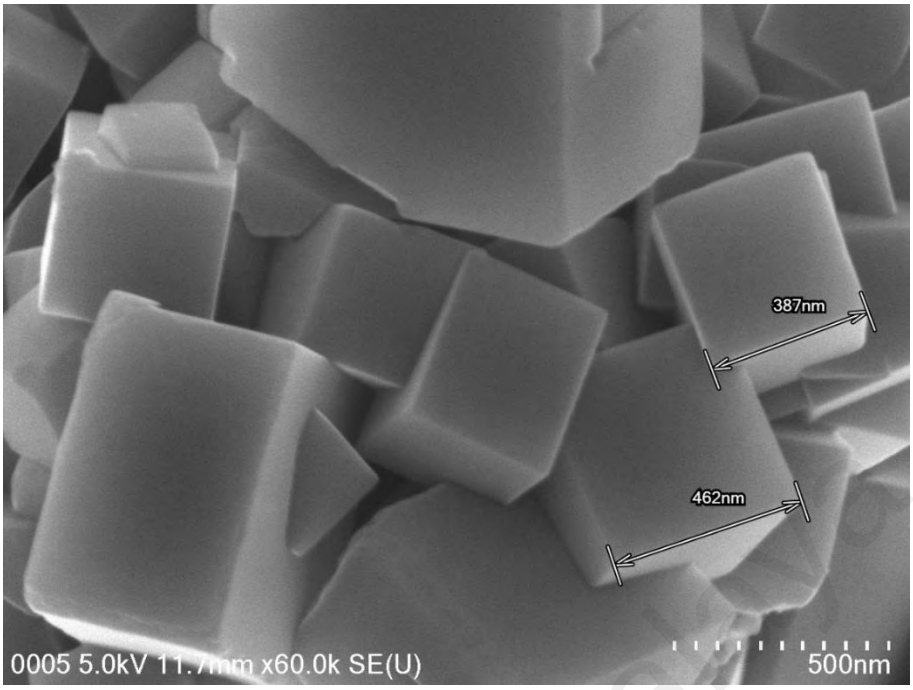

(b)

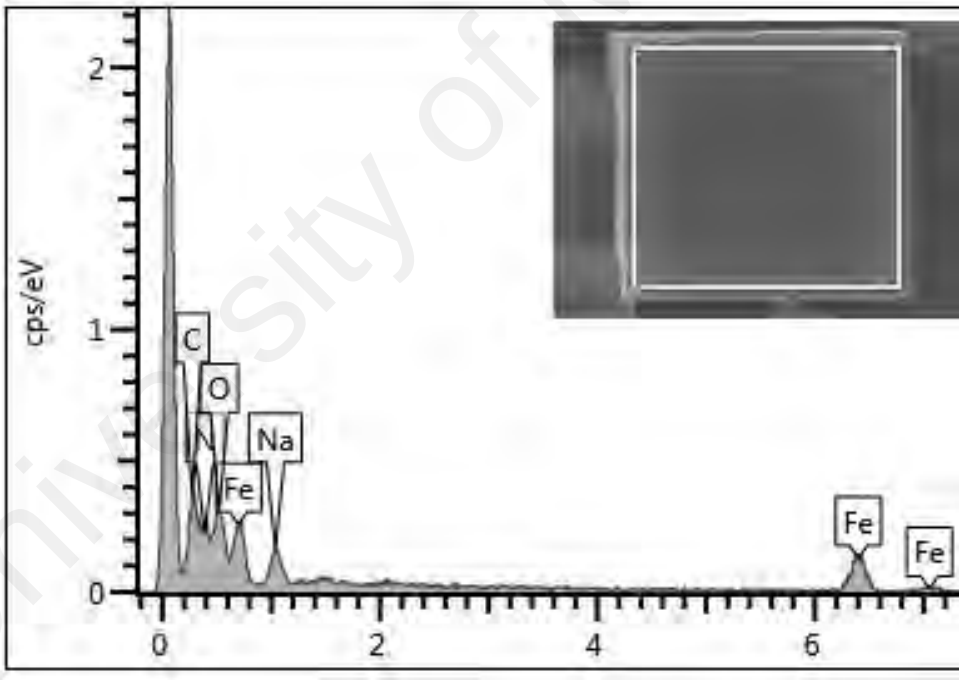

(c)

Figure 4.4, continued.

University of Malaya

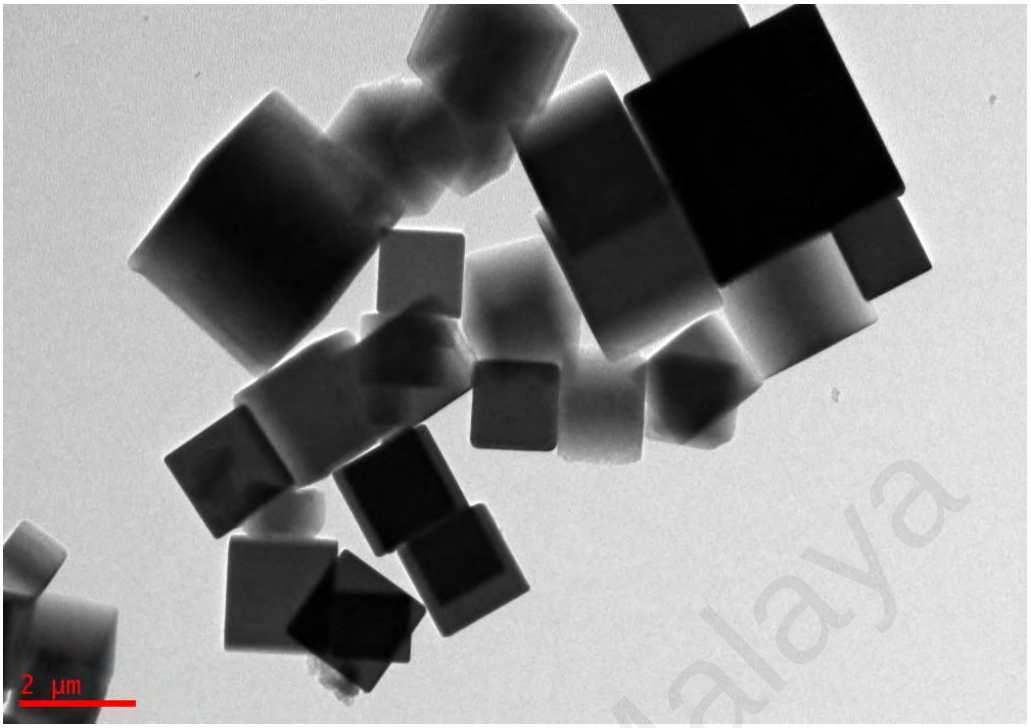

(d)

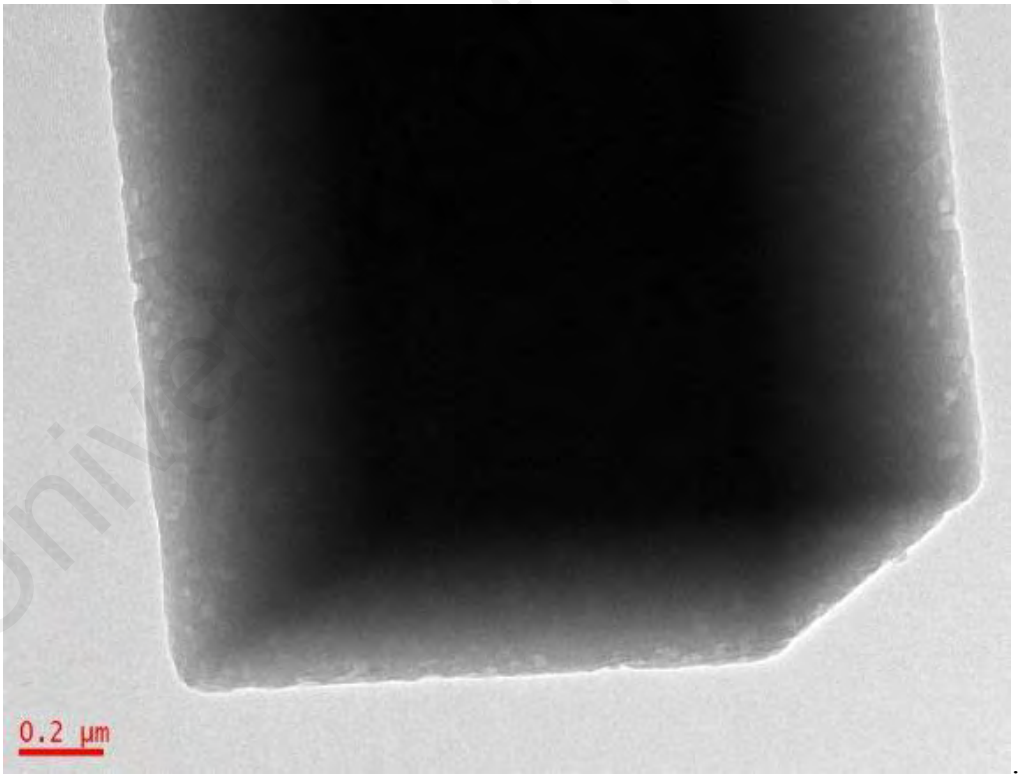

(e)

Figure 4.4, continued.

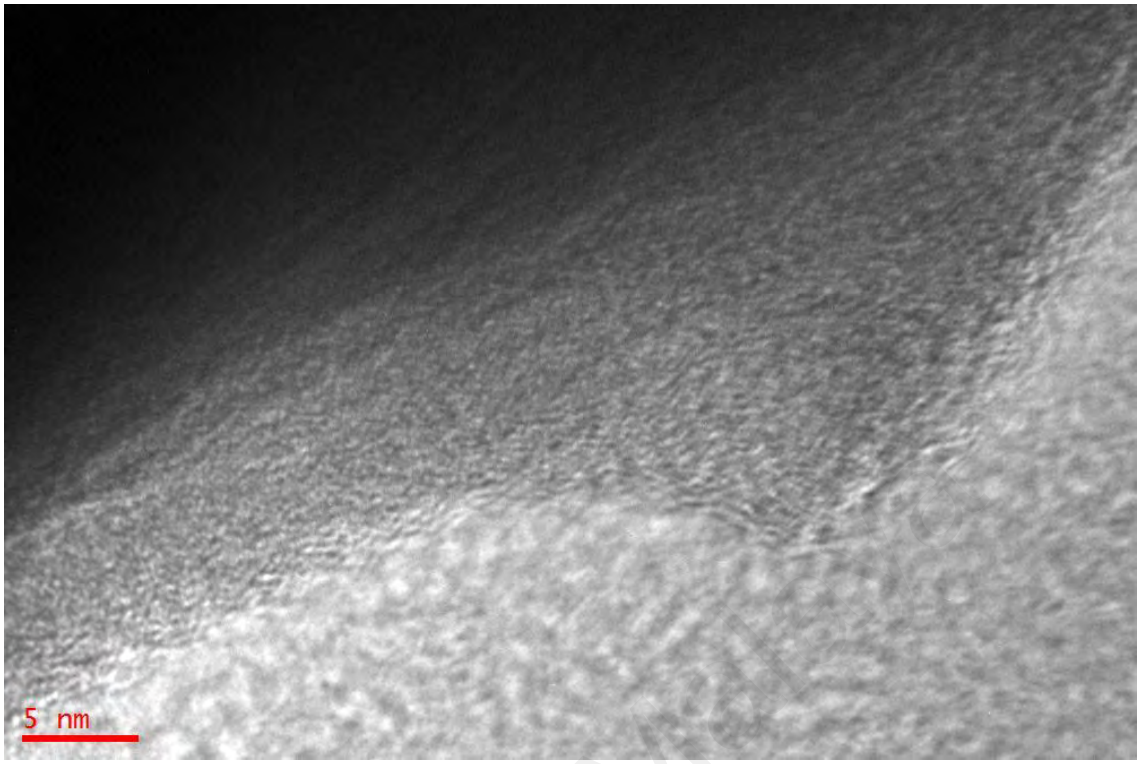

(f)

Figure 4.4, continued.

The EDX elemental result is shown in Figure 4.4(c). The elementary composition of the PB are Na, Fe, C, N and O. This indicates that the PB particles are not blended with other impurities which is in good agreement with XRD, demonstrating high purity of the particles.

4.1.5 X-ray Photoelectron Spectroscopy (XPS)

To confirm the different valence of Fe, X-ray photoelectron spectroscopy (XPS) testing was studied to determine the two valences of Fe ion. Figure 4.5 shows the XPS spectra of as-prepared PB from 0 eV to 1400 eV. The element includes C, N, Fe and Na. The peaks at 284.35 eV, 397.39 eV, 708.15 eV and 1070.82 eV correspond to C1s, N1s, Fe2p and Na1s, respectively. The binding energy of each element are shown in Table 4.2.

University of Malaya

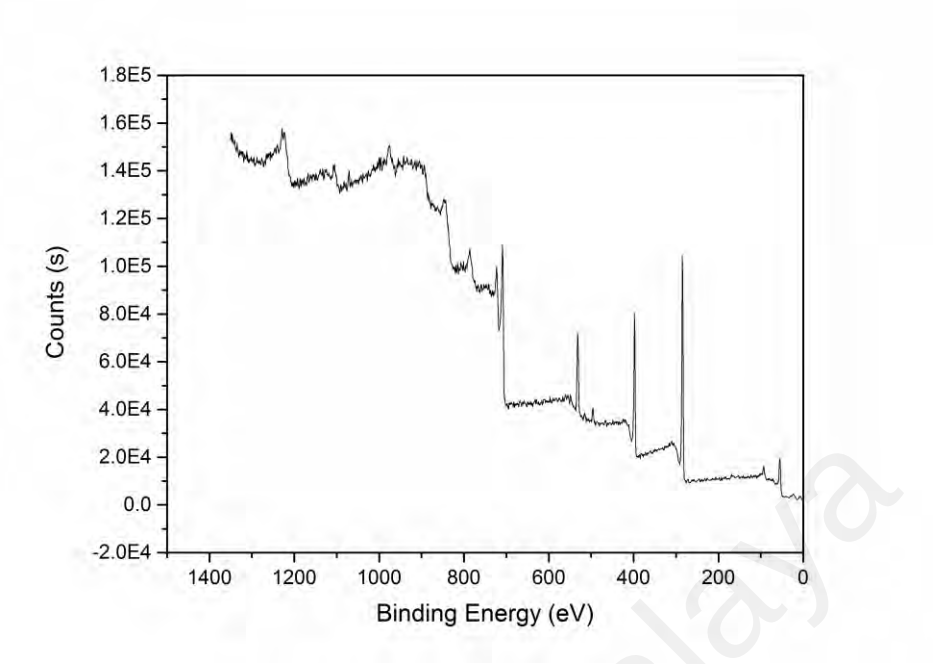

Figure 4.5: XPS spectra of as-prepared PB between 0 – 1400 eV

Table 4.2: Binding energy of C1s, N1s, Fe2p and Na1s.

Name	Start binding energy (eV)	End binding energy (eV)	Peak binding energy (eV)
C1s	297.98	279.18	284.35
N1s	410.03	392.13	397.39
Fe2p	739.98	700.18	708.15
Na1s	1079.03	1062.13	1070.82

In this work, only Fe ions have more than one valence. The enlarge XPS spectra of Fe are shown in Figure. 4.6. Two steps of data processing need to be carried out which are background correction and spectra deconvolution. Refer to Figure 4.6, the experimental XPS raw data of Fe spectra is shown as red line while the background spectrum is shown as black line.

University of Malaya

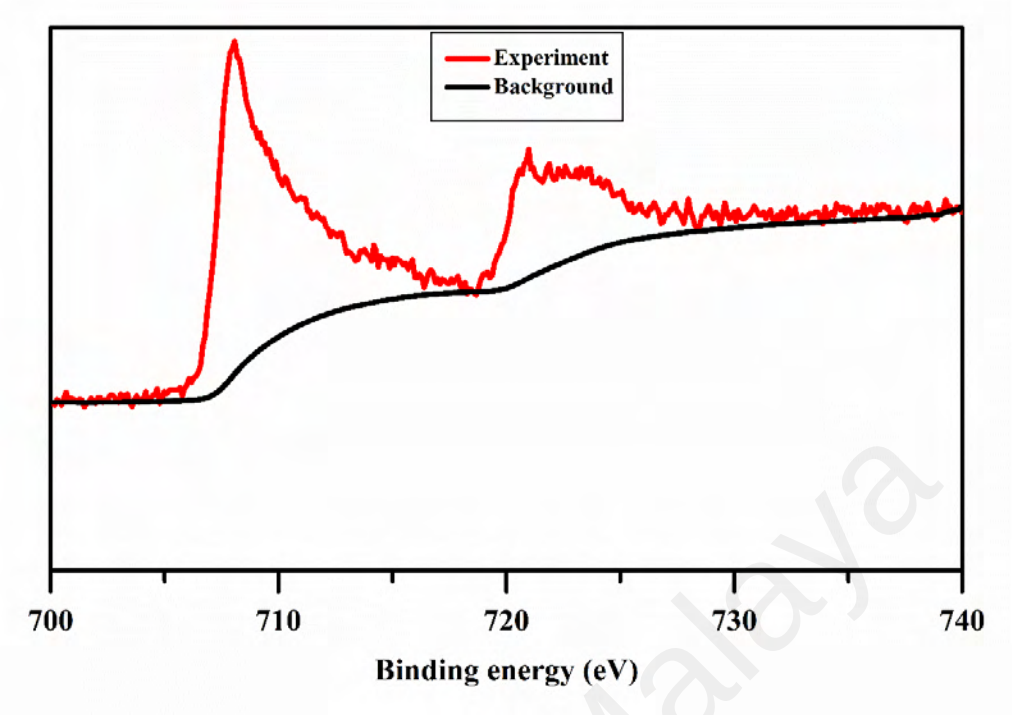

Figure 4.6: Enlarge XPS spectra of as-prepared PB between 700 – 740 eV.

Figure 4.7 shows the XPS spectra after background correction. Two main regions are observed from 705 – 718 eV and 718 – 730 eV. Area under the curve correspond to the content of Fe(III) and Fe(II). A closer look shows that each region is a broad envelope, composing two or more overlapping smaller peaks, corresponding to Fe^{3+} and Fe^{2+} in different states. The individual fitted curves centered at 708.0, 711.0, 721.1 and 723.7 eV are corresponded to Fe(II) $2P_{3/2}$, Fe(III) $2P_{3/2}$, Fe(III) $2P_{1/2}$ and Fe(II) $2P_{1/2}$, respectively and tabulated in Table 4.3. The area ratio of Fe(III) to Fe(II) is calculated as 1 : 0.93.The envelopes are then deconvoluted to split the overlapped/stacking peaks in Figure 4.8.

University of Malaya

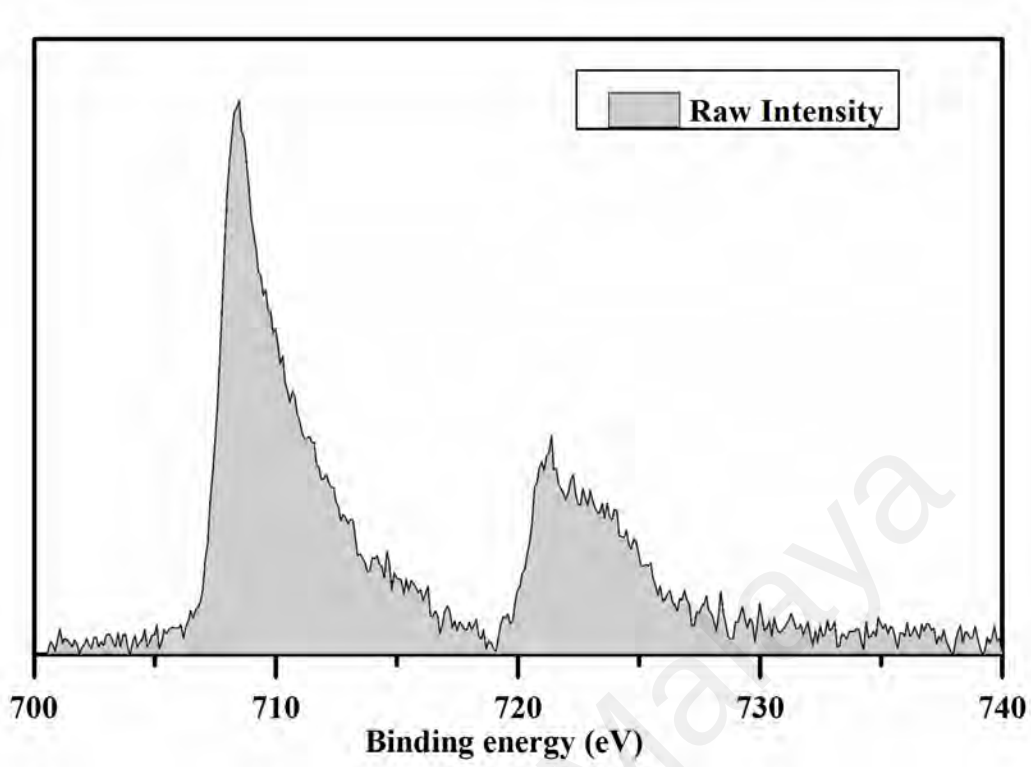

Figure 4.7: Enlarge XPS spectra of as-prepared PB after background correction.

Table 4.3: Binding energy of each spin state.

Spin state	Binding energy
Fe(II) $2P_{3/2}$	708.0
Fe(III) $2P_{3/2}$	711.0
Fe(III) $2P_{1/2}$	721.1
Fe(II) $2P_{1/2}$	723.7

University of Malaya

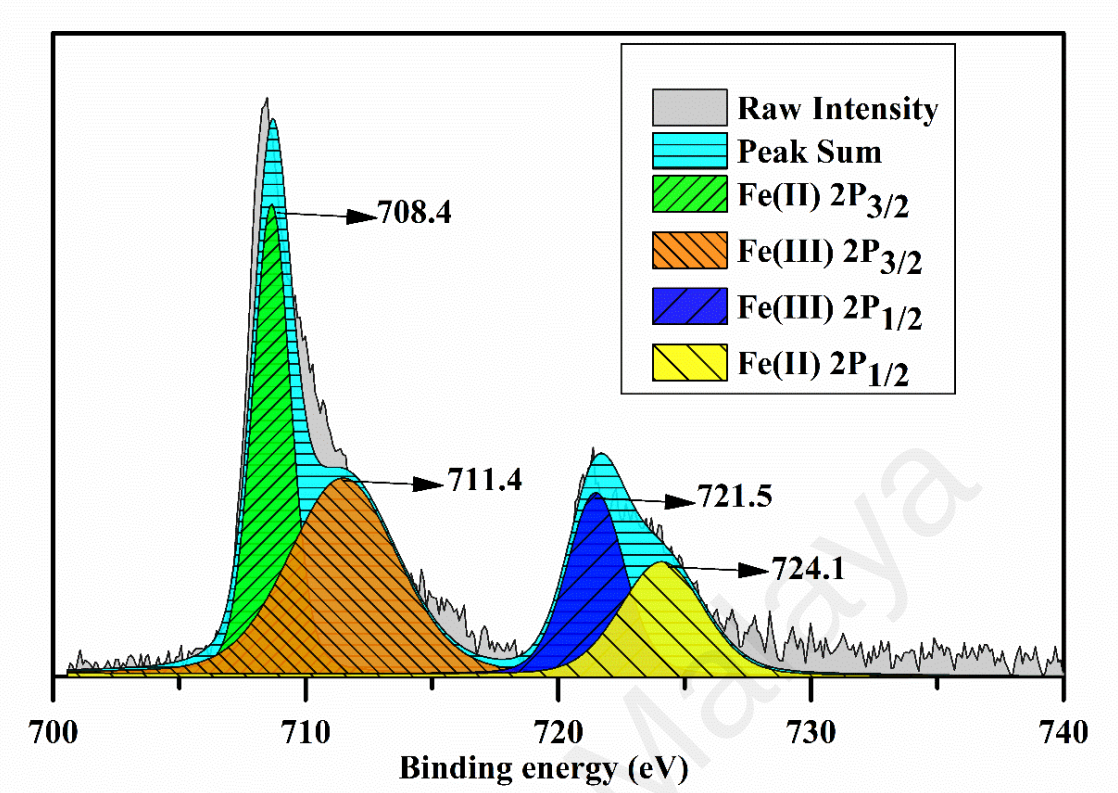

Figure 4.8: Deconvoluted XPS spectra of as-prepared PB.

4.2 Summary

- From elemental analysis, EDX and XPS results, the formula of as-prepared PB is determined as $Na_{0.58}Fe[Fe(CN)_6]_{0.93}\square_{0.07}\cdot 1.67H_2O$. The vacancies rate is 0.07 and the water content is low.
- In TGA analysis, the weight loss of water is estimated as 3 %
- XRD shows that the PB has a FCC structure with a lattice constant of 10.19 Å
- According to the TEM images and FESEM images, the size of as-prepared PB particles is in the range of 0.4 - 1 μm.
- XPS results confirmed there are two valences of Fe.

University of Malaya

CHAPTER 5: ELECTROCHEMICAL PERFORMANCE OF SIBS

5.1 Introduction

This chapter will show the electrochemical performance including cyclic voltammogram (CV) electrochemical impedance spectroscopy (EIS) and galvanostatic charge discharge (GCD) of half-cell SIBs using as-prepared PB as the cathode active material. The preparation of working electrode (cathode) by mixing PB, PVDF and super P has been shown in Section 3.4.1. Sodium metal is used as the counter electrode. In this work, two kinds of electrolyte were used to investigate the effect of FEC as additive. The electrolyte used throughout this work is 1M $NaPF_6$ in EC: PC=1:1(volume rate) with/without 5 % FEC.

5.2 Cyclic Voltammogram (CV)

To understand the redox voltage of PB, cyclic voltammogram (CV) was carried out. Figure 5.1 shows the CV plot of SIBs using the electrolyte with FEC and without FEC at a scan rate of 0.1 mV/s with voltage range between 2 - 4 V (vs. Na^+/Na).

Initially, there is no current from 2.0 - 2.75 V. The current is observed to increase after 2.75 V until the first peak appears at the voltage of 3.15 V. After that, the current reduces until 3.50 V where the current start to increase again which is showed the second peak at 3.78 V. The water starts to decompose at 4.0 V. In reverse direction, as the voltage is reduced from 4.0 V, multiple peaks are observed. The first peak appears from 3.63 V to 3.45 V while second peak (a small peak) is at 3.25 V. The third peak which is a strong peak appears at 2.74 V and current becomes to zero when the voltage drops below 2.5 V.

The CV curves for electrolyte without FEC are very similar to that with FEC, which indicates that the electrode is stable. This feature makes PB a potential to be a good

University of Malaya

cathode material for SIBs. Following from this experiment, two voltage ranges will be used in the GCD testing later.

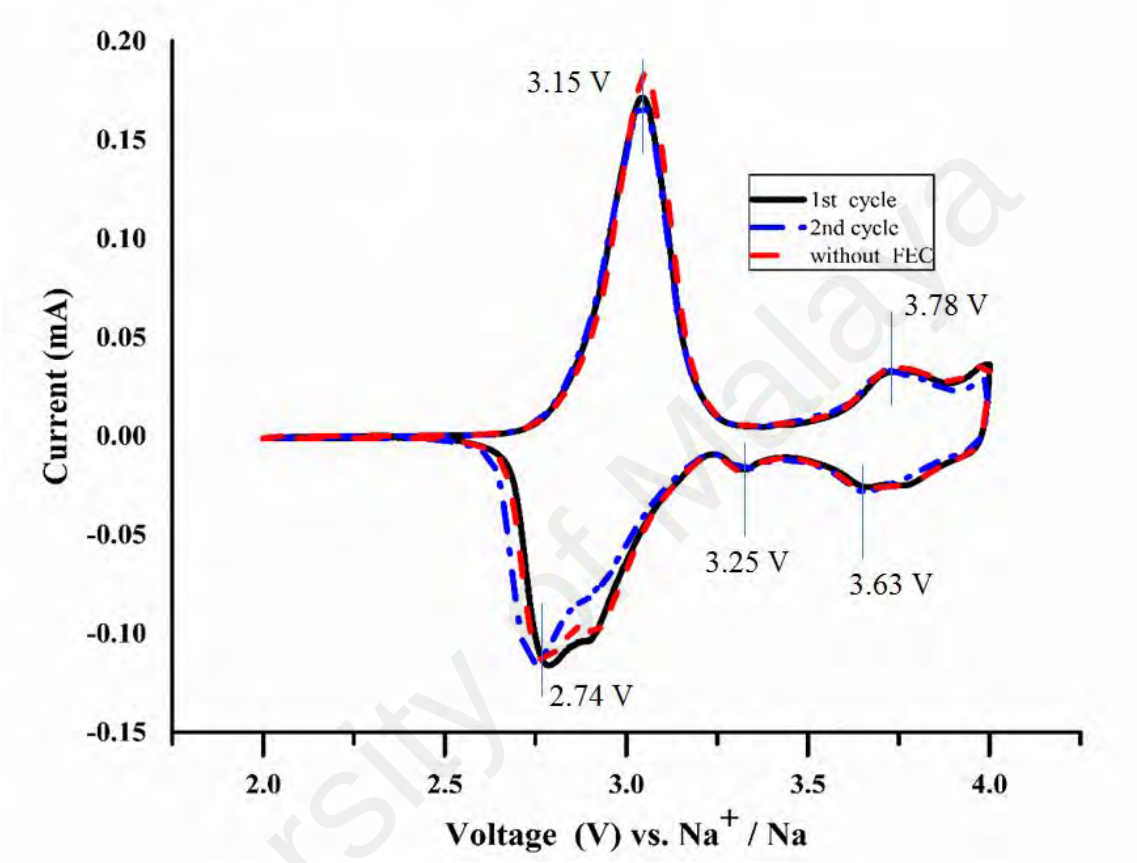

Figure 5.1: CV of SIBs at a scan rate of 0.1 mV/s with voltage range between 2 - 4 V (vs. Na+/Na).

5.3 Electrochemical Impedance Spectroscopy (EIS)

EIS was carried out and the Nyquist plot is shown in Figure 5.2. The Nyquist plots before cycling with FEC and without FEC indicate the ion kinetics in two different electrolyte systems. The EIS measurement is between 0.1 Hz and 100 kHz.

Diffusion coefficient, *D* can be calculated by Equation (3.2) and (3.3). The circuit shown in Figure 5.2 (b) is the fitting equivalent circuit of the testing process. By fitting the EIS result, *Rs* and R_{ct} can be obtained. R_{ct} with FEC is much lower (460 Ω) than R_{ct}

University of Malaya

without FEC (1337 Ω), indicating that FEC enhances the ion-transfer kinetics of Na^+ ion between electrode and electrolyte. From Equation (3.3), the slope of each line in Figure 5.2(c) corresponds to the Warburg coefficient, σ of each sample. σ^2 with FEC is smaller than σ^2 without FEC, which indicate that Na^+ is easier to move between electrode and electrolyte with FEC.

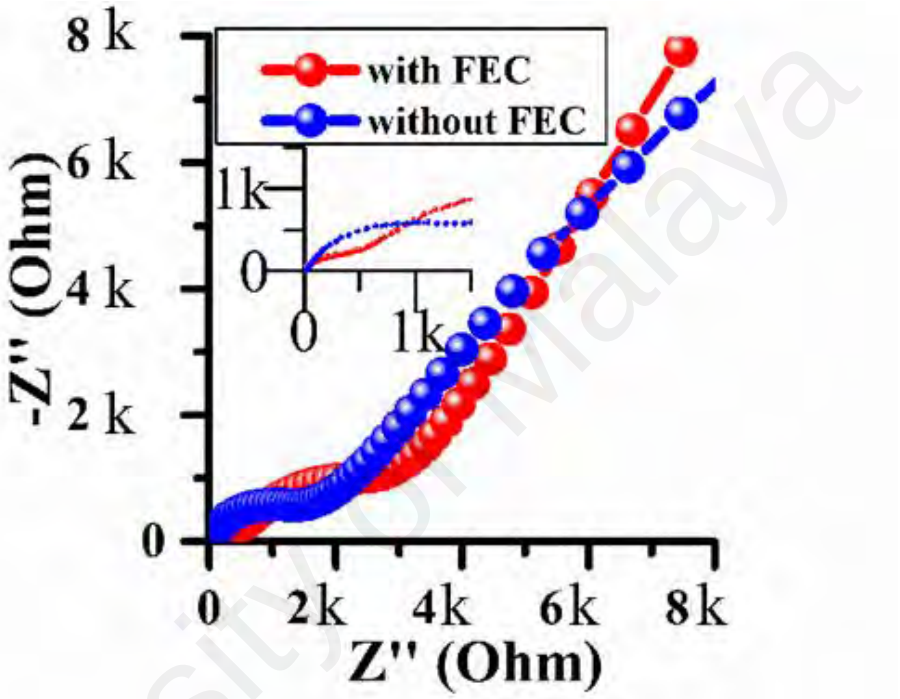

(a)

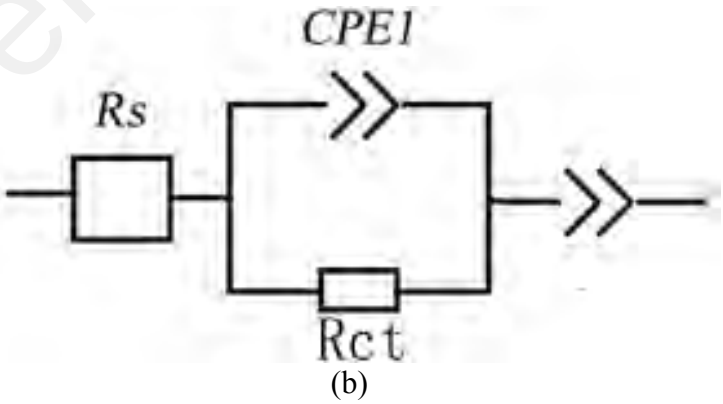

(b)

Figure 5.2: (a) Nyquist plot before cycling of half-cell using electrolyte with and without FEC between 0.1 Hz and 100 kHz, (b) simulated circuit and (c) plot of Z_{re} as a function of $\omega^{-1/2}$ in low frequency region.

University of Malaya

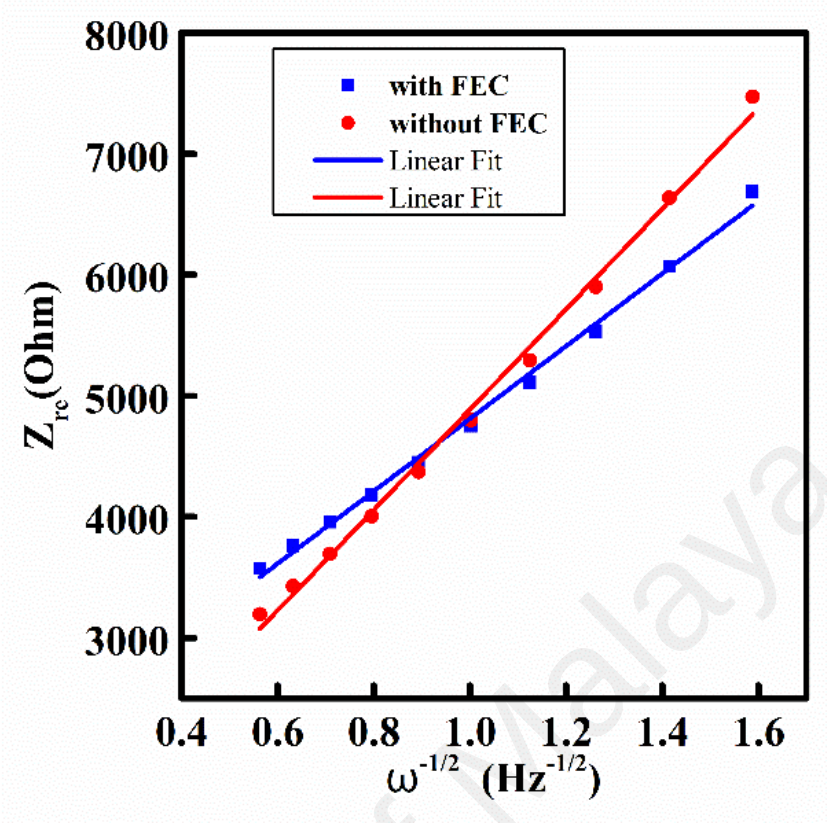

(c)

Figure 5.2, continued.

5.4 Galvanostatic Charge/discharge (GCD)

GCD section includes three parts. The first part is the rate performances of SIBs follows by voltage profile and cycling performance. From the CV testing, there are two pairs of redox peaks. Therefore, two voltage ranges are used in GCD, 2.0 – 3.6 V and 2.0 – 3.8 V, respectively. In addition, the electrolyte additive (FEC) is also investigated.

5.4.1 Rate Performances

The specific capability of the SIBs using electrolyte with FEC and without FEC at various rates of 0.1 C, 0.2 C and 0.3 C are investigated with voltage range between 2.0 V - 3.6 V.

University of Malaya

5.4.1.1 Rate performances of PB using electrolyte without FEC

Figure 5.3 shows the SC of SIBs using electrolyte without FEC at 0.1 C, 0.2 C, 0.3 C with voltage range between 2.0- 3.6 V. At the current of 0.1 C, SIBs using electrolyte without FEC has a discharge specific capacity (DSC) of 119.6 mAh g^{-1} with 97.8 % efficiency at the 1st cycle. The DSC increases to 122.0 mAh g^{-1} after few cycling. The increasing SC can be described as the activation of active material. For current of 0.2 C and 0.3 C, the DSC at first cycle is measured as 115.4 mAh g^{-1} and 112.5 mAh g^{-1}, respectively. At expected, this value is lower than that at 0.1 C. About 3 mAh g^{-1} has faded after 10 cycles. Low fading reflects good performance of the as-prepared PB as the cathode for SIBs. The efficiencies are generally maintained between 98-99 %.

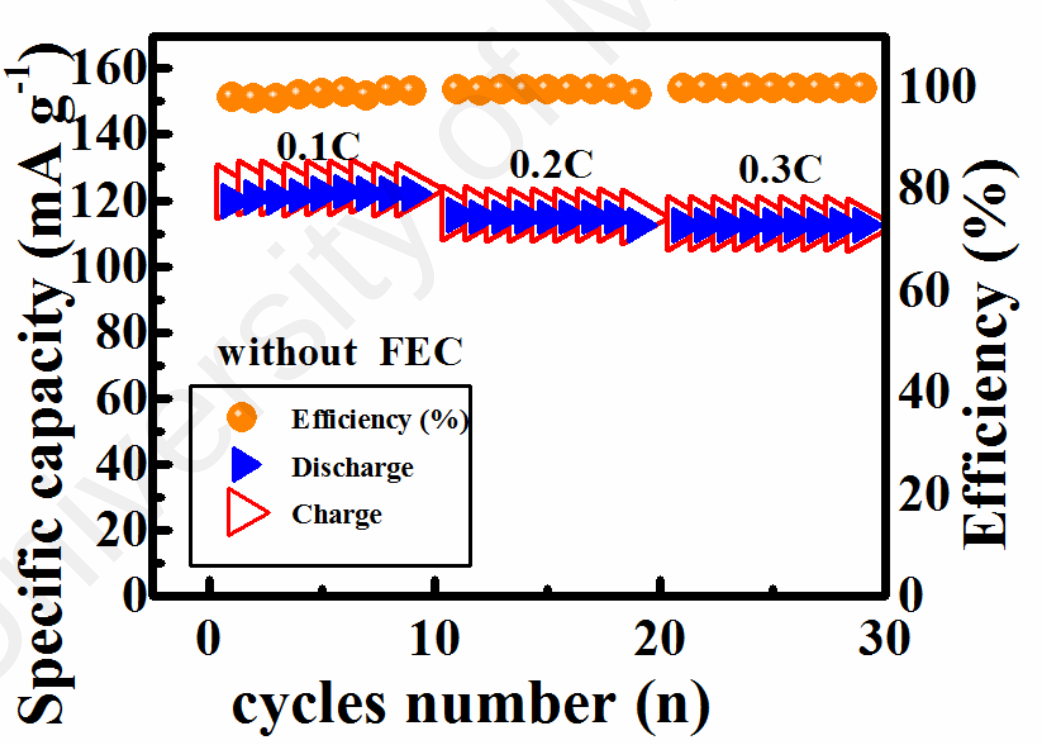

Figure 5.3: SC of SIBs using electrolyte without FEC at 0.1 C, 0.2 C, 0.3 C with voltage range between 2.0- 3.6 V vs Na^+ / Na.

University of Malaya

Table 5.1: SC using electrolyte without FEC at 0.1 C.

Cycle	Charge specific Capacity	Discharge specific Capacity	Efficiency
2	122.6	119.6	97.8
3	123.8	120.8	97.6
4	123.8	120.8	97.7
5	123.2	121.4	98.3
6	123.8	122.0	98.7
7	123.8	122.6	98.9
8	124.4	122.0	98.2
9	123.2	122.0	99.2
10	123.2	122.0	99.1

Table 5.2: SC using electrolyte without FEC at 0.2 C.

Cycle	Charge specific Capacity	Discharge specific Capacity	Efficiency
12	116.1	115.4	99.4
13	116.1	114.9	99.2
14	115.5	114.9	99.5
15	115.5	114.9	99.3
16	115.5	114.9	99.4
17	115.5	114.9	99.5
18	115.5	114.9	99.4
19	115.5	114.9	99.4
20	114.9	112.5	98.3

University of Malaya

Table 5.3: SC using electrolyte without FEC at 0.3 C.

Cycle	Charge specific Capacity	Discharge specific Capacity	Efficiency
22	113.1	112.5	99.7
23	113.1	112.5	99.7
24	113.1	112.5	99.6
25	113.1	112.5	99.7
26	113.1	112.5	99.7
27	113.1	112.5	99.7
28	113.1	112.5	99.7
29	113.1	112.5	99.6
30	112.5	112.5	99.7

5.4.1.2 Rate performance of PB using electrolyte with FEC

The rate performances of SIBs using electrolyte with FEC at 0.1 C, 0.2 C and 0.3 C. The testing voltage range is between 2.0 - 3.6 V and the results are shown in Figure 5.4,

Table 5.5 and Table 5.6. The DSC of 0.1 C is 118 mAh g^{-1} in the 1st cycle. It decreases slightly to 117.5 mAh g^{-1} over 10 cycles. High efficiencies are observed to maintain around 99 % and the SC is not obviously fading. At 0.2 C, DSC at the1st cycle is 115.4 mAh g^{-1}. The DSC reduces marginally to 114.9 mAh g^{-1} over 10 cycles. Discharge specific capacities at the 1st cycle is observed to drop from 113.2 mAh g^{-1} to 112.9 mAh g^{-1} at 10th cycle at 0.3 C. The addition of FEC in the electrolyte seems to increase the stability of the battery system.

University of Malaya

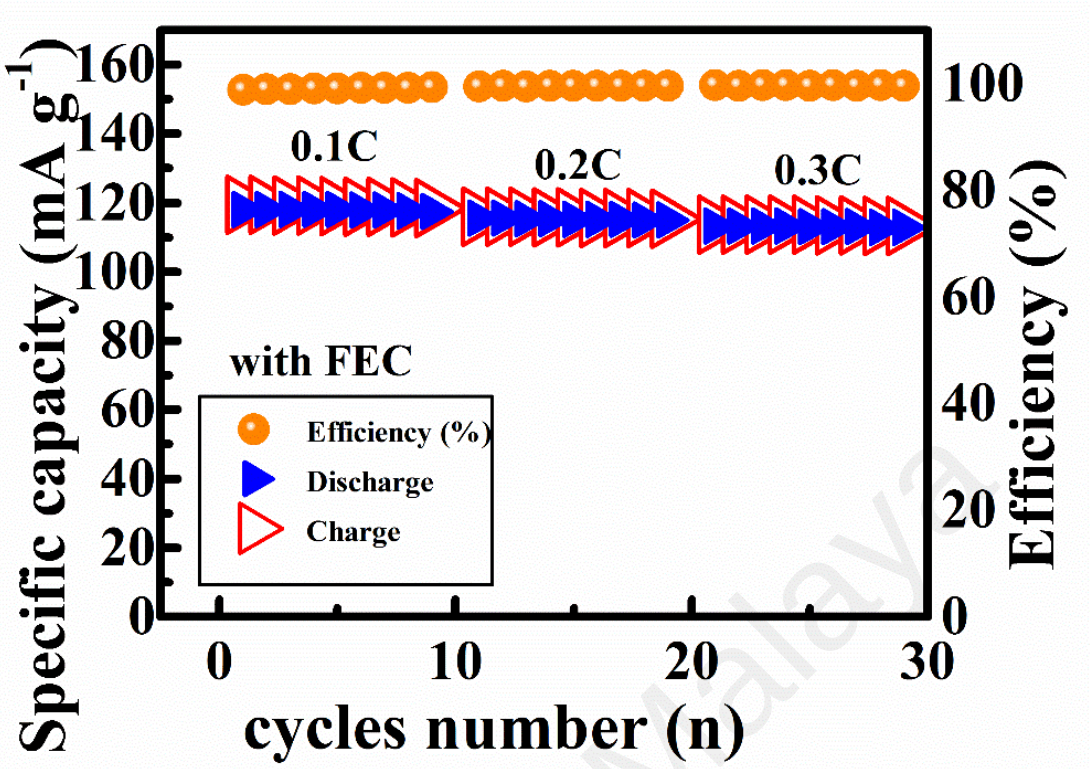

Figure 5.4: SC of the SIBs using electrolyte with FEC at 0.1 C, 0.2 C, 0.3 C with voltage range between 2.0- 3.6 V vs Na^+ / Na.

Table 5.4: SC using electrolyte with FEC at 0.1 C

Cycle	Charge specific Capacity	Discharge specific Capacity	Efficiency
2	119.4	118.0	98.8
3	119.2	118.0	98.9
4	119.1	118.0	99
5	119.1	118.0	99.1
6	119.0	117.9	99.1
7	118.8	117.9	99.2
8	118.8	117.9	99.2
9	118.6	117.7	99.2
10	118.4	117.5	99.3

University of Malaya

Table 5.5: SC using electrolyte with FEC at 0.2 C.

Cycle	Charge specific Capacity	Discharge specific Capacity	Efficiency
12	116.0	115.4	99.5
13	115.9	115.4	99.6
14	115.8	115.3	99.5
15	115.7	115.2	99.6
16	115.3	115.1	99.6
17	115.5	115.1	99.6
18	115.5	115.0	99.6
19	115.5	115.0	99.6
20	115.4	115.0	99.6

Table 5.6: SC using electrolyte with FEC at t 0.3 C.

Cycle	Charge specific Capacity	Discharge specific Capacity	Efficiency
22	115.0	115.4	99.5
23	115.9	115.4	99.6
24	115.8	115.3	99.5
25	115.7	115.2	99.6
26	115.6	115.1	99.6
27	115.5	115.1	99.6
28	115.5	115.0	99.6
29	115.5	115.0	99.6
30	115.4	115.0	99.6

University of Malaya

5.4.2 Galvanostatic Charge/Discharge Voltage Profile

This section shows the GCD voltage profiles of SIBs using electrolyte with FEC and without FEC for different cycles at 0.1 C with two voltage two voltage ranges, between 2.0 - 3.6 V and 2.0 - 3.8 V, respectively.

5.4.2.1 Galvanostatic Charge/discharge voltage profile using electrolyte without FEC

The GCD voltage profile using electrolyte without FEC is shown in Figure 5.5. At the first cycle, the GCD plateau is detected between 2.8 and 3.2 V, which corresponds to the CV curve at the peaks of 2.75 V. The first cycle charge specific capacity (CSC) is calculated about 140 mAh g^{-1}. However, the SC fades quickly to about 123 mAh g^{-1} in the 2nd cycle. The formation of SEI during 1st cycle and the side-reaction between electrolyte and electrode may cause the reduction of the SC.

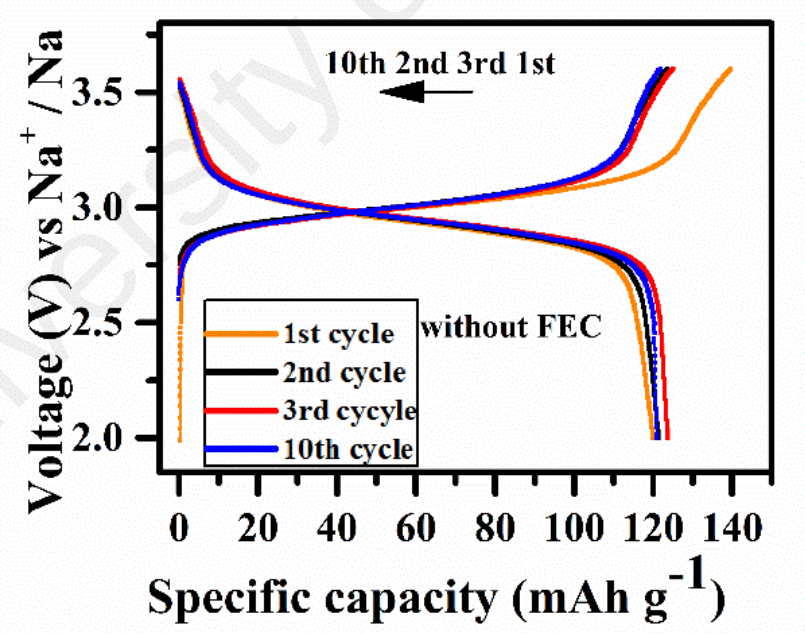

Figure 5.5: GCD voltage profiles using electrolyte without FEC at 0.1 C with voltage range between 2.0- 3.6 V vs Na^+ / Na.

University of Malaya

5.4.2.2 Specific capacity of PB using electrolyte with FEC

The GCD voltage profile using the electrolyte with FEC at 0.1 C with voltage range 2.0 – 3.6 V is shown in Figure 5.6(a). The GCD plateau at the first cycle is also found between 2.8 V - 3.2 V. The material exhibits a CSC of 125 mAh g^{-1} and DSC of 122 mAh g^{-1} in the 1st cycle. The DSC still remains 121 mAh g^{-1} over 10 cycles, indicating that the addition of FEC in the electrolyte helps to improve the performance.

To explore the different capacity offers by two active sites of PB, the ending voltage range is changed to 3.8 V. Figure 5.6(b) shows the voltage profiles with new voltage range between 2.0 - 3.8 V. After increasing the ending voltage from 3.6 - 3.8 V, the DSC at the first cycle increases from 125 mAh g^{-1} to 133 mAh g^{-1}. In the 2nd cycles, the DSC further increases to 135 mAh g^{-1} due to the activation of active material. After 10 cycles, the DSC still remains 134 mAh g^{-1} with 99 % of efficiency. This finding suggests that there are two active spots of PB in the GCD process. The second active spot at higher voltage will deliver additional SC.

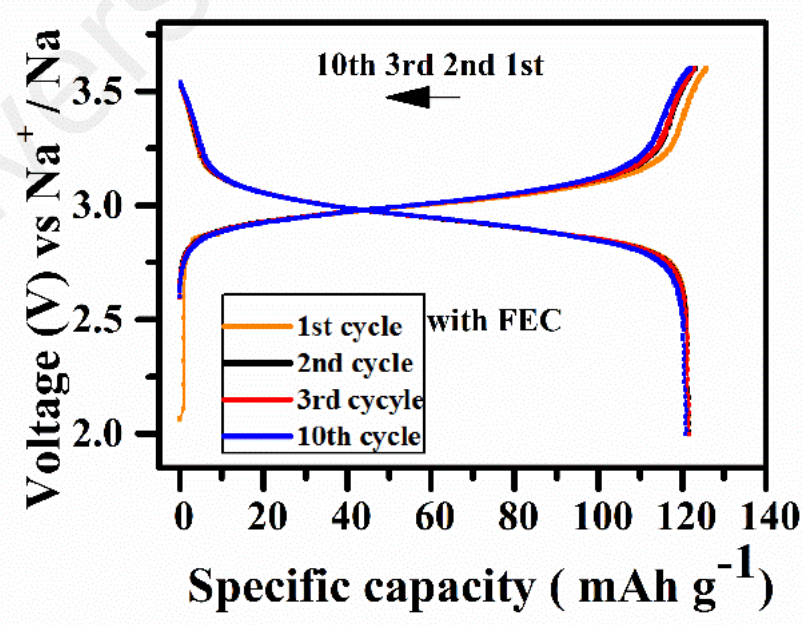

(a)

Figure 5.6: GCD voltage profiles using electrolyte with FEC at 0.1 C with two voltage ranges between (a) 2.0 - 3.6 V and (b) 2.0 -3.8 V.

University of Malaya

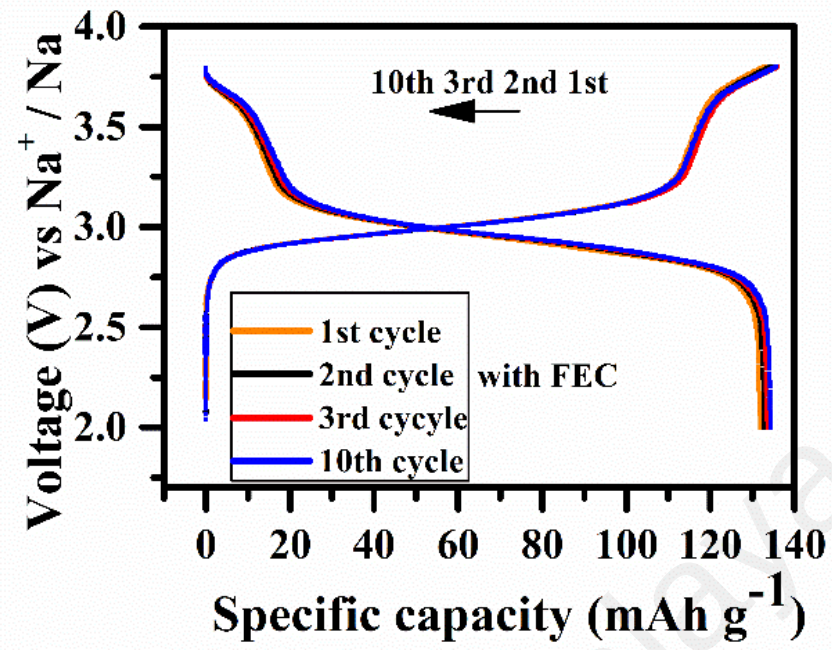

(b)

Figure 5.6, continued.

5.4.3 Cycling performance

Figure 5.7 shows the long cycling performance of SIBs using electrolyte with FEC at 2 C with voltage range between 2.0 - 3.8 V for 225 cycles. A very smooth SC plot is shown in Figure 5.7. After a few activation cycles, both the CSC and DSC are stabilized at 102 mAh g^{-1}. After more than 200 cycles, SIBs still exhibit a DSC of 87 mAh g^{-1} with an efficiency of near 100 %. The good long cycling performance of SIBs is corresponded to the low vacancies and low interstitial water of the as-prepared PB.

University of Malaya

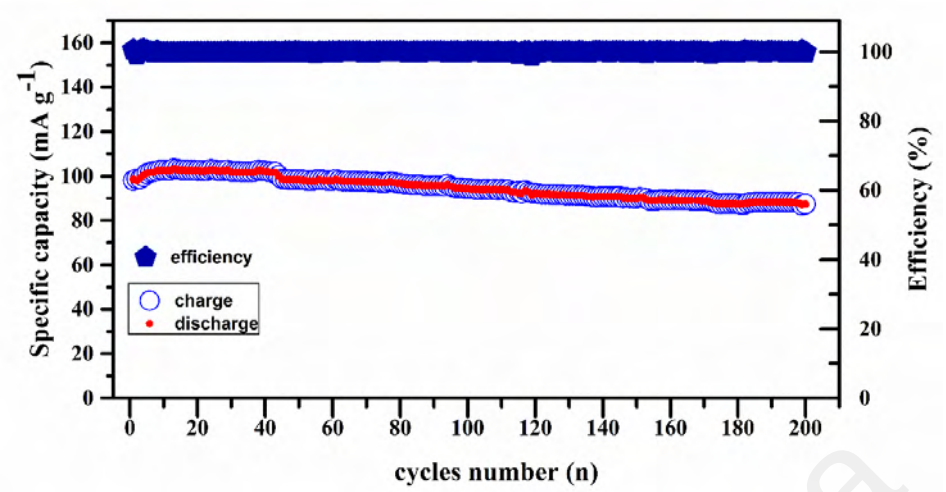

Figure 5.7: Cycling performance of SIBs using electrolyte with FEC at 2 C with voltage range between 2.0 – 3.8 V.

To understand the GCD in greater details, the cycling performance is divided into 4 parts. Figure 5.8 shows the GCD profile for the first 55 cycles. The SC is measured as 95 mAh g^{-1} at the 1st cycle. After 10 cycles, both the CSC and DSC are stabilized at 102 mAh g^{-1} for another 30 cycles before it drops a little bit to 98 mAh g^{-1}.

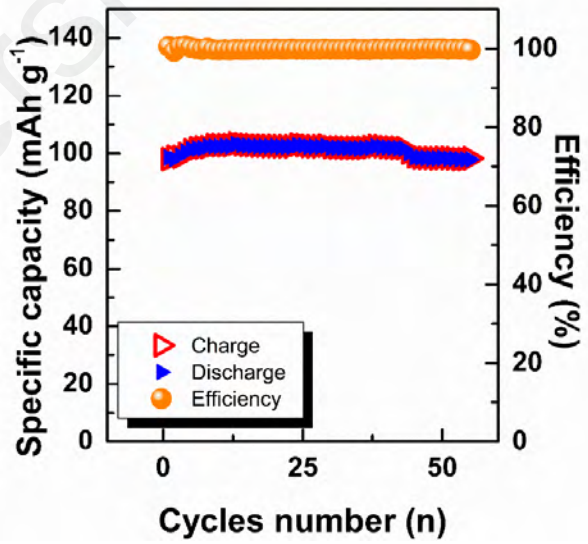

Figure 5.8: 1st – 55th cycles of SIBs using electrolyte with FEC at 2 C with voltage range between 2.0 - 3.8 V.

University of Malaya

In the cycle of 56th – 110th, cell shows a smooth marginal decrease. After 110 cycles the cell is still able to deliver a SC of 93 mAh g^{-1}.

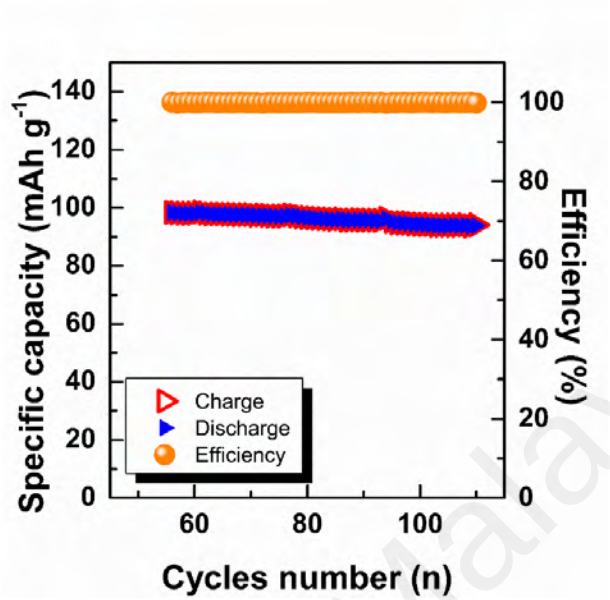

Figure 5.9: 56th – 110th cycle of SIBs using electrolyte with FEC at 2 C with voltage range between 2.0 - 3.8 V.

To continually charge and discharging, the SC decreases to 90 mAh g^{-1} after 165 cycles.

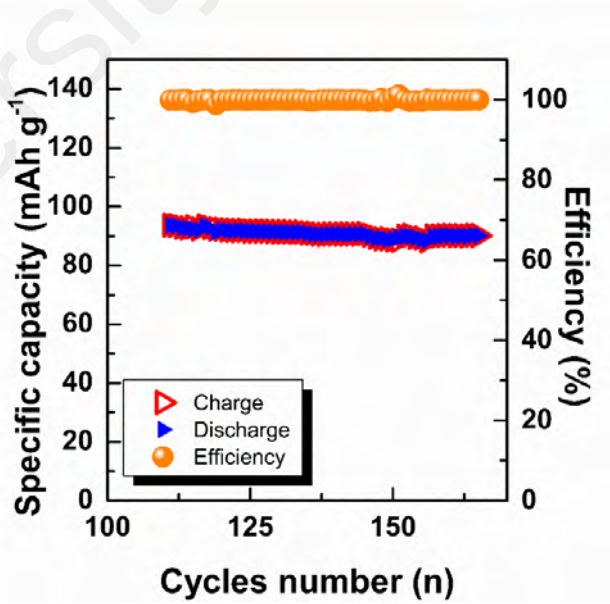

Figure 5.10: 111th – 165th cycle of SIBs using electrolyte with FEC at 2 C with voltage range between 2.0 - 3.8 V.

University of Malaya

After 225 cycling, the SC still remains 85 mAh g^{-1}.

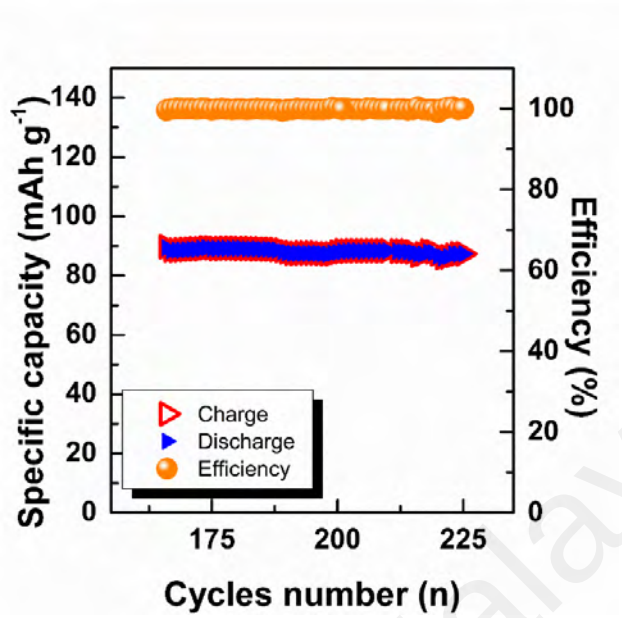

Figure 5.11: 166th -225th cycle of SIBs using electrolyte with FEC at 2 C with voltage range between 2.0 - 3.8 V.

5.5 Summary

- Cyclic voltammogram shows that there are two pairs of redox peak. The first pair of the symmetric peak is found at 3.15 V / 2.74 V while the second pair symmetric peak is determined at 3.78 V / 3.63 V.
- From EIS studies, R_{ct} of SIBs using electrolyte with FEC is 497 Ω, which is much lower than that using electrolyte without FEC (1870 Ω).
- In GCD studies, the DSC is observed to drop slightly from 0.1 C to 0.2 C and 0.3 C. These finding is the same for SIBs using electrolyte with FEC and without FEC.
- The addition of FEC in electrolyte seems to help to improve the efficiency and stability of cycling (above 99.7 %).
- From the study of two voltage ranges, there are two active spots of PB in the GCD process. After increasing the end voltage from 3.6 V to 3.8 V, the SC increases from 125 mAh g^{-1} to 133 mAh g^{-1}.

University of Malaya

- The SIBs show a DSC of 102 mAh g^{-1} in the current density of 2 C and still exhibits 87 mAh g^{-1} after more than 200 cycles.

University of Malaya

CHAPTER 6: RESULTS AND DISCUSSION

The general molecular formula of PB is written as Na_xFe^{III} $[Fe^{II}(CN)_6]_y\square_{1-y}\cdot nH_2O$ with □ represents $[Fe^{II}(CN)_6]$ vacancies in the structure, x, y, n are the stoichiometric numbers. The vacancies and interstitial water content of PB are very important. It has been shown that the performance of SIBs using as-prepared PB as cathode material is closely correlated to the vacancies available of PB crystal structure. As the vacancies increases, more coordinating interstitial water may occupy it causing less Na^+ storage into the PB open framework. In addition, high vacancies may incur high lattice distortion or instability of crystal structure leading to poor Na^+ insertion/extraction.

The aim of this work is to synthesis PB with low vacancies and low interstitial water content vis a facile method and use it as cathode material for SIB application. From literature review, as presented in Chapter 2, the synthesize of PB are normally optimized via a few steps and react at a temperature much higher than room temperature. In this work, the PB is synthesized via a facile one step solution-precipitation method at room temperature.

To determine the crystal structure, chemical composition and the formula of as-prepared PB, characterizations such as element analysis, EDX, TGA, XRD, TEM and XPS were carried out. The element ratio composition from element analysis and EDX is given in Table 4.1. XPS result in Section 4.1.5 shows that there are two valances of Fe ions, Fe(III) and Fe(II). The concentration ratio of Fe(III) to Fe(II) is calculated from the sum area under the respective filled curves as 1 : 0.93. Refer to Table 4.1, the concentration ratio of each element is first divided by the respective atomic weight to obtain the mole ratio. Then, the ratio of number of mole is simplified by normalizing the Fe^{III} mole ratio to 1. This eventually lead to a PB with the formula of

University of Malaya

$Na_{0.58}Fe[Fe(CN)_6]_{0.93}\square_{0.07}\cdot 1.67H_2O$. The exceptionally low vacancies (0.07) and low interstitial water (1.67) of PB obtained in this work is mainly due to the slow reaction of precipitation process that was taken place at room temperature (Wu et al., 2015). Low vacancies (0.07) mean the near perfect crystal with high purity, hence XRD and TEM are expected to provide evidences to support this result. The amount of interstitial water is low compared with other PB analogues i.e. $Na_{1.33}Fe[Fe(CN)_6]\cdot 3.5H_2O$ and $Na_{1.26}Fe[Fe(CN)_6]\cdot 3.8H_2O$ that was prepared from $Na_4Fe(CN)_6\cdot 10H_2O$ with and without NaCl, respectively (Li et al., 2015). By taking molar mass of H_2O as 18 and molar mass of whole PB crystal unit as 580, the water content is estimated to be 5 % ($1.67\times 18/580 \approx 5$ %.).

The TGA curves as depicted in Figure 4.1 presents the weight-loss processes. The weight loss in the range of 50 ℃ < T < 275 ℃ is ascribed to the loss of adsorbed water/interstitial water. From the first drop in the TGA curve, the water loss is estimated to be ~3 wt %, which is in good agreement to the water content estimated from PB chemical formula in the previous paragraph. It has been reported that the low interstitial water content will contribute to good stability and high sodium storage during GCD process. Therefore, it is anticipated that excellent cycling performance and high SC in the GCD process will be obtained in Chapter 5 (Song et al., 2015).

The XRD pattern of the PB is shown in Figure 4.2. The peaks of the PB are similar to the library data (JCPDS No. 52-1907), demonstrating the face-centered cubic crystal structure with the space group $Fm\bar{3}m$. The lattice constant of the as-prepared PB in this work is calculated to be 10.19 Å, which is very close to 10.20 Å of the ideal $FeFe(CN)_6$. The main peaks are strong, narrow and sharp with no presence of other impurity peak in the XRD diffractogram indicating the high purity of the PB. This finding is in agreement to the low vacancies of the as-prepared PB, in the first section. As compared to the

University of Malaya

conventional synthesis method performed at higher temperature (Wilde et al., 1970), this high purity PB is a result of slow reaction rate at room temperature throughout the precipitation process.

FESEM and TEM images as presented in Figure 4.4 shows the morphology of the PB. The particle size is estimated in the range of 0.4 μm - 1 μm. Both FESEM and TEM micrographs reveal that the crystals of the as-prepared PB show near perfect cubic structure which corroborates with the XRD results. It is known that different synthesized environment may affect the morphology of PB (Shen et al., 2009). In this work, the ascorbic acid and the PVP are added to set the synthesized environment. This structure of the as-prepared PB is the result of the slow growth rate and the cooperative chelation effect between ascorbic acid and PVP (Shen et al., 2009). Therefore, the vacancies inside the crystal lattice can be significantly reduced. Some of the interstitial water may occupy in the vacancies of PB, thus, the reduction of vacancies also reduces the amount of interstitial water, which improves the stability of PB to be used as electrode material (Song et al., 2015).

XPS testing was carried out to determine the two valences of Fe ions. Figure 4.8 shows the XPS spectrum of PB including the raw data, peak sum and individual fitted curves. Two main regions are observed from 705 – 718 eV and 718 – 730 eV where two enveloped of peaks are depicted. The peaks are then deconvoluted to split the overlapped peaks, indicating Fe(II) $2P_{3/2}$, Fe(III) $2P_{3/2}$, Fe(III) $2P_{1/2}$ and Fe(II) $2P_{1/2}$, respectively. Fe(II) $2P_{3/2}$ which linked with N atoms (Lu et al., 2012) has the lowest binding energy. This indicates that it will be first oxidized during the battery GCD process. By losing an electron to Fe, Na ions will be extracted from cathode and move to anode. The second step of reaction will be followed by Fe(III) $2P_{3/2}$ which linked with C atoms. In summary,

University of Malaya

the reaction sequence/priority in PB starts with the lower valence Fe (II) as it is more reactive than Fe (III).

The electrochemical performance of half-cell SIBs using as-prepared PB as the cathode material were investigated via CV, EIS and GCD. CV are tested in two different electrolytes environment. Figure 5.1 shows the CV of SIBs at the scan rate of 0.1 mV s^{-1} using the 1.0 M $NaPF_6$ electrolytes with and without FEC at voltage range between 2.0 – 4.0 V. Two pairs of redox peaks are significantly detected, indicating that there are two redox points of active sites which correspond to two different valence of Fe ions. This observation is in agreement with XPS result. The first pair of symmetrical peaks are found at 3.15 V/2.74 V and the second pair symmetric peak is observed at 3.78 V/3.63 V. This also demonstrates that there are two steps of Na^+ movement in the Na^+ insertion/extraction process.

Similar finding was reported in the literature. In the previous study of (Yan et al., 2017), peaks at 3.15 V/2.74 V correspond to the high-spin Fe^{3+}/Fe^{2+} bonding to N atoms of C≡N whereas those at 3.78 V/3.63 V relate to the low-spin Fe^{3+}/Fe^{2+} couple coordinated with C≡N via C atoms (Imanishi et al., 1999; Nie et al., 2015). In addition, some shoulder peaks can be depicted and this phenomenon can be explained by the extraction of interstitial water during Na^+ ion insertion/extraction process. At near 4 V, the extracted water and residual water have taken part in the side-reaction (Yang et al., 2016). The CV curves of the two kind of electrolytes environment are very similar, suggesting that the electrode is stable. This feature makes PB a good candidate as cathode material for SIBs. Based on this feature, the two voltage ranges are chosen i.e. 2 - 3.6 V and 2 - 3.8 V for the GCD testing.

The double redox site of Fe in PB give advantage to SIB application. Since there are two active sites per PB, the theoretical SC of PB is raised two times higher to 170 mAh

University of Malaya

g^{-1}. This make PB a promising cathode material as $LiPO_4$ in LIBs application with also a theoretical SC of 170 mAh g^{-1}. Fe is an abundant material in the earth crust, meaning the row material of PB is easy to obtain, low cost and environmentally friendly. Furthermore, SIBs have similar charge and discharge mechanism to LIBs, therefore SIBs should be the best alternative batteries to compliment LIBs.

EIS was firstly carried out to study the kinetics of cells using two types of electrolyte before GCD process. R_{ct} of SIBs using electrolyte without FEC is determined as 1337 Ω while electrolyte with FEC is determined to reduce to 460 Ω. The smaller R_{ct} (with FEC) implies that ions are easier to move between electrodes. This indicates that the addition of FEC can help to improve the ions movement. Besides, the relationship between Z_{re} and $\omega^{-1/2}$ in low frequency region is also plotted. From Equation 4.2 and Figure 5.2 (b), the slope of fitting line corresponds to σ, which is the only variable in Equation 4.1. Obviously, σ with FEC is found to be smaller than σ without FEC, which suggests that the addition of FEC improve the diffusion coefficient, D of the ions.

In GCD studies, two voltage ranges were used to investigate the SC contribution of two redox pairs. Both use the same starting voltage as 2.0 V but the ending voltage is 3.6 V and 3.8 V, respectively. Figure 5.3 and Figure 5.4 show the rate performances using two type of electrolytes. The SC of voltage range 2.0 – 3.8 V enhances from 125 mAh g^{-1} (2.0 – 3.6 V) to 133 mAh g^{-1}. The second active site at 3.6 V – 3.8 V provides additional SC. This SC is higher compared to the previous studies (Li et al., 2015; Wu et al., 2013; Wu et al., 2015). This high cyclability of SIBs could be explained from XPS and TGA results that show the as-prepared PB has low vacancies and low interstitial water. As shown in Figure 5.7, at high current density of 2 C, the SIBs show a DSC of 102 mAh g^{-1}. After 225 cycles, the SIBs still exhibit a SC of 87 mAh g^{-1} with an efficiency of near 100 %, indicating a good cyclability. The Na^+ ions can move smoothly inside the PB and

University of Malaya

occupy at the active site. The unblocked path of Na^+ is the only way to describe the excellent performance of as-prepared PB. The addition of FEC in the electrolyte also improves the efficiency and stability of cycling to be above 99 %.

University of Malaya

CHAPTER 7: CONCLUSION AND FUTURE WORK

This work is about synthesizing low vacancies and low interstitial water PB and using it as the cathode material for SIBs. The first part of the work focuses on the PB synthesis and electrochemical characterization of PB. Solution-precipitation method is used at room-temperature to obtain low vacancies and low interstitial water PB. PVP and ascorbic acid are incorporated as chelating agents to set the synthesis environment. This has resulted a low growth rate of high purity PB. Element analysis, XRD, TGA, HRTEM, FESEM, XPS are used to characterize the structure properties, chemical composition, thermal properties and morphology of the as-prepared PB. The chemical formula of the as-prepared PB are determined as $Na_{0.58}Fe[Fe(CN)_6]_{0.93}\square_{0.07}\cdot 1.67H_2O$ with 3 – 5 % water content. XRD pattern shows that the lattice structure of the as-prepared PB is face-centered cubic with lattice parameter 10.19 Å. HRTEM and FESEM present a nice cubic macro structure with dimension 0.4 - 1 μm. A series of electrochemical characterizations are also carried out to study the overall performance of SIBs using the PB as the cathode material. From CV analysis, two redox pairs are observed. The first pair of the symmetric peak is located at 3.15 V / 2.74 V while the second pair symmetric peak is found at 3.78 V / 3.63 V. The peaks at 3.15 V / 2.74 V correspond to the high-spin Fe^{3+}/Fe^{2+} bonding to N atoms of C≡N and those at 3.78 V / 3.63 V correspond to the low-spin Fe^{3+}/Fe^{2+} couple coordinated with C≡N by C atoms. EIS and GCD analysis concludes that the addition of FEC in electrolyte improve the stability and efficiency of SIB cycling processes. Without FEC, the SC fades quickly from 140 mAh g^{-1} of 1st cycle to 123 mAh g^{-1} of second cycle. After addition of FEC, the SC maintains for 10 cycles. Even at current density of 2 C, the cyclability of SIBs using electrolyte with FEC still performs well with 10 % fading after 225 cycles. This material is very suitable for long cycling rechargeable SIBs. Sodium-ion rechargeable batteries are only in the beginning of research. Na, as a

University of Malaya

rich-element in the earth crust and has similar nature with Li, should be the best alternative candidate of next-generation rechargeable batteries. It also works well in a large-scale energy storage system such as power grids and EVs.

For future work, the following directions are proposed:

- In the current work, the cycling performance is excellent, but the SC is not high enough. Therefore, a composite material base on PB should be developed with a higher SC.
- The theoretical SC of pure PB is about 170 mAh g^{-1}. However, the present SC is only 100 mAh g^{-1} at the current density of 2 C. Optimization of the synthesis method should be carried out. Carbon coating should be considered.

University of Malaya

REFERENCES

Avdeev, M., Mohamed, Z., Ling, C. D., Lu, J., Tamaru, M., Yamada, A., & Barpanda, P. (2013). Magnetic structures of $NaFePO_4$ maricite and triphylite polymorphs for sodium-ion batteries. *Inorganic Chemistry, 52*(15), 8685-8693.

Balogun, M.-S., Luo, Y., Qiu, W., Liu, P., & Tong, Y. (2016). A review of carbon materials and their composites with alloy metals for sodium ion battery anodes. *Carbon, 98*, 162-178.

Barpanda, P., Avdeev, M., Ling, C. D., Lu, J., & Yamada, A. (2012). Magnetic structure and properties of the $Na_2CoP_2O_7$ pyrophosphate cathode for sodium-ion batteries: A supersuperexchange-driven non-collinear antiferromagnet. *Inorganic Chemistry, 52*(1), 395-401.

Barpanda, P., Liu, G., Ling, C. D., Tamaru, M., Avdeev, M., Chung, S.-C., Yamada, Y., & Yamada, A. (2013a). $Na_2FeP_2O_7$: a safe cathode for rechargeable sodium-ion batteries. *Chemistry of Materials, 25*(17), 3480-3487.

Barpanda, P., Liu, G., Mohamed, Z., Ling, C. D., & Yamada, A. (2014). Structural, magnetic and electrochemical investigation of novel binary $Na_{2-x}(Fe_{1-y}Mn_y)P_2O_7$ ($0 \leqslant y \leqslant 1$) pyrophosphate compounds for rechargeable sodium-ion batteries. *Solid State Ionics, 268*, 305-311.

Barpanda, P., Lu, J., Ye, T., Kajiyama, M., Chung, S.-C., Yabuuchi, N., Komaba, S., & Yamada, A. (2013b). A layer-structured $Na_2CoP_2O_7$ pyrophosphate cathode for sodium-ion batteries. *RSC Advances, 3*(12), 3857-3860.

Baster, D., Maziarz, W., Świerczek, K., Stokłosa, A., & Molenda, J. (2015). Structural and electrochemical properties of $Na_{0.72}CoO_2$ as cathode material for sodium-ion batteries. *Journal of Solid State Electrochemistry, 19*(12), 3605-3612.

Billaud, J., Clément, R. J., Armstrong, A. R., Canales-Vázquez, J., Rozier, P., Grey, C. P., & Bruce, P. G. (2014). β-$NaMnO_2$: a high-performance cathode for sodium-ion batteries. *Journal of the American Chemical Society, 136*(49), 17243-17248.

Cao, Y., Xiao, L., Sushko, M. L., Wang, W., Schwenzer, B., Xiao, J., Nie, Z., Saraf, L. V., Yang, Z., & Liu, J. (2012). Sodium ion insertion in hollow carbon nanowires for battery applications. *Nano Letters, 12*(7), 3783-3787.

Chen, C.-Y., Matsumoto, K., Nohira, T., Ding, C., Yamamoto, T., & Hagiwara, R. (2014). Charge–discharge behavior of a $Na_2FeP_2O_7$ positive electrode in an ionic liquid electrolyte between 253 and 363K. *Electrochimica Acta, 133*, 583-588.

Chen, H., Hao, Q., Zivkovic, O., Hautier, G., Du, L.-S., Tang, Y., Hu, Y.-Y., Ma, X., Grey, C. P., & Ceder, G. (2013). Sidorenkite ($Na_3MnPO_4CO_3$): A new intercalation cathode material for Na-ion batteries. *Chemistry of Materials, 25*(14), 2777-2786.

University of Malaya

Chen, H., Hautier, G., & Ceder, G. (2012). Synthesis, computed stability, and crystal structure of a new family of inorganic compounds: carbonophosphates. *Journal of the American Chemical Society, 134*(48), 19619-19627.

Delmas, Saadoune, & Dordor. (1994). Effect of Cobalt Substitution on the Jahn-Teller Distortion of the $NaNiO_2$ Layered Oxide. *Molecular Crystals and Liquid Crystals Science and Technology. Section A. Molecular Crystals and Liquid Crystals, 244*(1), 337-342.

Delmas, C., Braconnier, J.-J., Fouassier, C., & Hagenmuller, P. (1981). Electrochemical intercalation of sodium in $NaxCoO_2$ bronzes. *Solid State Ionics, 3*, 165-169.

Delmas, C., Guignard, M., Didier, C., Carlier, D., Weill, F., Suchomel, M., Elkaim, E., & Darriet, J. (2013). *The Electrochemical Behavior of Sodium Vanadium Oxides in Sodium Batteries.* Paper presented at the Meeting Abstracts.

Didier, C., Guignard, M., Denage, C., Szajwaj, O., Ito, S., Saadoune, I., Darriet, J., & Delmas, C. (2011). Electrochemical Na-Deintercalation from $NaVO_2$. *Electrochemical and Solid-State Letters, 14*(5), A75-A78.

Ding, J.-J., Zhou, Y.-N., Sun, Q., & Fu, Z.-W. (2012). Cycle performance improvement of $NaCrO_2$ cathode by carbon coating for sodium ion batteries. *Electrochemistry Communications, 22*, 85-88.

Guignard, M., Didier, C., Darriet, J., Bordet, P., Elkaïm, E., & Delmas, C. (2013). P2-$NaxVO_2$ system as electrodes for batteries and electron-correlated materials. *Nature Materials, 12*(1), 74-80.

Hamani, D., Ati, M., Tarascon, J.-M., & Rozier, P. (2011). Na_xVO_2 as possible electrode for Na-ion batteries. *Electrochemistry communications, 13*(9), 938-941.

Han, S. C., Lim, H., Jeong, J., Ahn, D., Park, W. B., Sohn, K.-S., & Pyo, M. (2015). Ca-doped Na_xCoO_2 for improved cyclability in sodium ion batteries. *Journal of Power Sources, 277*, 9-16.

He, X., Wang, J., Qiu, B., Paillard, E., Ma, C., Cao, X., Liu, H., Stan, M. C., Liu, H., & Gallash, T. (2016). Durable high-rate capability $Na_{0.44}MnO_2$ cathode material for sodium-ion batteries. *Nano Energy, 27*, 602-610.

Huang, Y., Zheng, Y., Li, X., Adams, F., Luo, W., Huang, Y., & Hu, L. (2018). Electrode Materials of Sodium-Ion Batteries toward Practical Application. *ACS Energy Letters, 3*, 1604-1612.

Hwang, J.-Y., Myung, S.-T., & Sun, Y.-K. (2017). Sodium-ion batteries: present and future. *Chemical Society Reviews*, 46 (2017) 3529-3614.

Hwang, J.-Y., Yoon, C. S., Belharouak, I., & Sun, Y.-K. (2016). A comprehensive study of the role of transition metals in O3-type layered $Na[Ni_xCo_yMn_z]O_2$(x= 1/3, 0.5, 0.6, and 0.8) cathodes for sodium-ion batteries. *Journal of Materials Chemistry A, 4*(46), 17952-17959.

University of Malaya

Imanishi, N., Morikawa, T., Kondo, J., Takeda, Y., Yamamoto, O., Kinugasa, N., & Yamagishi, T. (1999). Lithium intercalation behavior into iron cyanide complex as positive electrode of lithium secondary battery. *Journal of Power Sources, 79*(2), 215-219.

Jian, Z., Zhao, L., Pan, H., Hu, Y.-S., Li, H., Chen, W., & Chen, L. (2012). Carbon coated $Na_3V_2(PO_4)_3$ as novel electrode material for sodium ion batteries. *Electrochemistry Communications, 14*(1), 86-89.

Kim, H., Park, C. S., Choi, J. W., & Jung, Y. (2016). Defect‐controlled formation of triclinic $Na_2CoP_2O_7$ for 4 V sodium-ion batteries. *Angewandte Chemie International Edition, 55*(23), 6662-6666.

Kim, H., Park, I., Lee, S., Kim, H., Park, K.-Y., Park, Y.-U., Kim, H., Kim, J., Lim, H.-D., & Yoon, W.-S. (2013). Understanding the electrochemical mechanism of the new iron-based mixed-phosphate $Na_4Fe_3(PO_4)_2(P_2O_7)$ in a Na rechargeable battery. *Chemistry of Materials, 25*(18), 3614-3622.

Kim, H., Park, I., Seo, D.-H., Lee, S., Kim, S.-W., Kwon, W. J., Park, Y.-U., Kim, C. S., Jeon, S., & Kang, K. (2012). New iron-based mixed-polyanion cathodes for lithium and sodium rechargeable batteries: combined first principles calculations and experimental study. *Journal of the American Chemical Society, 134*(25), 10369-10372.

Komaba, S., Nakayama, T., Ogata, A., Shimizu, T., Takei, C., Takada, S., Hokura, A., & Nakai, I. (2009). Electrochemically reversible sodium intercalation of layered $NaNi_{0.5}Mn_{0.5}O_2$ and $NaCrO_2$. *ECS Transactions, 16*(42), 43-55.

Langrock, A., Xu, Y., Liu, Y., Ehrman, S., Manivannan, A., & Wang, C. (2013). Carbon coated hollow Na_2FePO_4 F spheres for Na-ion battery cathodes. *Journal of Power Sources, 223*, 62-67.

Lee, E., Brown, D. E., Alp, E. E., Ren, Y., Lu, J., Woo, J.-J., & Johnson, C. S. (2015). New insights into the performance degradation of fe-based layered oxides in sodium-ion batteries: Instability of Fe^{3+}/Fe^{4+} Redox in α-$NaFeO_2$. *Chemistry of Materials, 27*(19), 6755-6764.

Lee, H.-W., Wang, R. Y., Pasta, M., Lee, S. W., Liu, N., & Cui, Y. (2014). Manganese hexacyanomanganate open framework as a high-capacity positive electrode material for sodium-ion batteries. *Nature Communications, 5*, 5280-5286.

Lee, M., Hong, J., Lopez, J., Sun, Y., Feng, D., Lim, K., Chueh, W. C., Toney, M. F., Cui, Y., & Bao, Z. (2017). High-performance sodium–organic battery by realizing four-sodium storage in disodium rhodizonate. *Nature Energy, 2*, 861-868.

Li, S., Dong, Y., Xu, L., Xu, X., He, L., & Mai, L. (2014). Effect of carbon matrix dimensions on the electrochemical properties of $Na_3V_2(PO_4)_3$ nanograins for high-performance symmetric sodium‐ion batteries. *Advanced Materials, 26*(21), 3545-3553.

University of Malaya

Li, W.-J., Chou, S.-L., Wang, J.-Z., Kang, Y.-M., Wang, J.-L., Liu, Y., Gu, Q.-F., Liu, H.-K., & Dou, S.-X. (2015). Facile method to synthesize na-enriched $na_{1+x}fefe(cn)_6$ frameworks as cathode with superior electrochemical performance for sodium-ion batteries. *Chemistry of Materials, 27*(6), 1997-2003.

Li, Z. Y., Zhang, J., Gao, R., Zhang, H., Hu, Z., & Liu, X. (2016). Unveiling the role of co in improving the high-rate capability and cycling performance of layered $Na_{0.7}Mn_{0.7}Ni_{0.3-x}Co_xO_2$ cathode materials for sodium-ion batteries. *ACS Applied Materials & Interfaces, 8*(24), 15439-15448.

Liu, Q., Hu, Z., Chen, M., Gu, Q., Dou, Y., Sun, Z., Chou, S., & Dou, S. X. (2017). Multiangular rod-shaped $Na_{0.44}MnO_2$ as cathode materials with high rate and long life for sodium-ion batteries. *ACS Applied Materials & Interfaces, 9*(4), 3644-3652.

Lu, Y., Wang, L., Cheng, J., & Goodenough, J. B. (2012). Prussian blue: A new framework of electrode materials for sodium batteries. *Chemical Communications, 48*(52), 6544-6546.

Luo, W., Allen, M., Raju, V., & Ji, X. (2014). An Organic Pigment as a High‐Performance Cathode for Sodium‐Ion Batteries. *Advanced Energy Materials, 4*(15), 1400554-1400560.

Martin, G., Rentsch, L., Höck, M., & Bertau, M. (2017). Lithium market research–global supply, future demand and price development. *Energy Storage Materials, 6*, 171-179.

Mendiboure, A., Delmas, C., & Hagenmuller, P. (1985). Electrochemical intercalation and deintercalation of $NaxMnO_2$ bronzes. *Journal of Solid State Chemistry, 57*(3), 323-331.

Nie, P., Shen, L., Pang, G., Zhu, Y., Xu, G., Qing, Y., Dou, H., & Zhang, X. (2015). Flexible metal–organic frameworks as superior cathodes for rechargeable sodium-ion batteries. *Journal of Materials Chemistry A, 3*(32), 16590-16597.

Niu, Y., Xu, M., Cheng, C., Bao, S., Hou, J., Liu, S., Yi, F., He, H., & Li, C. M. (2015). $Na_{3.12}Fe_{2.44}(P_2O_7)_2$/multi-walled carbon nanotube composite as a cathode material for sodium-ion batteries. *Journal of Materials Chemistry A, 3*(33), 17224-17229.

Niu, Y., Xu, M., Shen, B., Dai, C., & Li, C. M. (2016). Exploration of $Na_7Fe_{4.5}(P_2O_7)_4$ as a cathode material for sodium-ion batteries. *Journal of Materials Chemistry A, 4*(42), 16531-16535.

Onoda, M. (2008). Geometrically frustrated triangular lattice system $NaxVO_2$: superparamagnetism in x= 1 and trimerization in $x \approx 0.7$. *Journal of Physics: Condensed Matter, 20*(14), 145205- 145214.

Pang, W. K., Kalluri, S., Peterson, V. K., Sharma, N., Kimpton, J., Johannessen, B., Liu, H. K., Dou, S. X., & Guo, Z. (2015). Interplay between electrochemistry and phase evolution of the P2-type $Na_x(Fe_{1/2}Mn_{1/2})O_2$ cathode for use in sodium-ion batteries. *Chemistry of Materials, 27*(8), 3150-3158.

University of Malaya

Parant, J.-P., Olazcuaga, R., Devalette, M., Fouassier, C., & Hagenmuller, P. (1971). Sur quelques nouvelles phases de formule Na_xMnO_2 (x<1). *Journal of Solid State Chemistry, 3*(1), 1-11.

Qian, J., Zhou, M., Cao, Y., Ai, X., & Yang, H. (2012). Nanosized $Na_4Fe(CN)_6$/C composite as a low-cost and high-rate cathode material for sodium-ion batteries. *Advanced Energy Materials, 2*(4), 410-414.

Ren, W., Zhu, Z., An, Q., & Mai, L. (2017). Emerging prototype sodium-ion full cells with nanostructured electrode materials. *Small, 13*(23), 1604181-1604207.

Sauvage, F., Laffont, L., Tarascon, J.-M., & Baudrin, E. (2007). Study of the insertion/deinsertion mechanism of sodium into $Na_{0.44}MnO_2$. *Inorganic Chemistry, 46*(8), 3289-3294.

Shen, X., Wu, S., Liu, Y., Wang, K., Xu, Z., & Liu, W. (2009). Morphology syntheses and properties of well-defined Prussian blue nanocrystals by a facile solution approach. *Journal of Colloid and Interface Science, 329*(1), 188-195.

Skundin, A. M., Kulova, T. L., & Yaroslavtsev, A. B. (2018). Sodium-ion batteries (a review). *Russian Journal of Electrochemistry, 54*(2), 113-152.

Song, J., Wang, L., Lu, Y., Liu, J., Guo, B., Xiao, P., Lee, J.-J., Yang, X.-Q., Henkelman, G., & Goodenough, J. B. (2015). Removal of interstitial H_2O in hexacyanometallates for a superior cathode of a sodium-ion battery. *Journal of the American Chemical Society, 137*(7), 2658-2664.

Su, D., Ahn, H.-J., & Wang, G. (2013). Hydrothermal synthesis of α-MnO_2 and β-MnO_2 nanorods as high capacity cathode materials for sodium ion batteries. *Journal of Materials Chemistry A, 1*(15), 4845-4850.

Sun, A., Beck, F. R., Haynes, D., Poston, J. A., Narayanan, S., Kumta, P. N., & Manivannan, A. (2012). Synthesis, characterization, and electrochemical studies of chemically synthesized $NaFePO_4$. *Materials Science and Engineering: B, 177*(20), 1729-1733.

Szajwaj, O., Gaudin, E., Weill, F., Darriet, J., & Delmas, C. (2009). Investigation of the new P´3-$Na_{0.60}VO_2$ phase: structural and physical properties. *Inorganic chemistry, 48*(19), 9147-9154.

Vassilaras, P., Ma, X., Li, X., & Ceder, G. (2013). Electrochemical properties of monoclinic $NaNiO_2$. *Journal of the Electrochemical Society, 160*(2), A207-A211.

Wang, H., Liao, X.-Z., Yang, Y., Yan, X., He, Y.-S., & Ma, Z.-F. (2016a). Large-scale synthesis of $NaNi_{1/3}Fe_{1/3}Mn_{1/3}O_2$ as high performance cathode materials for sodium ion batteries. *Journal of the Electrochemical Society, 163*(3), A565-A570.

Wang, L., Song, J., Qiao, R., Wray, L. A., Hossain, M. A., Chuang, Y.-D., Yang, W., Lu, Y., Evans, D., & Lee, J.-J. (2015). Rhombohedral Prussian white as cathode for rechargeable sodium-ion batteries. *Journal of the American Chemical Society, 137*(7), 2548-2554.

University of Malaya

Wang, S., Wang, L., Zhu, Z., Hu, Z., Zhao, Q., & Chen, J. (2014). All organic sodium‐ion batteries with $Na_4C_8H_2O_6$. *Angewandte Chemie International Edition, 53*(23), 5892-5896.

Wang, Y., Ding, Y., Pan, L., Shi, Y., Yue, Z., Shi, Y., & Yu, G. (2016b). Understanding the size-dependent sodium storage properties of $Na_2C_6O_6$-based organic electrodes for sodium-ion batteries. *Nano Letters, 16*(5), 3329-3334.

Wessells, C. D., Huggins, R. A., & Cui, Y. (2011). Copper hexacyanoferrate battery electrodes with long cycle life and high power. *Nature Communications, 2*, 550-555.

Whiteside, A., Fisher, C. A., Parker, S. C., & Islam, M. S. (2014). Particle shapes and surface structures of olivine $NaFePO_4$ in comparison to $LiFePO_4$. *Physical Chemistry Chemical Physics, 16*(39), 21788-21794.

Wilde, R. E., Ghosh, S. N., & Marshall, B. J. (1970). Prussian blues. *Inorganic Chemistry, 9*(11), 2512-2516.

Wood, S. M., Eames, C., Kendrick, E., & Islam, M. S. (2015). Sodium ion diffusion and voltage trends in phosphates $Na_4M_3(PO_4)_2P_2O_7$ (M= Fe, Mn, Co, Ni) for possible high-rate cathodes. *The Journal of Physical Chemistry C, 119*(28), 15935-15941.

Wu, L., Hu, X., Qian, J., Pei, F., Wu, F., Mao, R., Ai, X., Yang, H., & Cao, Y. (2014). Sb–C nanofibers with long cycle life as an anode material for high-performance sodium-ion batteries. *Energy & Environmental Science, 7*(1), 323-328.

Wu, X., Deng, W., Qian, J., Cao, Y., Ai, X., & Yang, H. (2013). Single-crystal $FeFe(CN)_6$ nanoparticles: a high capacity and high rate cathode for Na-ion batteries. *Journal of Materials Chemistry A, 1*(35), 10130-10134.

Wu, X., Luo, Y., Sun, M., Qian, J., Cao, Y., Ai, X., & Yang, H. (2015). Low-defect Prussian blue nanocubes as high capacity and long life cathodes for aqueous Na-ion batteries. *Nano Energy, 13*, 117-123.

Xia, X., & Dahn, J. (2012). $NaCrO_2$ is a fundamentally safe positive electrode material for sodium-ion batteries with liquid electrolytes. *Electrochemical and Solid-State Letters, 15*(1), A1-A4.

Xu, F., Xia, J., & Shi, W. (2015). Anthraquinone-based polyimide cathodes for sodium secondary batteries. *Electrochemistry Communications, 60*, 117-120.

Xu, F., Xia, J., Shi, W., & Cao, S.-a. (2016). Sulfonyl-based polyimide cathode for lithium and sodium secondary batteries: Enhancing the cycling performance by the electrolyte. *Materials Chemistry and Physics, 169*, 192-197.

Yabuuchi, N., Yoshida, H., & Komaba, S. (2012). Crystal structures and electrode performance of alpha-$NaFeO_2$ for rechargeable sodium batteries. *Electrochemistry, 80*(10), 716-719.

University of Malaya

Yamashita, T., Momida, H., & Oguchi, T. (2016). Crystal structure predictions of $Na_xC_6O_6$ for sodium-ion batteries: First-principles calculations with an evolutionary algorithm. *Electrochimica Acta, 195*, 1-8.

Yan, X., Yang, Y., Liu, E., Sun, L., Wang, H., Liao, X.-Z., He, Y., & Ma, Z.-F. (2017). Improved cycling performance of prussian blue cathode for sodium ion batteries by controlling operation voltage range. *Electrochimica Acta, 225*, 235-242.

Yang, Y., Liu, E., Yan, X., Ma, C., Wen, W., Liao, X.-Z., & Ma, Z.-F. (2016). Influence of structural imperfection on electrochemical behavior of Prussian blue cathode materials for sodium ion batteries. *Journal of the Electrochemical Society, 163*(9), A2117-A2123.

Ye, H., Wang, Y., Zhao, F., Huang, W., Han, N., Zhou, J., Zeng, M., & Li, Y. (2016). Iron-based sodium-ion full batteries. *Journal of Materials Chemistry A, 4*(5), 1754-1761.

Yoshida, H., Yabuuchi, N., Kubota, K., Ikeuchi, I., Garsuch, A., Schulz-Dobrick, M., & Komaba, S. (2014). P2-type $Na_{2/3}Ni_{1/3}Mn_{2/3-x}Ti_xO_2$ as a new positive electrode for higher energy Na-ion batteries. *Chemical Communications, 50*(28), 3677-3680.

Yu, C.-Y., Park, J.-S., Jung, H.-G., Chung, K.-Y., Aurbach, D., Sun, Y.-K., & Myung, S.-T. (2015). $NaCrO_2$ cathode for high-rate sodium-ion batteries. *Energy & Environmental Science, 8*(7), 2019-2026.

Yuan, Y., Wang, J., Hu, Z., Lei, H., Tian, D., & Jiao, S. (2016). $Na_2Co_3[Fe(CN)_6]_2$: A promising cathode material for lithium-ion and sodium-ion batteries. *Journal of Alloys and Compounds, 685*, 344-349.

Zhang, H., Hasa, I., Buchholz, D., Qin, B., & Passerini, S. (2017). Effects of nitrogen doping on the structure and performance of carbon coated $Na_3V_2(PO_4)_3$ cathodes for sodium-ion batteries. *Carbon, 124*, 334-341.

Zhao, C., Liu, L., Qi, X., Lu, Y., Wu, F., Zhao, J., Yu, Y., Hu, Y. S., & Chen, L. (2018). Solid‐State Sodium Batteries. *Advanced Energy Materials*. 8 (2018) 1703012-1703032.

Zheng, X., Bommier, C., Luo, W., Jiang, L., Hao, Y., & Huang, Y. (2019). Sodium metal anodes for room-temperature sodium-ion batteries: Applications, challenges and solutions. *Energy Storage Materials, 16*, 6-23.

Zhou, M., Li, W., Gu, T., Wang, K., Cheng, S., & Jiang, K. (2015). A sulfonated polyaniline with high density and high rate Na-storage performances as a flexible organic cathode for sodium ion batteries. *Chemical Communications, 51*(76), 14354-14356.

Zhu, Y., Xu, Y., Liu, Y., Luo, C., & Wang, C. (2013). Comparison of electrochemical performances of olivine $NaFePO_4$ in sodium-ion batteries and olivine $LiFePO_4$ in lithium-ion batteries. *Nanoscale, 5*(2), 780-787.

University of Malaya

LIST OF PUBLICATIONS AND PAPERS PRESENTED

List of Publications

1. Chen, Y., Woo, H. J., Kufian, M. Z., Teo, L. P., Wang, F., Zhao, C., & Arof, A. K. (2018). Synthesis of low vacancies PB with high electrochemical performance using a facile method. *Materials Technology*, 1, 1-8.

Paper presented

1. Chen, Y., Woo, H. J., Arof, A. K. (2017), Low vacancies Prussian blue as the sodium batteries cathode. Paper presented at the 6th International Conference on Functional Material and Devices (ICFMD), 15-18 August 2017, Melaka, Malaysia.

University of Malaya